GEO-3900

MASTER'S THESIS IN GEOLOGY

Late Weichselian and Holocene sedimentary
processes and environments in Billefjorden, Svalbard

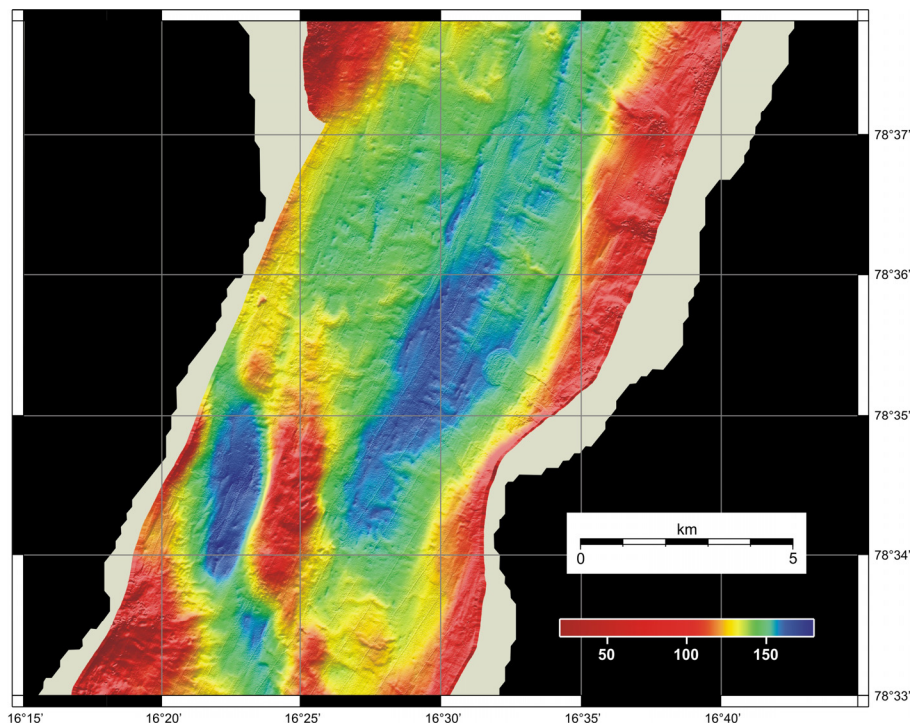Nicole J. Baeten

November, 2007

GEO-3900

MASTER'S THESIS IN GEOLOGY

Late Weichselian and Holocene sedimentary processes and environments in Billefjorden, Svalbard

Nicole J. Baeten

November, 2007

<u>Acknowledgements</u>

I would never have succeeded without the help of many, and would therefore like to thank the following persons:

Nicole J. Baeten

Tromsø, November 2007

Abstract

Three sediment cores, swath multibeam bathymetry data and high-resolution seismic data from Billefjorden, Svalbard have been analysed for a better understanding of the Late Weichselian and Holocene glacier activity as well as sedimentary process and glacigenic deposits in the fjord.

The physical properties, sedimentology and mineralogy of the cores were studied. Seven radiocarbon dates provide the basis for the chronology. The occurrence, distribution and relative age of deposition of different morphological features in the fjord were analysed. The sediment cores have been correlated to high-resolution seismic data in order to get a better understanding of the lateral extent of the different lithostratigraphic units.

The data reveal that glacial linear features were generated in the central part of Billefjorden while it was filled with ice draining the Svalbard-Barents Sea ice sheet during the Last Glacial. A till in the bottom of a sediment core from the central part of the fjord is inferred to have been deposited before the ice front retreated into Billefjorden around 11230 cal. years BP. An overlying glacimarine unit deposited between c. 11230 and 11200 cal. years BP indicates that the glacier retreated from central parts of the fjord to the fjord head in approximately 30 years. Annual recessional moraines deposited during this period suggest that the glacier front retreated approximately 330 m/ year at the end of the last Glacial.

High concentration of shells, low amounts of IRD and XRD results indicate a Holocene climatic optimum between c. 11200 – 7930 cal. years BP in which Nordenskiöldbreen was most likely much smaller than it is at present.

XRD results and comparatively high amounts of IRD point to a complex pattern of ice rafting between c. 7930 and 3230 cal. BP. IRD deposited before c. 5470 cal. years BP was most likely transported by sea ice, whereas IRD after 5470 cal. years points towards a growth of Nordenskiöldbreen.

The time after c. 3230 is mainly characterised by suppressed rafting of sea ice and icebergs because of the possible presence of multi-year shorefast sea ice during the Neoglacial maximum. Glacial lineations on a bedrock terrace in the inner fjord were formed during a Neoglacial advance of Nordenskiöldbreen. Iceberg ploughmarks and recessional moraines

were most likely generated during the retreat after the maximum Neoglacial extent of Nordenskiöldbreen.

Mass-transport activity in Billefjorden probably occurred throughout the entire Holocene. There might haven been an increased mass-transport activity shortly after the deglaciation of the fjord, because high rates of isostatic uplift might have caused seismic activity. Other triggering mechanisms include the development of oversteepened slopes by high sediment supply and the pushing of sediments at the grounding line of the glacier.

Pockmarks in the central part of the fjord were most likely generated by the seepage of thermogenic gas along the Billefjorden fault zone.

Table of contents

1. Introduction

1.1 Objectives

Three sediment cores, swath bathymetry data and two seismic profiles were used to reconstruct the glacial history and to investigate the sedimentary processes in Billefjorden, central Spitsbergen, Svalbard (Fig 1). The following objectives were addressed:

- Inferring the origin of landforms in the fjord
- Elucidating glacimarine/marine sedimentary processes
- Reconstructing the glacier-retreat pattern at the end of the last glacial
- Elucidating variations in the Holocene glacial activity in the fjord

1.2 Background

This study is a part of the strategic university program *Sedimentary Processes and Palaeoenvironments on Northern Continental Margins* (SPONCOM), funded by the Research Council of Norway. The overall goal of this program is to assess the changes in the physical environment of the sea-floor and overlying water and ice in selected fjords and continental margins in northern Norway and West Spitsbergen during the last glacial – interglacial cycle. Glacial history is very important because of its close relationship to climate change. However this relationship is not yet fully understood and needs more investigation (http://www.ig.uit.no/sponcom/).
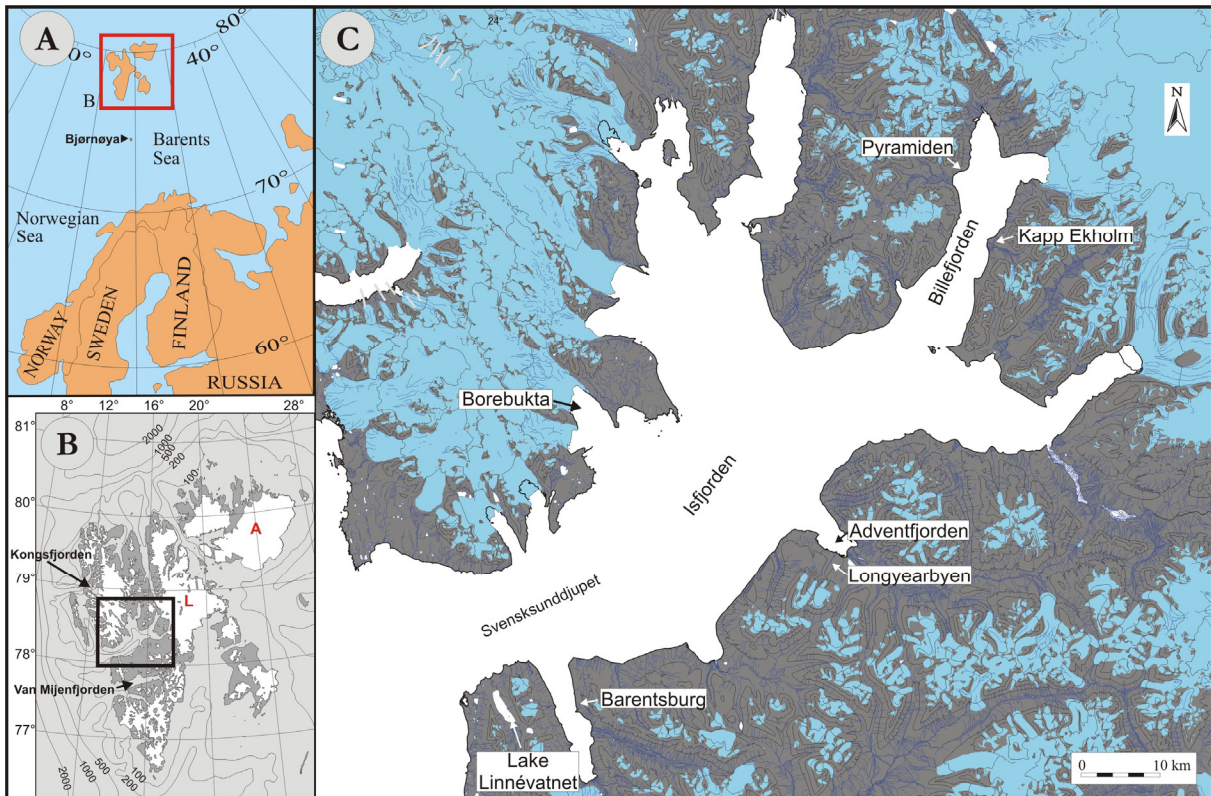
Fig. 1.1 A shows an overview map of northern Europe with the position of Svalbard, B shows Svalbard with indicated the Isfjorden system, and C shows the Isfjorden system on Svalbard. Light blue represents glacier coverage and the dark blue lines show the positions of rivers. The red letters in B shows the positions of the two ice caps Lomonosovfonna (L) and Austfonna (A).

1.3 Previous investigations

During the Last Glacial, fjords on Spitsbergen acted as pathways for fast-flowing ice streams draining the Svalbard-Barents-Sea Ice Sheet (e.g. Ottesen et al., 2005). The retreat of the ice stream draining the LGM ice sheet through the Isfjorden area started around 14.8 ^{14}C ka BP (radiocarbon years before the present; Elverhøi et al. 1995A, Svendsen et al. 1996, Fig. 1.2). Around 13 ^{14}C ka BP, glacial retreat accelerated. This correlates well with the first major warming of the high-latitude North Atlantic region (Svendsen et al. 1996). Marine cores show a short glacial readvance around 12.4 ^{14}C ka BP (Fig. 1.2, Svendsen et al., 1996).

The deglaciation of the mouth of Isfjorden started around 12.3 ^{14}C ka BP (Mangerud et al., 1992).

Based on a single radiocarbon date, Boulton (1979) interpreted a till at Kapp Ekholm (for location see Fig. 1.1) in Billefjorden to indicate a major glacial readvance between 11 and 9.7 ^{14}C ka BP (Fig. 1.2). Mangerud and Svendsen (1990) could, however, not reproduce this date,

and question Boulton's interpretations. Also Forwick & Vorren (2005B) did not find any evidence for a Late Weichselian glacier readvance in Billefjorden.

Based on sediments overridden by glaciers, Forwick & Vorren (2005B) suggest that during the Younger Dryas, glaciers readvanced up to 25 km in the north and east of Isfjorden.

Minor morainal banks in the innermost part of Isfjorden suggest the retreating glaciers had a short halt subsequent to the Younger Dryas readvance (Forwick & Vorren, 2005B).

According to Forwick & Vorren (2005) the deglaciation of Billefjorden took place during the Late Younger Dryas and during the Early Preboreal. Recessional moraines in the fjord indicate a stepwise retreat of the glaciers. The main glacier retreat terminated at c. 10 ^{14}C ka BP in the inner fjords (e.g. Elverhøi et al., 1995A). Several dates from emerged sediments show that most glaciers had retreated close to or behind their present margins by 10 to 9 ^{14}C ka BP (Salvigsen, 1979, Forman et al., 1987).
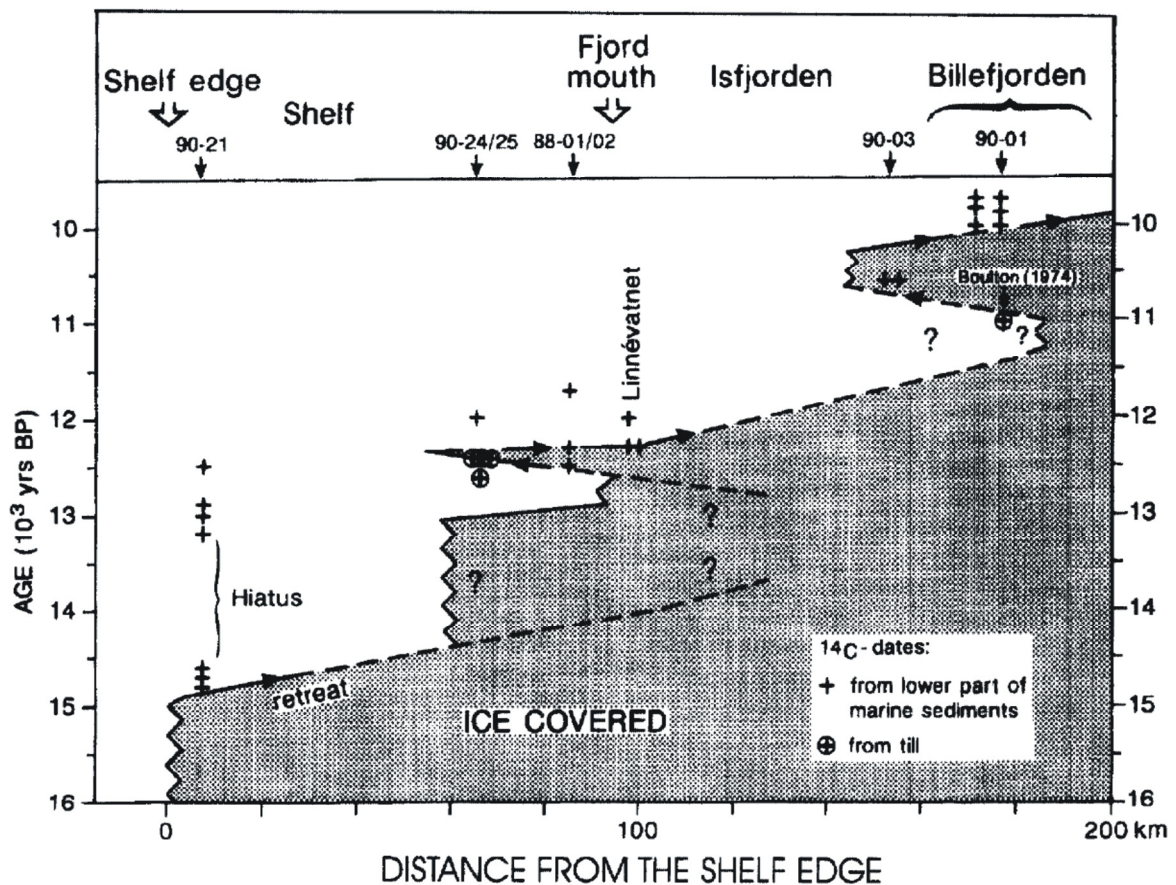
Fig. 1.2: Time-distance diagram for the glacier front in Billefjorden, Isfjorden and the adjacent shelf, from Svendsen et al. 1996.

Previous work by Svendsen and Mangerud (1997), Elverhøi et al. (1995A), suggested that, based on a constant low sedimentation rate during the early and mid- Holocene, glaciers in Billefjorden were small or absent during this interval. Possible glacier expansion, in which the glacier Nordenskiöldbreen would reach the fjord, after 2800 cal. BP is indicated by a pronounced increase in sedimentation rate.

Recent studies on sea surface temperature and IRD indicate that central parts of Spitsbergen have never been ice-free during the Holocene and that the glacial activity increased around 8000 ^{14}C BP and c. 4000 ^{14}C BP (Hald et al., 2004, Forwick & Vorren, 2005A).

2. Description of the area

2.1 Physiographic setting

Billefjorden is a tributary of Isfjorden, the largest fjord on western Spitsbergen (Fig.1.1). It is located between 78° 25' and 77° 45' N and 15° 50' and 17° 00' E. It is 30 km long, between 5 and 8 km wide and has a maximum water depth of 225 m (Fig. 2.1). The area of the fjord is approximately 202 km^2 (Forwick & Vorren, 2005A).

Sediment supply occurs from several rivers and the tidewater glacier Nordenskiöldbreen at the innermost parts of the fjord (Fig. 2.1). The catchment area of Billefjorden is 907 km^3, and it has a glacier coverage of 43.8% (Hagen et al., 1993). The fjord is narrower and steeper and with a rougher seafloor than some of the other fjords in the Isfjorden area. This may be related to the bedrock types and structures in the fjord (Forwick & Vorren, 2005A).

Fig. 2.1: Bathymetry map of Billefjorden (Norske sjøkart, Isfjorden, 1978).

2.2 Geology

2.2.1 Tectonic history

The first movement along the Billefjorden Fault Zone took place during the early Caladonian tectonic events. This event included both compressional and strike-slip movement in this area. Intensive faulting took place during the mid-Carboniferous. This east side was down-faulted and resulted in a half-graben structure, the Billefjorden through (Hjelle et al., 1993). This fault zone is running sub-parallel to the fjord axis (Fig. 2.2). Eroded material was transported eastwards from the Nordfjorden High in the west and deposited in the Billefjorden through. More than 1000 m of sediments were deposited in the central part of the through (Fig. 2.3). The strata thicken and coarsen towards the fault zone.

2.2.2 Pre-Quaternary geology

The different strata present in the area are indicated in figure 2.3 and 2.4. Under the glacier Nordenskiöldbreen, Precambrian basement rocks occur. These mainly crystalline rocks are very resistant and form a terrace in front of the present glacier front. Along the fjord sides the rocks mainly consist of Billefjorden through strata (Dallmann et al., 2004). Difference in lithologic composition of the sediments in the fjord eroded by the glacier should therefore indicate difference in glacier regime (Svendsen & Mangerud, 1997).

The rocks entering the fjord or occurring close to the fjord in the north-west part mainly consist of limestones, dolomites, conglomerates, sandstones and shale (Dallmann et al., 2004). The groups or formations, timing of deposition and the depositional environment of these rocks are described in figure 2.4. In the western and eastern part of the fjord the strata consist of shale, sandstone, limestone, gypsum/anhydrite and dolomite. In the eastern part mudstone can be found in addition (Dallmann et al., 2004).

Some rocks in the mouth of the fjord, including the little island in the mouth of the fjord (Fig. 2.1) consist of some intrusive dolerite. These sills and dikes were mainly formed during the Early Cretaceous when the North Atlantic region was subject to tensional tectonics due to initial mid-ocean rifting of the future North Atlantic Ocean (Dallmann et al., 2004).

Fig. 2.2: The tectonic overview of Billefjorden, from Dallmann et al., 2004.

Fig. 2.3: A W-E profile across the Billefjorden fault zone and the adjoining areas. The tectonic setting and sedimentary formations are indicated. From Svalsim, Statoil, modified from Johannesen and Steel, 1992.

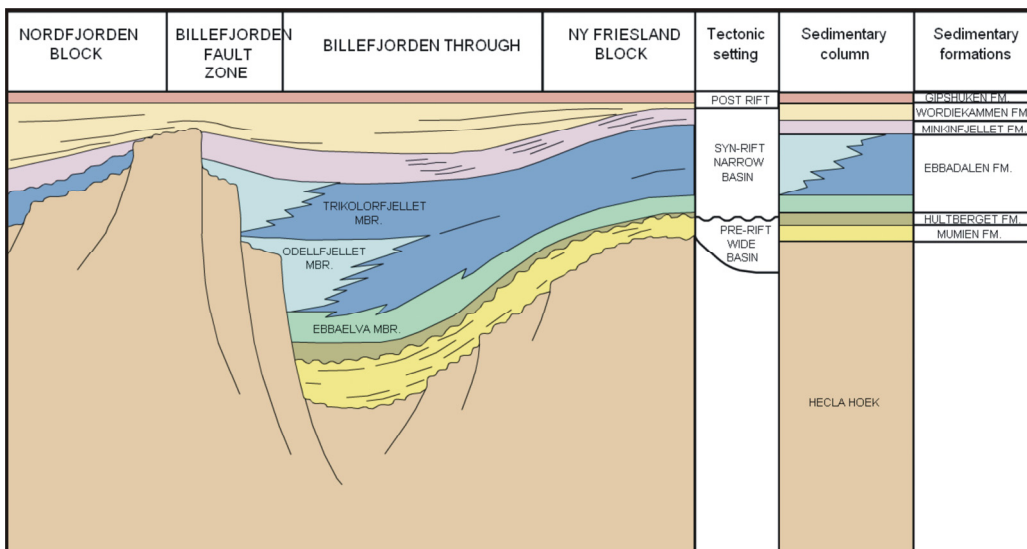| Era	Series	Stage	Age (Ma)	Stratigraphic units	Tectonic events and geological setting	Lithology and environments
Cainozoic	Quaternary		1.64	Bockfjorden Volcanic Cpl.	glaciation; volcanism in NW Spitsbergen	**Bockfjorden Volcanic Complex:** Quaternary pyroclastics and lavas, 3 eruptive centres.
	Tertiary	Neogene (Plio., Mio.)	23.5	Seidfjellet Fm.	no record; uplift, tilting / local volcanism	**Seidfjellet Formation:** Max. thickness < 400 m. Plateau basalts, consisting of up to 15 individual lava flows.
		Palaeogene (Oli., Eoc., Pal.)	65	Buchananisen Grp. / Calypsostranda Grp. / Van Mijenfjorden Grp.	no record; regional uplift? / fault-thrust belt deformation and uplift in W Svalbard; pull-apart basins, clastic sedimentation	**Buchananisen Group:** Max. thickness > 4000 m (?). Conglomerates, sandstones, siltstones, and shales. Continental (alluvial fan, fluvial, deltaic) to shallow marine environments. **Calypsostranda Group:** Max. thickness 265 m. Sandstones, siltstones, shales, coal seams and subordinate conglomerates.
Mesozoic	Cretaceous	Late	97		no record; regional uplift	**Van Mijenfjorden Group:** Max. thickness 1900 m. Sandstones, siltstones, and shales with subordinate coals and conglomerates, deposited within coastal (deltaic) to shallow-marine environments.
		Early	146	Adventdalen Grp. / Janusfjellet Subgrp.	deltaic sedimentation / coastal progradation / marine shelf / organic-rich shale deposition	**Adventdalen Group:** Max. thickness 1600 m. Shales, siltstones and sandstones, deposited on a shallow marine shelf. Deltaic sediments at the top.
		Late	157			
	Jurassic	Middle	178	Wilhelmøya Subgrp.	condensed succession regional hiatuses	**Kapp Toscana Group:** Max. thickness 475 m. Shales, siltstones and sandstones, deposited within coastal (deltaic) and shallow marine environments.
		Early	208	Kapp Toscana Grp.		**Sassendalen Group:** Max. thickness 700 m. Shales and siltstones with sandstone inter-vals in the west. Coastal (deltaic) to shallow marine environments.
	Triassic	Late	235	Storfjorden Subgrp.	stable shelf conditions	**Tempelfjorden Group:** Max. thickness 460 m. Siliceous (spiculitic) shales, siltsones and cherts with intercalated sandstone and lime-stone intervals. Sediments deposited within deeper marine environments.
		Middle / Early	241 / 245	Sassendalen Grp.	deltaic and shelf sedimentation	
Palaeozoic	Permian	Late	256	Tempelfjorden Grp.	no record; regional uplift	
		Early	290	Dickson Land Subgrp.	extended marine shelf	**Gipsdalen Group:** Max. thickness 1800 m. Carbonates and clastic rocks, intercalated with evaporites. Development from a clastic continental graben into an open, shallow-marine shelf.
	Carboniferous	Late	323	Gipsdalen Grp. / Charlesbreen Subgrp. / Campbellryggen Subgrp. / ?Treskelen Subgrp.	transtensional tectonic activity; individual depositional areas (Inner Hornsund, St. Jonsfjorden, Billefjorden troughs)	**Billefjorden Group:** Max. thickness 2500 m. Mainly conglomerates, sandstones and shales, locally intercalated with coal seams. Continental (fluvial, swamp and lacustrine) environments.
		Early	362	Billefjorden Grp.	clastic basin / Svalbardian Event	**Andrée Land Group:** Max. thickness > 3000 m. Fining upward sequence, consisting of conglomerates, sandstones, siltstones and claystones, locally with limestone interbeds. Continental (fluvial, lacustrine) to marginal-marine (delta, lagoon) environments.
	Devonian	Late	382.5	no record		
		Middle	394	Andrée Land Grp.	Old Red Sandstone, continental molasse basin	**Red Bay Group:** Max. thickness 2500 m. Fining upward sequence, consisting mainly of conglomerates and sandstones, deposited within continental (alluvial fan, fluvial) high-energy environments.
		Early	418	Red Bay Grp.	Haakonian Event	**Siktefjellet Group:** Max. thickness 750-1400 m (?). Fault-controlled, fining upward se-quence, consisting of conglomerates and sandstones, deposited within alluvial fan and fluvial environments. Bounded by angular unconformities.
	Silurian	Late	423	Siktefjellet Grp.	continental molasse basin / Late Caledonian Event; E-directed folding a. thrusting; granitic intrusions	
		Early	443	Bullbreen Grp. / Arkfjellet Formation (age ?)	flysch sedimentation	**Bullbreen Group:** Max. thickness ca. 1500 m. Conglomerates interlayered with sandstones and shales in the upper part. Lower part consists of carbonates, containing marine fossils of Late Ordovician to Early Silurian age.
	Ordovician	Late	458			**Arkfjellet unit:** Sandstone/shale succession of some 100 m in thickness. Bounded by angular unconformities. Occurs only in Sørkapp Land area.
		Middle	470	Early Caledonian Event; subduction of Vestgötabreen Cpl.; multiple thrust duplexes (S and W Spitsbergen); upright tight faults (NE Svalbard)		
		Early	495	Sørkapp Land Grp. (S Spitsbergen) / upper part of Oslobreen Grp. (NE Svalbard)	shallow marine carbonate shelf	**Sørkapp Land Group:** Cumulative thickness ca. 1400 m. Low-grade metamorphic marble succession with basal quartzites.
	Cambrian	Late		Hornsundian Event; unconformity		**Oslobreen Group:** Cumulative thickness > 1200 m. Carbonate succession with basal sandstones; dark limestones with bituminous shales in the upper part.
		Middle	518	Sofiekammen Grp. / lower part of Oslobreen Grp.	shallow marine carbonate shelf	
		Early	545	Jarlsbergian Event; unconformity		**Sofiekammen Group:** Cumulative thickness 935 m. Low-grade marble succession with intercalated slates and quartzitic sandstones.
Proterozoic	Neoproterozoic	Vendian	610	W / NW Spitsbergen: Kapp Lyell Grp., Comfortlessbreen Grp., Ferrierfjellet Grp. / W Ny Friesland / E Ny Friesland / Nordaustlandet: Polarisbreen Grp., Sveanor Fm.		**Proterozoic:** Three geological terranes with contrasting development. All, except for W Ny Friesland, experienced Grenvillian age events and are overlain by Neoproterozoic succes-sions. All terranes were juxtaposed during the Caledonian Orogeny.
			1000	Daudmannsodden Grp., Sofiebogen Grp., other time equivalents / Planetfjella unit (age ?) / Murchisonfjorden Supergrp., Akademikarbreen Grp., Veteranen Grp.	Grenvillian Events; granitic intrusions, volcanic activity	**Neoproterozoic:** Thickness of several km, significantly varying. Unmetamorphosed to low-grade metasedimentary rocks. W Spitsbergen: Basal conglomerates and marbles with stromatolites, clastics and tilloids. Nordaustl.: 3-4 deepening upward, shallow marine shelf rhythms, up to 1 km thick. E Ny Friesland: > 5 km thick, quartzitic graywacke deposited within a distal shelf slope environment; two tilloid successions.
	Mesoproterozoic		1600	Krossfjorden Grp., Smeerenburgfj. Cpl., Biscayarhuken unit, Mont Blanc unit, Richarddalen Cpl., Pinkiefjellet unit, Kongsvegen Grp., St. Jonsfjorden Grp., Magnethøgda unit, Nordbukta Grp., Isbjørnhamna Grp., Skålfjellet Grp., Deilegga Grp. / Sørbreen unit, Vassfaret unit, Rittervatnet unit, Polhem unit, Smutsbreen unit, Planetfjella unit ? / Kapp Hansteen Cpl., Brennevinsfjorden Grp., Duvefjorden Cpl.		**Mesoproterozoic:** Thickness of several km, significantly varying. Medium- to high-grade supracrustal and igneous rocks, intruded by ca. 950 Ma old granites in Western Spitsber-gen and Nordaustlandet. In Ny Friesland, a stack of thrust sheets, each containing Palaeoproterozoic basement gneisses and younger cover sequences, is folded in the Atomfjella Antiform.
	Palaeoproterozoic			Sveco-Karelian Event (radiometric age data) / Bangenhuk unit, Instrumentberget-Flåtan unit, Eskolabreen unit		**Palaeoproterozoic:** High-grade metamorphic complexes of gneisses, migmatites and
	Archaean		2500	Residual zircons (3.2 Ga), Biscayarhalvøya / Quartz-monzonite (2.7 Ga), E of Femmilsjøen		Detrital zircons suggest late Archaean source rocks for Mesoproterozoic metasediments

Western and eastern part of the fjord

North-west part of the fjord

Fig. 2.4: Geological timetable for Svalbard, Norwegian Polar Institute, Geo-NP Net (http://npolar.no/geonet/).

2.2.3 Quaternary stratigraphy

The Kapp Ekholm sections are situated 14 km from the front of Nordenskiöldbreen (Fig. 2.1). This indicates that when Kapp Ekholm was ice free, glaciers could not have been much larger than at present (Mangerud et al., 1998). The sections contain four sedimentary cycles, each consisting of a diamicton overlain by a coarsening-upward sequence of glacial and marine sediments. The diamictons are interpreted as basal tills, and the coarsening-upward sequences reflect regression caused by glacio-isostatic uplift after the preceding glaciation (Mangerud et al., 1998). Dates on shells just above the last glacial till give a concluded age of 10 ka ^{14}C BP (Mangerud & Svendsen, 1992). At this time the site must have been deglaciated. Other sedimentary cycles give evidence for at least three other glaciations before the last Glacial. A composite glaciation curve is shown in Figure 2.5.
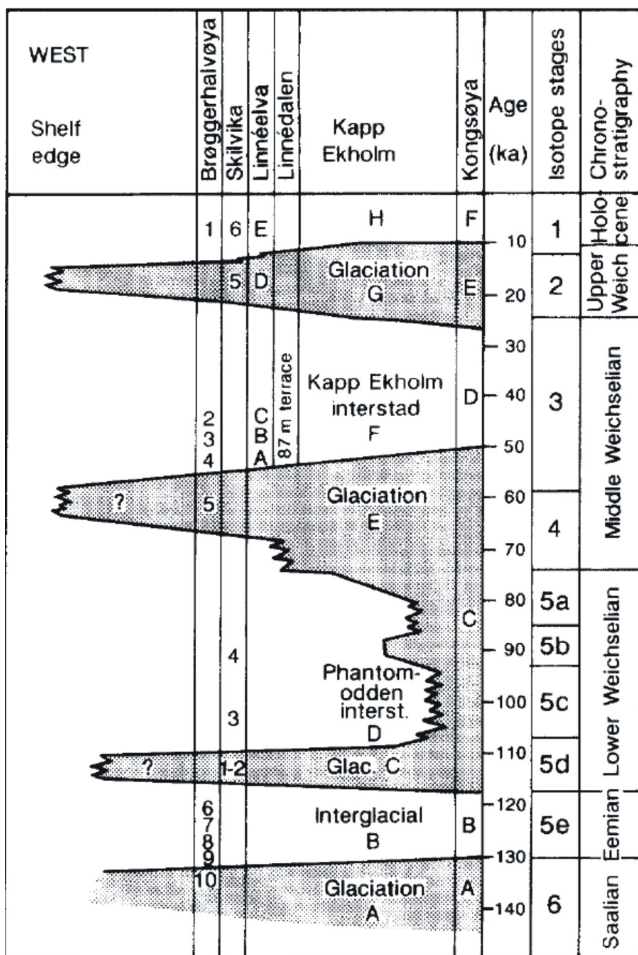

Fig. 2.5: Glaciation curve for the Northern Barents Sea and Svalbard. Constructed from onshore sections on Svalbard. From Mangerud et al. 1998.

2.4 Geomorphology/sediment distribution

The geomorphology of Billefjorden is characterised by very shallow areas and deeper basins (Fig. 2.1). The roughest topography can be found at the mouth of the fjord, ranging between the water surface and 226 m water depth (Fig. 2.1). The bathymetry is probably partly related to tectonic activity within the Billefjorden fault zone.

Several mounds of up to 10 m high and 100 m wide were identified on high-resolution seismic profiles parallel to the fjord axis. These mounds have an acoustically chaotic internal structure and were suggested to be recessional moraines that have been deposited during halts or minor readvances within a period of general glacier retreat (Forwick & Vorren, 2005A)

Approximately 2 km beyond the glacier front of Nordenskiöldbreen, the water depth changes rapidly from a bedrock terrace (approximately 100 m deep) to an up till 211 m deep basin (Fig. 2.1). The bedrock terrace consists of Precambrian crystalline rock. A sub-aerial marginal moraine on this terrace was interpreted as the terminal moraine deposited during the Neoglacial maximum around 1900 AD (Plassen et al., 2004). On the slope from the terrace to the basin, a debris flow with a thickness up to 25 m was identified (Plassen et al., 2004). Seismic data indicate that the thickest sediment accumulation (up to 65 m) is found in the innermost parts of Billefjorden, in front of Nordenskiöldbreen (Plassen et al., 2004; Forwick & Vorren, 2005A). The shallow areas at the mouth of the fjord are covered with a sediment package that is less then 10 m thick. In the central part of the fjord the sediments predominantly drape the underlying topography (Forwick and Vorren, 2005A).

2.5 Climate

Studies on molluscs found in deposits along the coastline of the fjords in Svalbard give some indications about the climate in the early Holocene (Salvigsen et al., 1992). Dates on different species in Isfjorden and western Spitsbergen indicate optimal climate conditions around 8700 to 7800 ^{14}C BP. The species living around this time (*Zirphaea crispate and Modiolus modiolus*) require highest temperatures of all the investigated species. *Mytulis edulis* was common on Svalbard during the warmer part of the Holocene and lived in Svalbard from at least 9500 to 3500 ^{14}C BP. It has not been found on Svalbard since then, but very recently it was observed again. So according to Salvigsen et al. (1992), during the largest part of the Holocene the marine climate was warmer than it is today.

During the past few hundred years, the climate change in the Artic was dominated by the generally cool Little Ice Age and the subsequent warming of up to several degrees marking the termination of this cold period (Grove, 1988). Ice cores in the Lomonosovfonna and Austfonna ice caps (for location see Fig. 1.1) respectively show the cooling towards the Little Ice Age and the subsequent warming (Issakson et al., 2003; Fig. 2.6). Note that Nordenskiöldbreen is an outlet glacier of Lomonosovfonna.
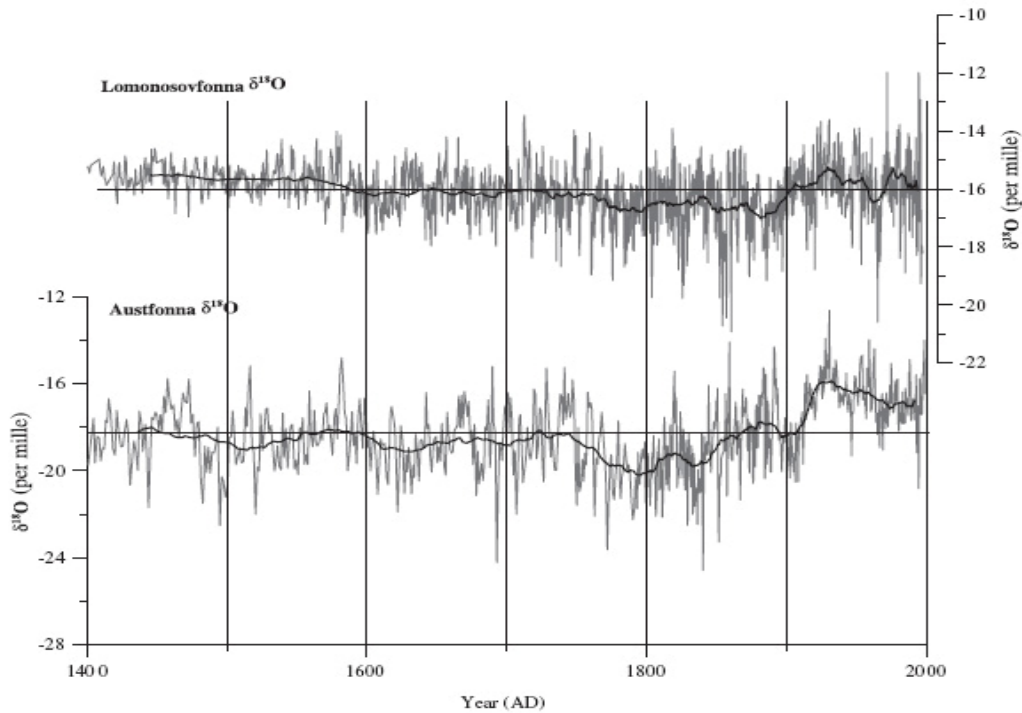
Fig. 2.6: The $\delta^{18}O$ records from Lomonosovfonna and Austfonna ice caps from 1400 AD to present. The grey line is the unsmoothed data and the black line the running mean for an equivalent of 25 years. From Issakson et al. 2003.

The present climate on Svalbard is warmer than in other areas at similar latitude because of the influx of temperate Atlantic water and the passage of low pressure systems from the south (Svendsen et al. 2002). Throughout the year temperatures vary a lot because of Svalbards position in the boarder zone between cold polar and mild maritime air masses (Isaksson et al., 2003). The average temperature on central Spitsbergen is circa -6 ºC (Nordli et al., 1996). The area is generally snow covered from late September to late May. The precipitation is 190 mm/year at Svalbard Airport (Førland et al., 1997).

2.6 Oceanography-hydrography

Oceanographic conditions in the western Spitsbergen fjord are strongly determined by the West Spitsbergen Current, the northernmost extension of the Norwegian Atlantic Current (Fig. 2.7). This current transports warm and saline water along the continental slope of west Spitsbergen northward. Because of this current the area west of the shelf is essentially ice free (Aagaard et al., 1987; Gascard et al., 1995). This heat input from the south makes Svalbard very susceptible to climatic changes (Svendsen et al., 2002). On the shelf, cold and relatively fresh Arctic water rounds the southern tip of Spitsbergen and flows north as a coastal current (Fig. 2.7). Sea-ice conditions vary seasonally (Dowdeswell and Dowdeswell, 1989).

The water masses on the shelf can flow into the Isfjorden system because of the lack of a sill at the mouth of the fjord. The bedrock sill at the mouth of Billefjorden restricts however the inflow there. Inflow of water into the fjord does not occur every year, hence the bottom current activity is very low.

Fig. 2.7: Map of Svalbard showing the major currents. With the West Spitsbergen Current in red and the Arctic-type coastal water in blue. The dashed black line indicates the frontal area between the two currents. From: Svendsen et al. 2002.
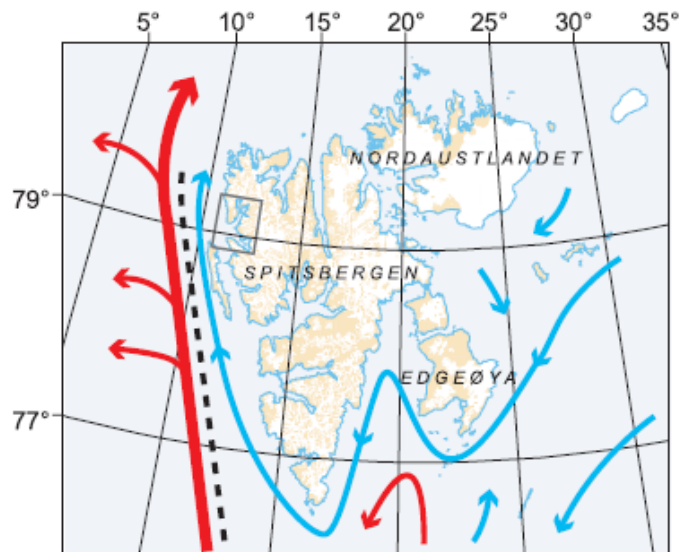
3. Material and methods

3.1 Sediment cores

Three sediment cores were retrieved with the R/V Jan Mayen, the research vessel of the University of Tromsø. They are all gravity cores. JM97-943-GC and JM97-941-GC were taken in 1997 and JM02-979-GC in 2002 (Table 3.1; for location see Fig. 3.1).

A gravity core penetrates the sediments at the seafloor because of a 1600 kg weight on the top of the 6 m long steel barrel. At the bottom of the barrel, a core catcher was used to avoid the sediment sliding out when the core is retrieved. Inside the barrel a plastic liner with an outer diameter of 11 cm contains the sediment sample. This plastic liner was cut into one meter sections, marked and sealed with plastic caps at both ends. The sections were stored at 4 ºC.

Table 3.1: Positions, water depths, core lengths and penetration depths of the three sediment cores.

Station	Latitude	Longitude	Water depth	Core length	Penetration
JM97-941-GC	78º 39.7'	16º 43.5'	193 m	495 cm	7 m
JM97-943-GC	78º 35.7'	16º 29.1'	154 m	459 cm	5.5 m
JM02-979-GC	78º 39.7'	16º 47.3'	196 m	116 cm	~6 m
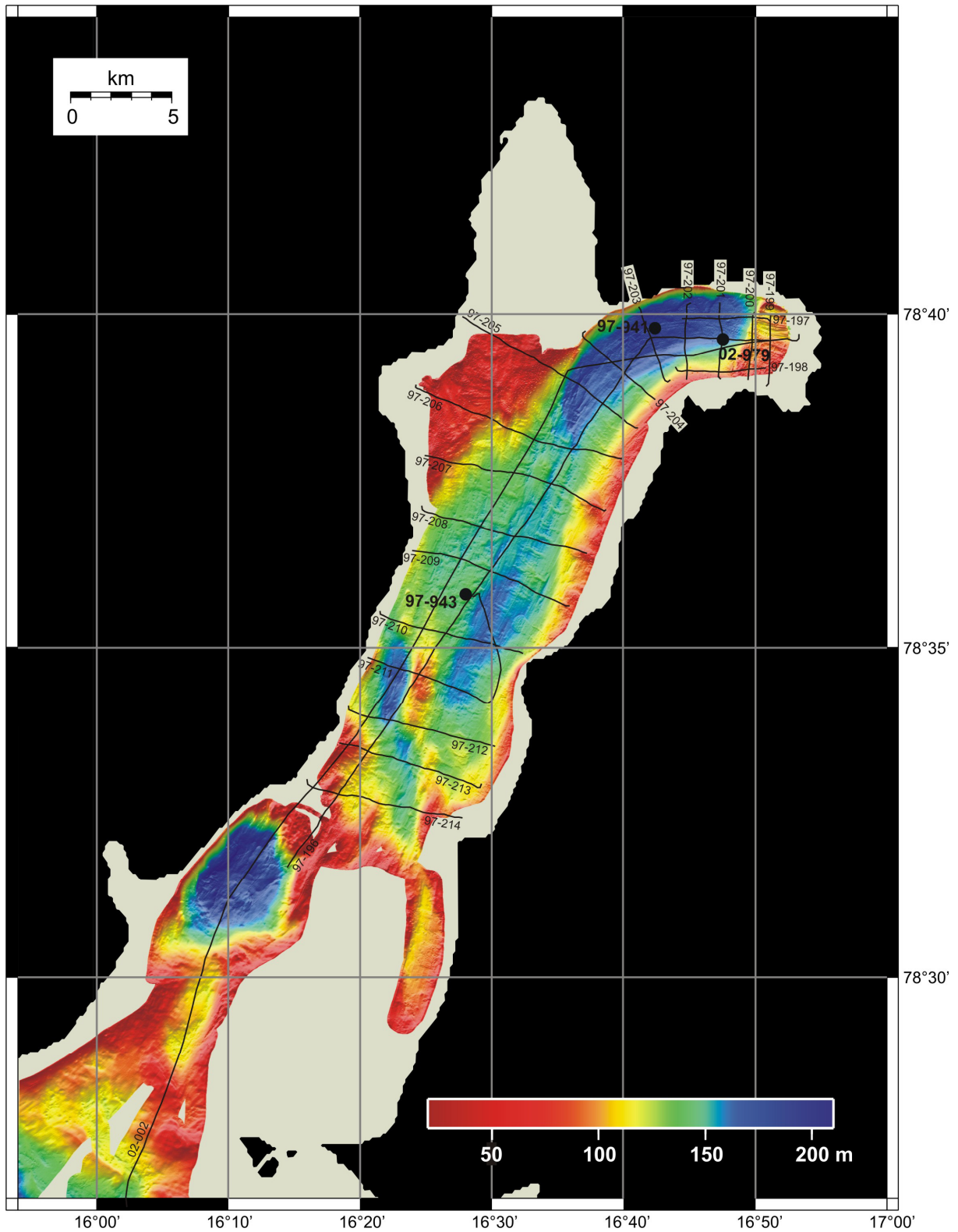
Fig. 3.1: Multibeam bathymetry dataset of Billefjorden with the core positions and seismic lines.

3.2 Laboratory work - sediment cores

3.2.1 Multi Sensor Core Logger (MSCL)

The cores were first logged with the MSCL (developed by the company Geotek Ltd in the UK) when they were still unopened (Fig. 3.2). The MSCL measures the physical parameters of the cores including gamma-ray attenuation, p-wave velocity, p-wave amplitude, core thickness, magnetic susceptibility (with a loop sensor) and temperature. Bulk density, acoustic impedance and the fractional porosity were calculated subsequently.

After the splitting of the cores, the MSCL was used for the acquisition of colour images of the cores. Additionally the magnetic susceptibility of the cores was measured with a point sensor.

A change in temperatures can influence some physical parameters like the p-wave velocity (Weber et al., 1997). The cores were stored in the laboratory the day before they were measured to avoid this. Before measuring the sediment cores, the different sensors were calibrated. The different physical parameters are shortly described below, using information provided in the user manual (MSCL manual, 2000).
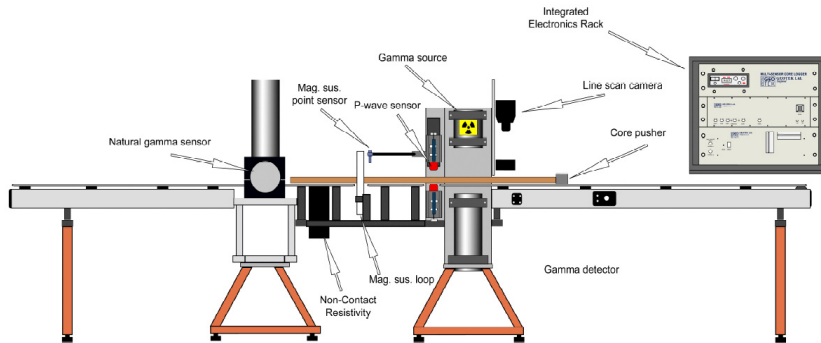
Fig. 3.2: A typical MSCL split/whole core configuration for soft sediments, from MSCL manual, 2000.

3.2.1.1 Gamma-ray attenuation

Gamma photons sent through the core are scattered by electrons inside the core. The loss of energy in the beam is therefore related to the core thickness and the electron density in the sediments. From the gamma-ray attenuation, the bulk density of the sediments can be calculated.

3.2.1.2 P-wave velocity

The travel time of an ultrasonic pulse travelling through the sediments in the liner is measured. From this travel time the p-wave velocity can be calculated. For measuring the p-

wave velocity it is important that there is a good coupling between the core liner and the sediments.

3.2.1.3 P-wave amplitude

The p-wave amplitude measures the intensity of the p-wave pulse at the receiver. This intensity can provide information about the contact between the sediments and the liner. A bad contact between the sediments and the liner gives low values and a good contact gives high values. The p-wave amplitude values may also give information about the porosity of the sediments. The lower the p-wave amplitude value, the higher the porosity.

3.2.1.4 Core thickness

The core thickness is measured with a reference to a known thickness. The deviation from that thickness is recorded.

3.2.1.5 Magnetic susceptibility

The magnetic susceptibility is measured with a loop sensor before opening of the core. Any material with a magnetic susceptibility that comes near to the sensor will cause a change in the oscillatory frequency of the magnetic field in the loop sensor. This frequency information is converted into magnetic susceptibility values.

After the splitting of the cores, the magnetic susceptibility was measured with a point sensor. The magnetic susceptibility measured with the point sensor has a better spatial resolution then measured with the magnetic field in the loop. The loop is however more sensitive. It works according to the same principle as the loop sensor. The point sensor measurements for JM02-979-GC and JM97-943-GC were carried out automatically with an interval of 1 cm.

Due to a malfunction in the point sensor, the magnetic susceptibility of core JM97-941-GC was measured by hand. The intervals were determined according to the lamination of the core and consisted of 0.5 or 1 centimetre.

3.2.1.6 Acoustic impedance

The acoustic impedance is the product of P-wave velocity and density and is calculated after the measurements.

3.2.1.7 Fractional porosity

The fractional porosity (FP) can be calculated from the bulk density (BD) if the following can be assumed:

a) The sediment is fully saturated (this can be water, air or other material)

b) The mineral grain density (MGD) is known

c) The fluid density (FD) is known

FP = (MGD-BD) / (MGD-FD)

3.2.1.8 Colour images
The colour images were taken with a Geoscan colour line scan digital camera. The images consist of 25 separate images per meter section, put together as a whole afterwards.

3.2.2 Logging of the cores
The cores were split lengthwise into two equal parts with a circular saw. The sediments were split with an osmotic knife. One half of the split core, the archive part, was sealed in plastic and stored in a cold storage room. The other half, the working half, was used for taking radiographs. Radiographs show the difference in absorption of x-rays by different densities in the sediments. Sediments or clasts with a high density appear lighter than objects with a lower density. The radiographs were studied for structures, clasts and shells in the sediments.

The structures and the sediments on the surface of the working half were logged, and the colours were determined using the Munsell Colour Charts.

The undrained shear strengths of the cores were not measured because parts of the core were dry.

3.2.3 Samples
Samples from all three cores were taken. From core JM97-941-GC, 29 samples were taken. These samples were taken approximately every 20 cm. From core JM02-979-GC, 7 samples were taken and 25 samples were taken from core JM97-943-GC. The sampling depths in JM97-943-GC and JM02-979-GC were depended on the lithological variations with the purpose of giving a good representation of the various litological units. The samples were put into small petri-dishes and were frozen. All the in total 61 samples were dried in a freeze-dryer (Alpha-1-4, Christ). In a freeze-dryer, the samples are frozen in a vacuum. During the drying process, the water in the samples sublimates from ice into vapour (Brukermanual frysetørkning, UITØ, 2007).

The samples were not weighed before they were dried to calculate the water content because of the age of the cores.

3.2.4 XRD

X-ray diffraction (XRD) measurements were performed by Dr. Christoph Vogt at the Central Laboratory of Crystallography and Applied Material Sciences (ZEKAM), University of Bremen. Powder X-ray diffraction analysis was performed using an X'Pert Pro MD, Cu-radiation and X'Celerator detector system. The settings used were a 1/4° fixed divergence slit with a first angle of 3° 2 theta and a last angle of 85° 2 theta and a step size of 0.016° 2 theta. The calculated time per step was 100 s.

Quantification of the mineral content was carried out with QUAX (for further information see Vogt et al., 2002). Before measuring the sediments were grounded to a fine powder.

The XRD measurements give specific information on the mineral content of a sediment sample. The sediment compositions of the samples can assist in the reconstruction of the sediment transport pathways, and the sedimentary environment of the fjord (Vogt et al. 2002). The mineral contents in the samples are expressed as percentages of the bulk material.

3.2.5 Sieving

The samples were sieved for the grain-size distribution analysis. To separate the particles, the samples were put into glasses partly filled with water and shaken for approximately one hour. Afterwards the samples were wet-sieved, in order to separate the finest fraction (<0.063 mm) from the rest of the sediments. The material coarser than 63 μm was first dried on a hotplate, weighed and dry sieved afterwards. For the dry sieving the following sieves were used: 0.063 mm, 0.125 mm, 0.250 mm, 0.50 mm, 1.0 mm and 2.0 mm. The different fractions were weighed and stored in small glass pots.

From the weight of the different fractions and the total weight of the sample, the weight percentages for the different fraction were calculated.

The fraction <63 μm was dried in a drying cupboard, then weighed and subsequently used for sedigraph and Leco measurements.

3.2.6 Sedigraph

The material finer than 0.063 mm was analysed with a sedigraph (Micromeritics Sedigraph 5100) in order to determine the silt and clay fraction. In the sedigraph, samples in suspension are x-rayed. The time it takes for a grain to sink can be used to determine its size. The percentage of silt or clay can be calculated from the amount of x-rays arriving at the detector (Sedigraf brukermanual UITØ, 2001).

3.2.7 Leco (TC, TOC & CaCO₃)

The total carbon content (TC) and total organic carbon content (TOC) of the finest fraction (< 63 μm) were determined with a Leco carbon analyser (LECO CS-200). The Leco carbon analyser uses infrared absorption to measure the quantities of carbondioxide (and sulphurdioxide) generated by the burning of the sample in an induction furnace in a pure oxygen environment.

During the burning process, the carbon is released and reacts with the oxygen to form CO and CO_2. Carbon dioxide absorbs infrared energy of a known wavelength. The reduction of the amount of infrared energy reaching the detector is a measure of the concentration of CO_2 in the sample. Before measuring the organic carbon (TOC), the samples were treated with HCL (Leco user manual).

The percentage of $CaCO_3$ in the samples was calculated using the formula:

$$CaCO_3 = (TC - TOC) * (100/12)$$

100/12 represents the ratio of the relative atomic masses of $CaCO_3$ and C.

3.2.8 Radiocarbon dating

Radiocarbon dating uses ^{14}C to date carbonaceous materials. ^{14}C is produced in the atmosphere by the impact of cosmic rays on nitrogen. It is an unstable isotope and starts to decay immediately after the death of the organism that incorporated the ^{14}C into its skeleton. The half-life of ^{14}C is 5570 years (Stuiver & Polach, 1977). The ratio of the unstable isotope ^{14}C to the stable isotope ^{12}C is used to calculate the age of the sample. Seven samples from core JM97-943-GC were prepared at the Laboratory of Radiometric Dating in Trondheim, Norway. They have been dated with the AMS (Accelerator Mass Spectrometry) method in the Ångstrøm laboratory in Uppsala, Sweden. In this method all the ^{14}C atoms can be counted directly, rather then only the ones decaying during a certain time interval as with the conventional method.

Because the samples were retrieved from marine sediments, they had to be corrected for the reservoir age of 440 years (Mangerud and Gulliksen, 1975). The radiocarbon ages are reported as ^{14}C yrs BP.

The production of ^{14}C in the atmosphere has not been constant over time. It is therefore not possible to simply calculate the calendar age of a radiocarbon dated sample. Fluctuations in the atmospheric ^{14}C have been largely produced by changes in the solar magnetic field,

producing positive ^{14}C anomalies during intervals of a weaker geomagnetic field. The radiocarbon ages therefore have to be calibrated. Dendrochronology is used for calibration. The tree rings are dated and can be counted back in time. This method can be used to 11,857 cal BP. The Uranium-thorium (U-Th) dating of corals extends the calendar age range for radiocarbon dating to 24,000 cal BP (from Stuiver et al., 1998).

All the radiocarbon ages in this study have been calibrated using the software *Calib Rev 5.0.2* (Stuiver & Reimer, 1993). A Δ R and a Δ R uncertainty of 99 ± 39 have been used. This value is a local average and was determined with the ^{14}Crono marine reservoir database (http://calib.qub.ac.uk/marine). The marine dataset used was *marine 04.14C* by Hughen et al. (2004).

3.3 Accoustic data

3.3.1 Swath bathymetry

The multibeam data was collected with R/V Jan Mayen using a *Kongsberg Maritime Simrad EM 300 multibeam echo sounder.* This is a hull-mounted system with up to 135 beams. It can be used to map the seafloor between 10 and 5000 m depth. The nominal operational frequency is 30 kHz with an angular coverage sector of up to 150º. Pulse length and sampling rate are variable with depth for the best resolution. The ping rate goes up to 10 Hz and is corrected in real time for the effects of sound speed and vessel attitude (Kongsberg, 2003).

The first part of the multibeam data survey was carried out in the summer of 2005. This was most of the data inside of the fjord. In the summer 2006 some data was added to the sides in the fjord and the dataset was extended into the inner parts of Isfjorden. In this thesis only the data from inside the fjord will be used (Fig. 3.1).

After acquisition, data cleaning and processing was performed using the post-processing system *Neptune* version 4.1.2. Gridding and visualising of the results has been carried out in *GMT* (*The Generic Mapping Tools, http://gmt.soest.hawaii.edu*). The program *Fledermaus 6.4* was also used for visualising.

3.3.2 Seismic data

High-resolution seismic profiles oriented approximately parallel and perpendicular to the axis of the fjord were taken in 1997 and 2002 with R/V Jan Mayen (Fig 3.1). The seismic lines from 1997 were collected with a 3.5 kHz echo sounder (10 kW hull-mounted echo sounder with a bandpass-filter setting 3-5 kHz) and a sparker (700 j Bennex multi-electrode sparker with a bandpass-filter setting 500-2000 Hz). The lines taken in 2002 were taken with a 3.5 kHz echo sounder and a boomer (300 J O.R.E model 5813A with a bandpass-filter setting 300-1500 Hz).

For the digital interpretation of the seismic data *Kingdom Software* from *Seismic Micro-Technology Inc.* (version 7.4 and 7.5) were used.

For plotting the cores in the seismic profiles, a p-wave velocity of 1600 m/s was used. This value has been suggested for Holocene sediments from the Isfjorden area (Elverhøi et al., 1995B; Plassen et al., 2004).

4. Multibeam data

4.1 Large scale bathymetry

The swath bathymetry data analysed in this study is shown in figure 4.1. The data shows the imprint of glacial activity in the fjord, but also tectonic activity, like the Billefjorden fault zone. Very shallow and deep areas are associated with this fault zone. The height difference between the highest and lowest point in the fault zone is about 80 m (Profile A, Fig. 4.2). Two comparatively large basins occur in the mouth of the fjord and in the inner part of the fjord. A less pronounced basin occurs in the central part of the fjord. The innermost part of the fjord is characterized by a bedrock terrace changing into a deep basin, defined by a break in the slope. The difference in height between the bedrock terrace and the basin is around 80 meters (Profile C, Fig. 4.5).

Both in the inner part of the fjord and in the central part of the fjord linear features perpendicular and parallel to the ford axis can be distinguished. On the eastern side several lobe shape deposits come down from the steep fjord side walls. In the shallow area in the north-west and eastern part of the fjord, chaotically oriented slightly elongated depressions occur. In the central part of the fjord, especially within some of the linear features parallel to the fjord axis, circular depressions were identified. The mouth of the fjord is characterised by significant variations in water depth. Large parts were too shallow to sail over by boat, therefore data is lacking here. The above mentioned morphological features are discussed in more detail below.
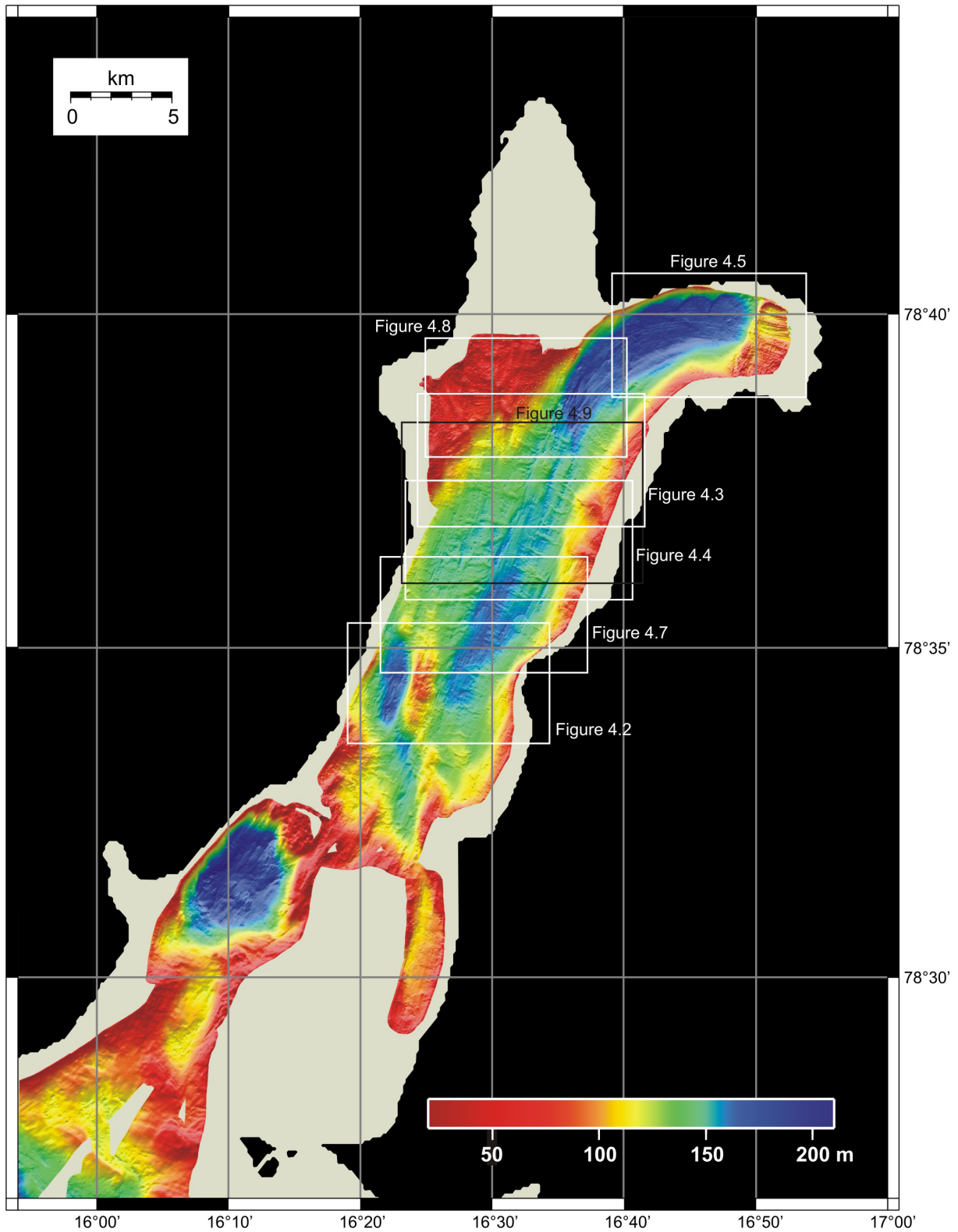
Fig. 4.1: Swath bathymetry dataset of Billefjorden going out into Isfjorden. The indicated areas are shown and discussed in more detail below.
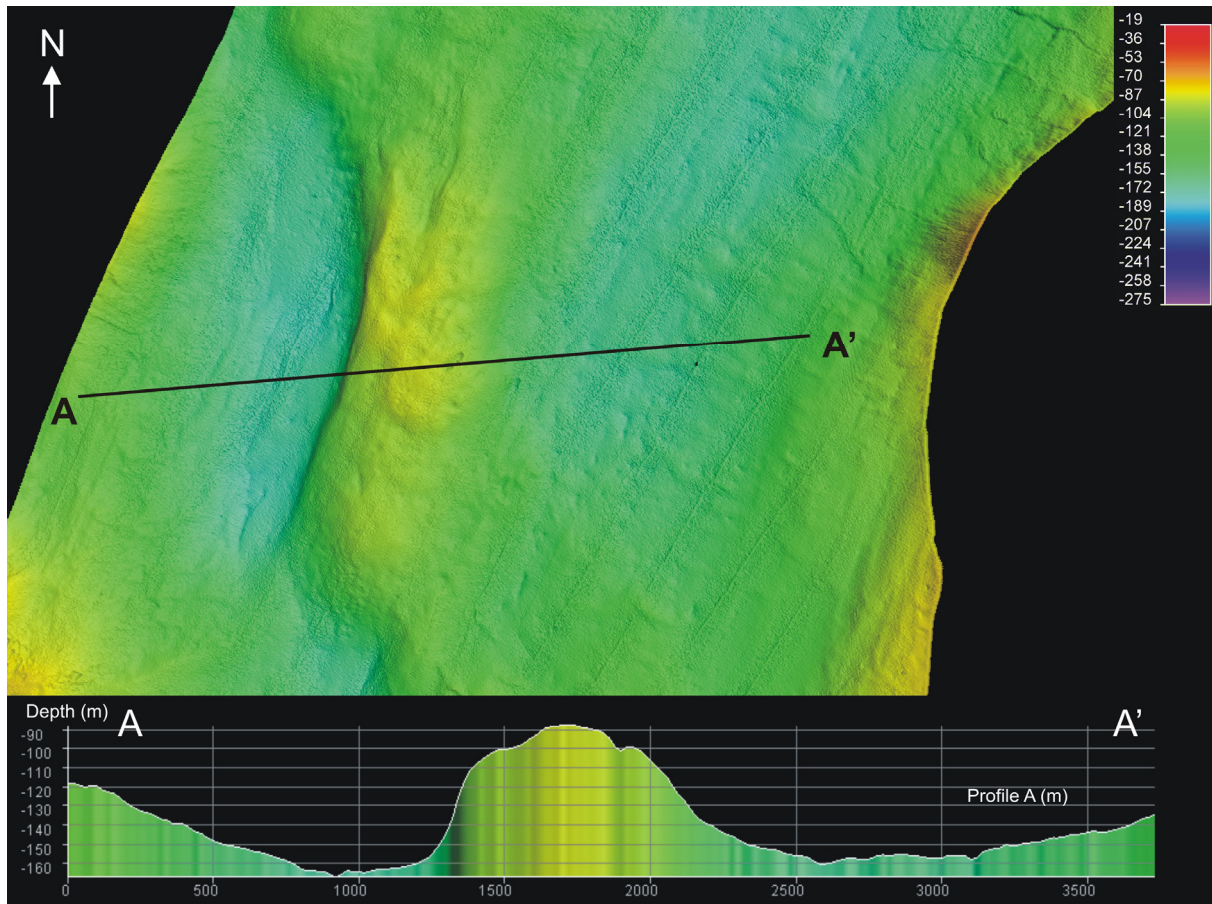
Fig. 4.2: Swath bathymetry data zoom up and profile, for location see figure 4.1. The profile shows the topography of the Billefjorden Fault Zone running through the fjord.

4.2 Glacial linear features

Profile B (Fig. 4.3) shows two linear features running parallel to the direction of glacier flow in the central part of the fjord. The linear features in profile B have a vertical relief of up to 6 m and are approximately 300 m wide. They are not very sharp outlined and are therefore assumed to have been covered with sediment. Most of the linear features are suggested to be glacial lineations. Glacial lineations are elongated ridges and grooves oriented parallel to ice flow (Clark, 1994), and are often associated with high velocity glacier flow (Ottesen & Dowdeswell, 2006). However, a few linear features observed in the north-western part of the fjord are suggested to be crag and tail features because of the 'tails' behind possibly more resistant small shallow obstacles of bedrock (Fig. 4.4; Benn & Evans, 1998). A few larger features with a teardrop shape are suggested to be drumlins (Fig. 4.4; Benn & Evans, 1998). Similar shaped features with corresponding sizes were found in Kongsfjorden (Howe et al., 2003). Because the maximum glacier extent during the Holocene was at the edge of the

bedrock terrace during the Neoglacial maximum (Plassen et al., 2004), the linear features in the central part of the fjord are suggested to have been deposited during the Last Glacial. The orientation of these linear features indicates that, during the time of their deposition, the ice was coming from at least two different directions (Fig. 4.4).

Profile B in figure 4.5 shows linear features parallel to the direction of glacier flow in the inner part of the fjord. The linear features have a vertical relief of up to 14 m. They are up to 300 m wide and their length exceeds 500 m. Their absolute extent cannot be calculated due to a limited extend of the dataset. Because of the fact that they look very sharply outlined (in comparison to the linear features in the central part of the fjord), and were deposited within the area of maximum Neoglacial ice extent, they were interpreted to have been formed during the Neoglacial glacier advance.
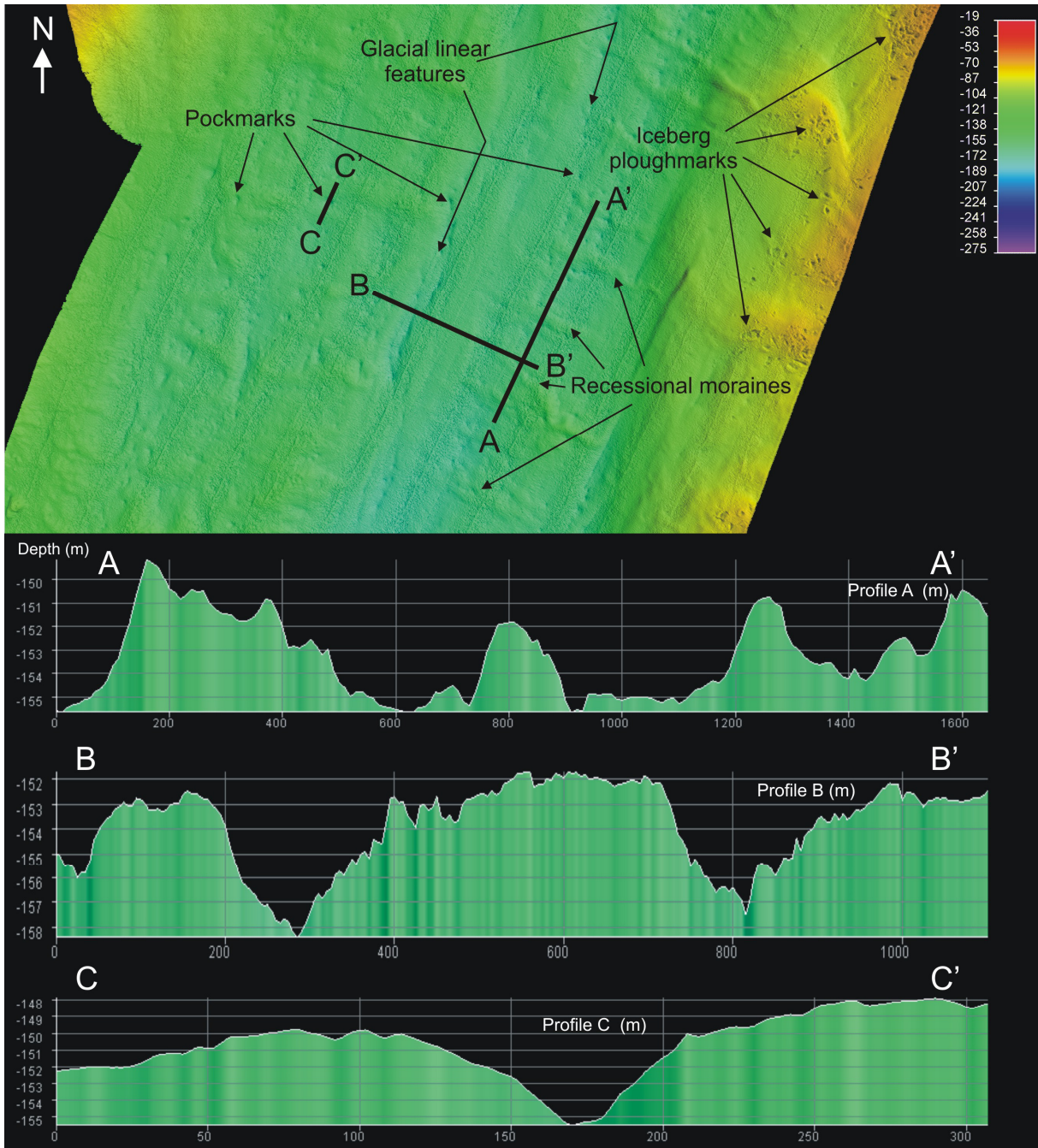
Fig. 4.3: Swath bathymetry data and profiles of the central part of Billefjorden, for location see figure 4.1. Profile A shows moraines orientated perpendicular to the fjord axis, profile B shows glacial linear features orientated parallel to the fjord axis, profile C shows the topography of a pockmark. Iceberg plough marks are indicated in east.
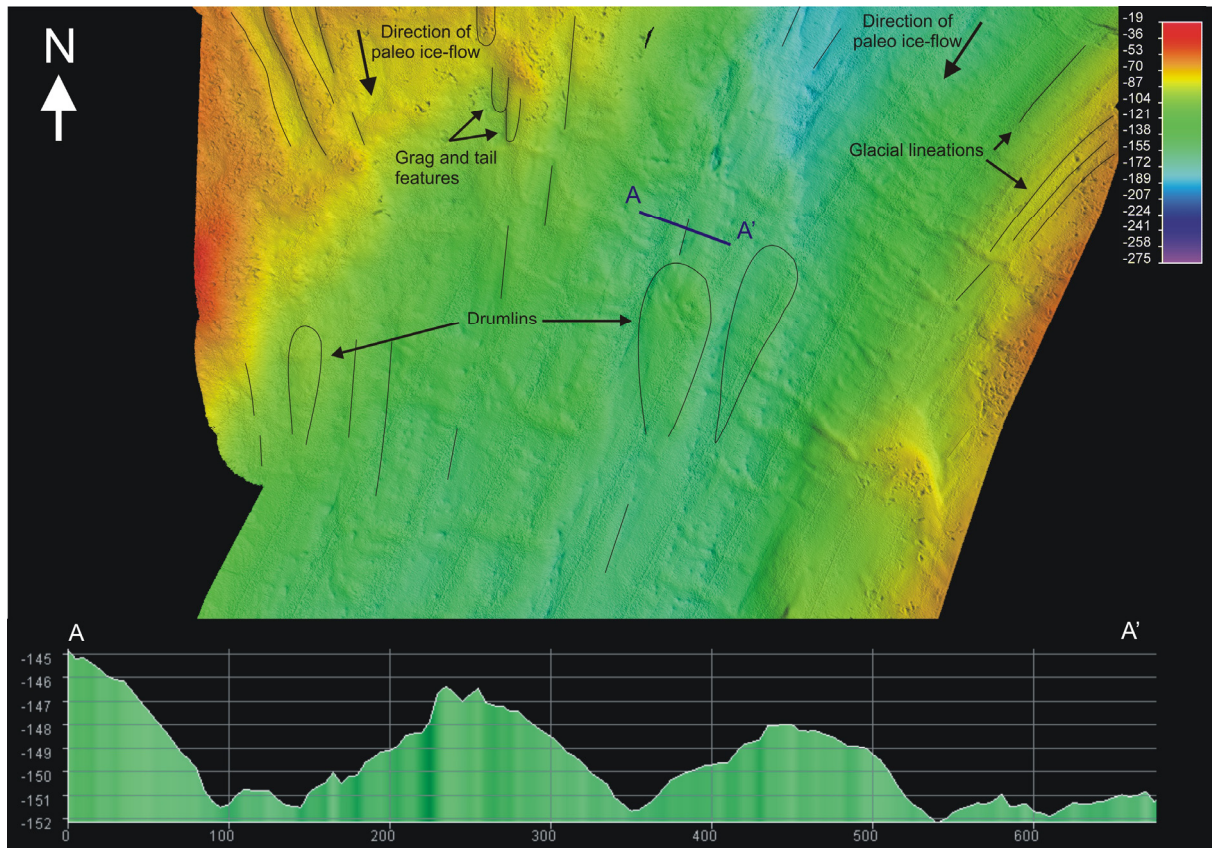
Fig. 4.4: Glacial linear features in the central part of the fjord. Paleo ice-flow directions, crag and tail features, glacial lineations and drumlins are indicated. Profile A displays the morphology of some glacial linear features.
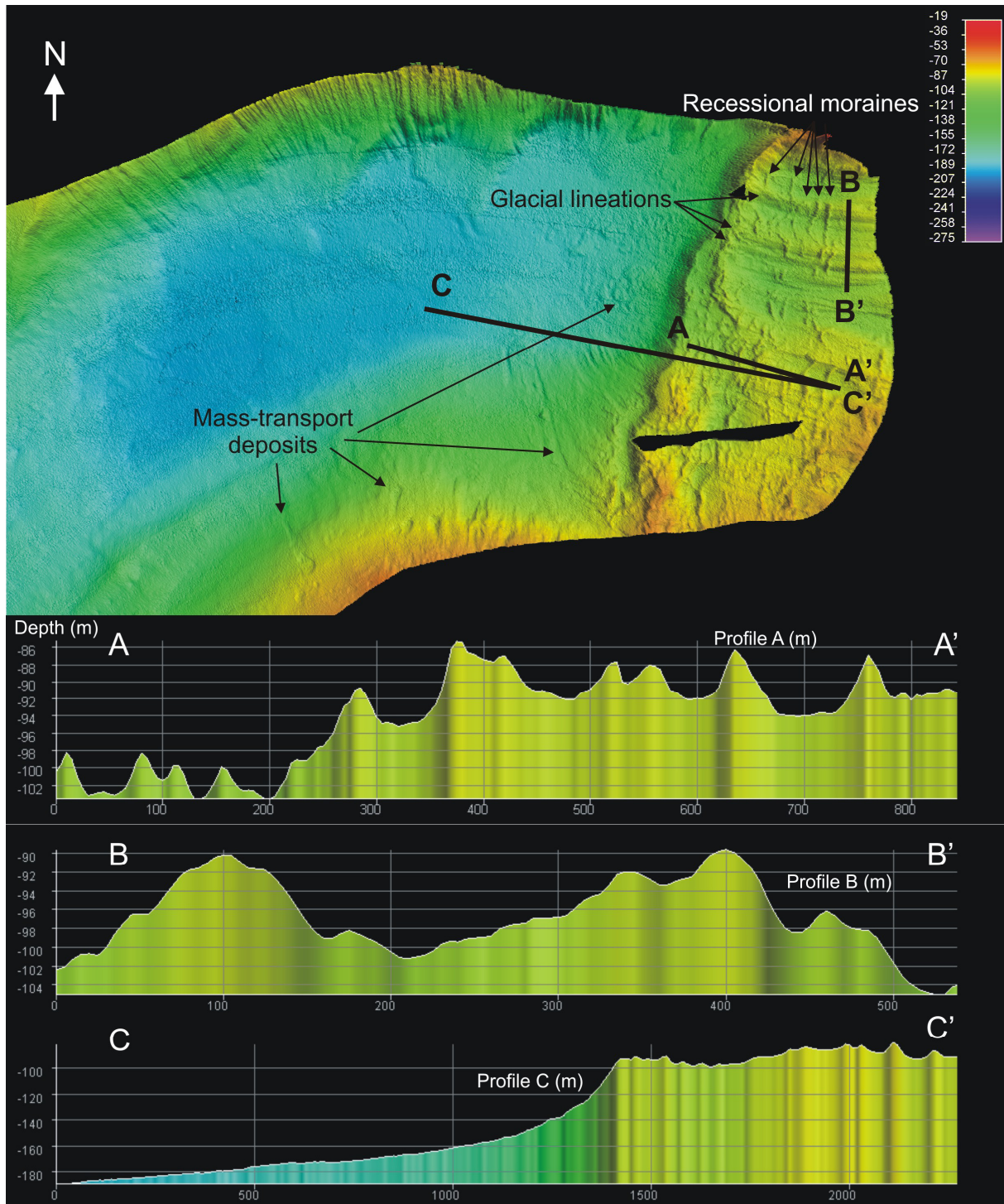
Fig. 4.5: Swath bathymetry data and profiles from the innermost part of the fjord, for location see figure 4.1. Profile A shows the moraines on the bedrock terrace running perpendicular to the direction of glacier flow. Profile B shows the lineations parallel to the direction of glacier flow. And profile C shows the topography of the bedrock terrace changing into a deep basin. Mass-transport deposits are indicated.

4.3 Moraines

Figure 4.3A shows some ridges perpendicular to the fjord axis. The ridges in the profile are between 4 and 6 m high and 200 to 600 m wide. Like the glacial linear features in the central part of the fjord, they are not very sharp outlined and are therefore assumed to have been covered by a sediment package. They superpose the glacial linear features described in chapter 4.2 and are assumed to be younger. The ridges were therefore interpreted as recessional moraines, probably formed during halts or minor readvances within a period of general glacier retreat after the Last Glacial. Annual retreat moraines are produced during a late winter readvance, followed by a summer retreat (Boulton, 1986). Whether these recessional moraines are annual cannot be concluded, since no record of glacier front positions exists this far out into the fjord.

Figure 4.5A shows the topography of some transverse ridges in the inner part of the fjord. The height of these ridges ranges between 2 and 8 m, and they are up to 100 m long. The transverse ridges clearly overprint the glacial lineations described in chapter 4.2 and are therefore assumed to be younger. The position of the glacier front in 1896 and 1908 has been documented to be on the edge of the bedrock terrace (De Geer, 1910; Fig. 4.6). These positions correspond to the crest of the ice-marginal deposit mapped by Plassen et al. (2004). This ice marginal deposit have been interpreted as the terminal moraine deposited during the Neoglacial maximum around 1900 AD (Plassen et al., 2004). The transverse ridges occur within the area of the maximum Neoglacial extent, and are therefore interpreted to be recessional moraines deposited during retreat of the glacier most likely after the Neoglacial maximum.
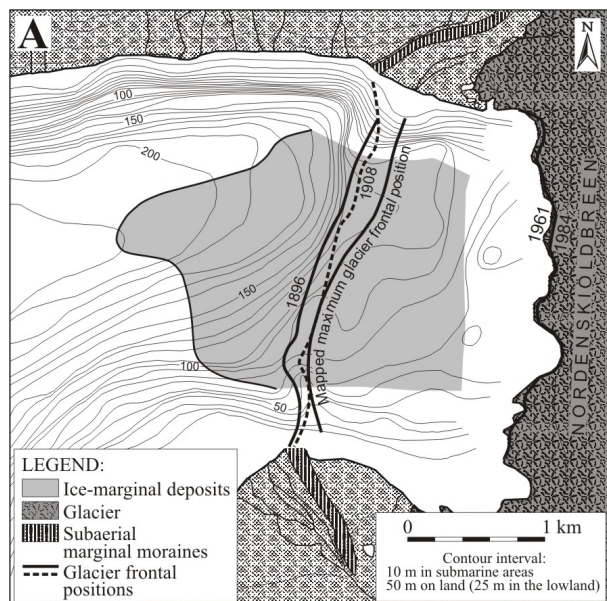
Fig. 4.6 Map of inner Billefjorden showing the lateral distribution of ice-marginal deposits and previously documented frontal positions of Nordenskiöldbreen (in years AD; from Plassen et al., 2004).

4.4 Mass-transport deposits

Several mass-transport deposits occur on eastern side of the fjord. In figure 4.7 two mass-transport deposit coming from the fjord side are indicated. Profile A show the incision on the upper part of the slope and profile B the sediment lobe on the fjord bottom.

The depth of the incision shown in profile A (Fig. 4.7) is 7 to 8 meter. The sediment lobe in profile B (Fig. 4.7) reaches a thickness of 6 to 7 meter. The surface of the lobe is rugged. The resolution of the data is not high enough to determine whether this rugged surface is because of different smaller sediment lobes or channels. The other mass-transport deposit indicated in figure 4.6 does not show an incision in the upper part of the slope, and has a different overall shape. Other mass-transport deposits are indicated in figure 4.5. The two on the southern fjord slopes are comparatively small and do not show any lobe deposits. The mass-transport deposits coming down from the bedrock terrace were earlier described by Plassen et al. (2004) and interpreted as a debris flow.

Slope failures in fjords are in general controlled by the topography, the supply of material, the physical properties of the sediments and the triggering mechanism. Triggering mechanisms include sediment loading, earthquakes, sea level fluctuations, climate change and anthropogenic activity (Syvitski et al., 1987). The mass-transport deposits (Fig. 4.7) are situated close to a delta at Kapp Ekholm (Fig. 2.1). Side-entry deltas are sites of intermittent slides and slumps where the frequency is related to the development of oversteepened slopes

(Syvitski et al., 1987). This could have been a reason for the mass-transport deposits to have been triggered at this specific location.
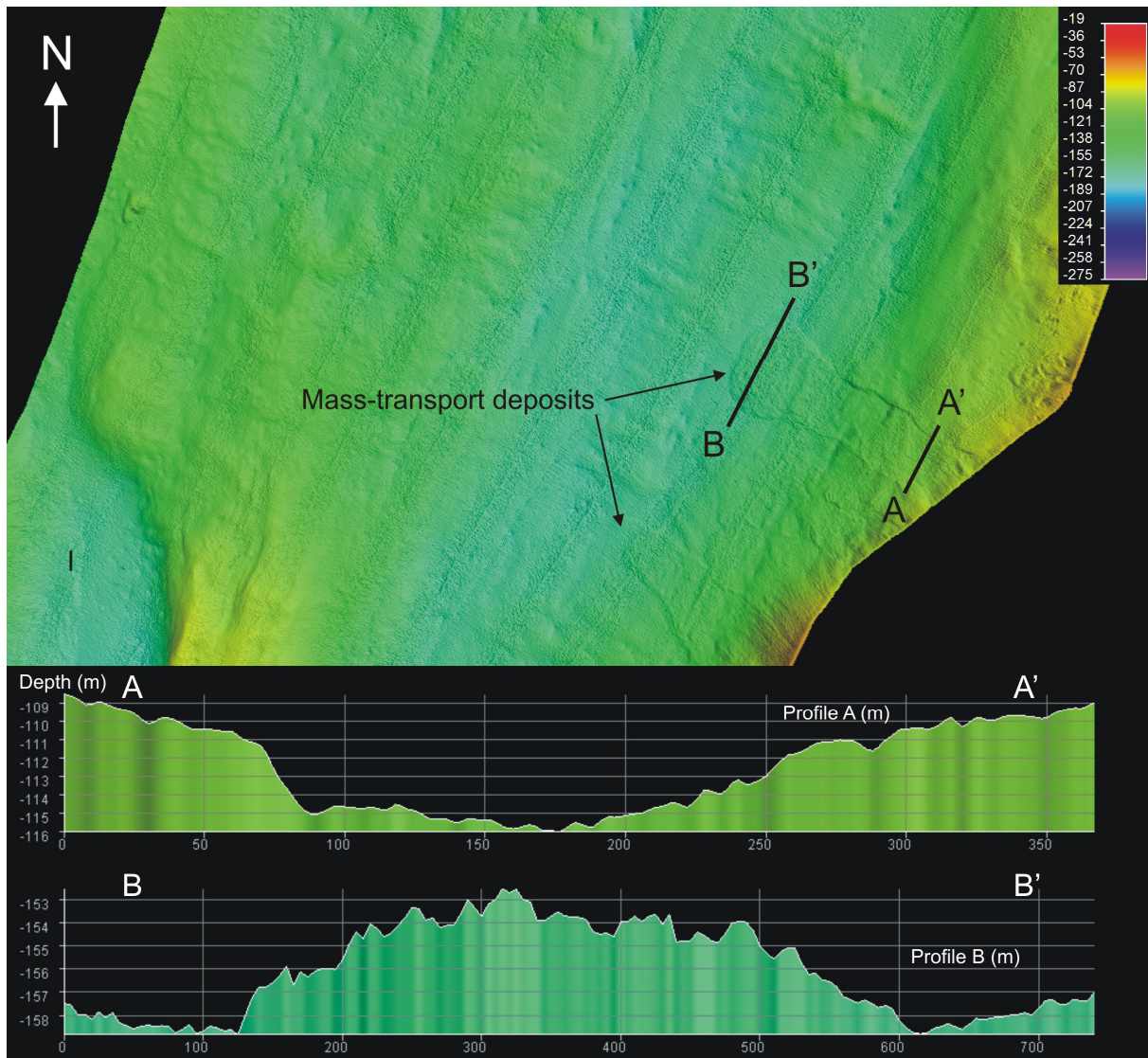
Fig. 4.7: Swath bathymetry data and profiles of the central part of Billefjorden, for location see figure 4.1. Both profiles show the topography of the mass-transport deposit. Profile A shows an incision on the upper part of the slope and profile B shows the deposition of the sediment lobe at on the bottom of the fjord.

4.5 Iceberg ploughmarks

Most areas between 100 and 20 m water depth are covered by slightly elongated depressions in a chaotic pattern (Fig. 4.8, also indicated on Fig. 4.3). Profile A (Fig. 4.8) shows an example of the morphology of these depressions. Their depths range from 2 to 5 meters, their widths vary between 30 and 50 meter, and they are on average 30-80 meter long. These

depressions were interpreted as iceberg ploughmarks because of their presence in shallow areas and chaotic pattern and orientation. Similar sized features (a few meters deep and tens of metres wide) on the shelf off Antarctica were interpreted as formed by grounding ice bergs (Barnes & Lien, 1988). The depressions look sharply outlined on the multibeam data. This could indicate that these features are comparatively young. The icebergs most probably came from the glacier Nordenskiöldbreen.
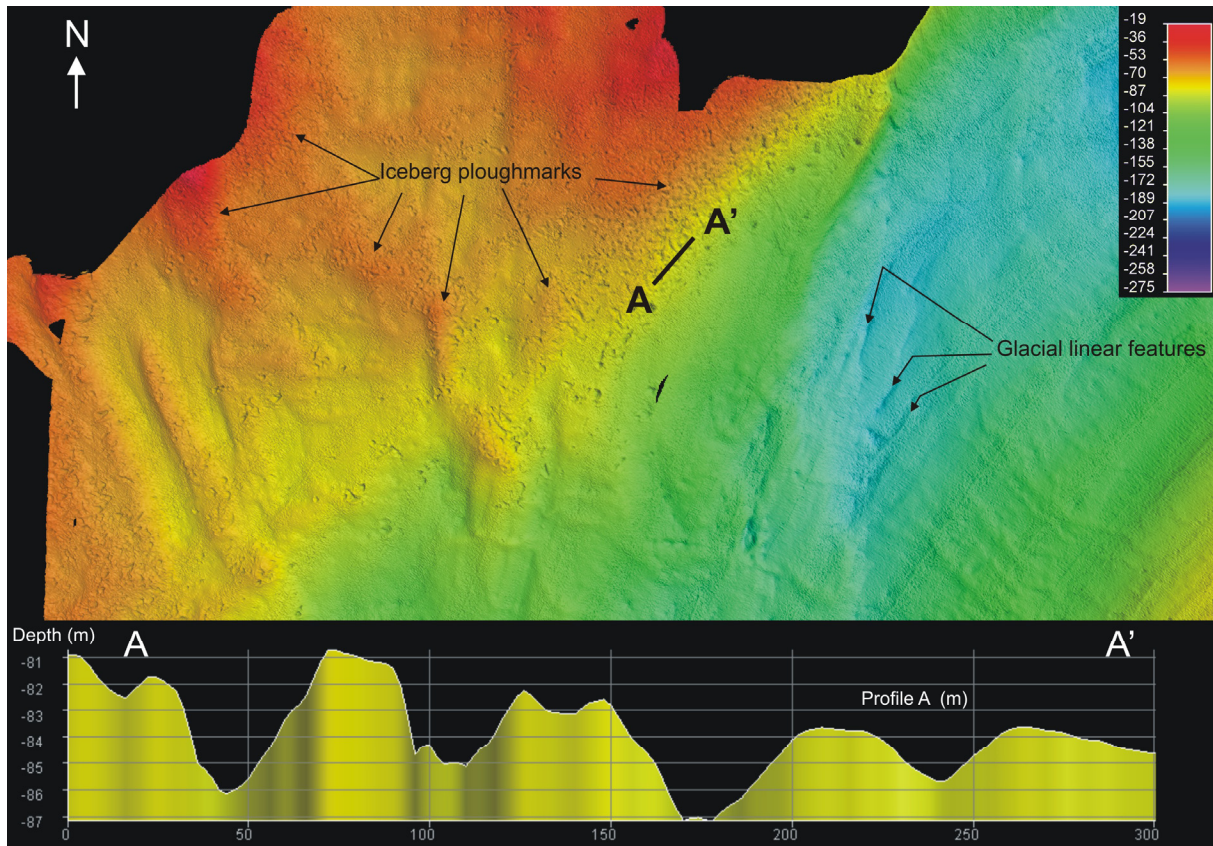
Fig. 4.8: Swath bathymetry data and profiles the northern part of Billefjorden, for location see figure 4.1. The profile shows the morphology of iceberg ploughmarks. Glacial liniations are also indicated.

4.6 Pockmarks

Pockmarks occur in the central part of the fjord. The pockmarks are relatively sharply outlined and occur at depths between 125 and 175 m. Most of them are linearly aligned and occur within the elongated grooves interpreted as glacial liniations (Fig. 4.9). A couple of pockmarks align in a more N-S direction. Profile C (Fig. 4.3) was taken over a pockmark. The pockmark in profile C has a diameter of about 140 m and is 5 to 6 m deep. Most of the pockmarks in the area are however smaller than this one. Pockmarks are defined as roughly

conical depressions formed by the escape of natural gas or interstitial water from muddy, unconsolidated sediments (Hovland and Judd, 1988; Judd and Hovland, 1992).
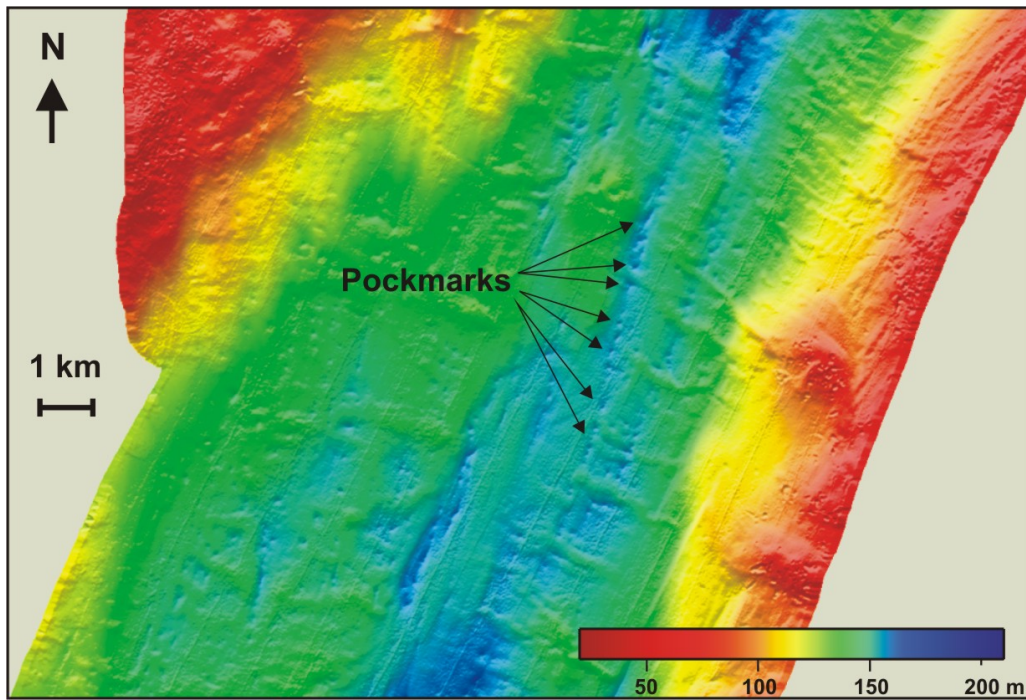
Fig. 4.9: Swath bathymetry data , showing the morphology of aligned pockmarks in more detail. For location see figure 4.1.

5. Sediment cores

Three sediment cores; JM02-979-GC, JM97-941-GC and JM97-943-GC have been analysed. Core JM02-979-GC was retrieved from the slope off Nordenskiöldbreen, core JM97-941-GC from the large basin in the inner part of the fjord and core JM97-943-GC from the central part of the fjord. Their positions are shown in Figure 3.1. Boundaries between the lithological units within the cores are defined by changes in grain-size, sediment colour and physical properties. The different units are be described in detail below.

5.1 JM02-979-GC

Core JM02-979-GC was retrieved in front of Nordenskiöldbreen (Fig. 3.1). It penetrates a sediment lobe deposited during the Neoglacial (Plassen et al., 2004).

5.1.1 Unit 979-A (110-116 cm)
The lowermost unit of this core has a matrix of sandy mud and contains comparatively many clasts, up to 2 cm in diameter (Fig. 5.1). Its upper boundary is defined by an erosional surface. The sediment colour is greyish brown (Munsell code 10YR 5/2). The unit does not seem to have any internal structures on the x-ray pictures (Fig. 5.2). The sediments are characterised by comparatively high bulk density, acoustic impedance and p-wave velocity values, and low p-wave amplitude, fractional porosity and magnetic susceptibility (Fig. 5.3). These high and low values change at the upper boundary of the unit. The magnetic susceptibility (MS) measured with the loop sensor is low at the base of the core because it also measures air there, towards the top of the unit the values increase. The TC and TOC contents (Fig. 5.4) are rather low in this unit, while the $CaCO_3$ values are comparatively high throughout the whole core. No trend can be observed because only one sample was taken in this unit. The unit contains some shell fragments.

5.1.2 Unit 979-B (100-110 cm)
This unit is grading from coarser to finer sand, to muddy sand in the top. The grain-size distribution diagram (Fig. 5.1) shows that it mostly consists of sand, with up to 0.5 % of gravel. Both boundaries of this unit are irregular and probably erosive (Fig. 5.2). The colour

of the sediments are greyish brown (Munsell code 10 YR 5/2). The bulk density, acoustic impedance and p-wave velocity (Fig. 5.3) are lower than in the underlying unit, but still higher then in the overlying unit. The P-wave amplitude, fractional porosity and the MS measured with the loop sensor are slightly higher than in the underlying unit. The majority of the physical properties remains constant or changes only slightly within the unit. However, the MS measured with the point sensor measurements show some fluctuations. Both the loop and the point sensor measurements indicate an increase in MS towards the top of the unit. The TC, TOC and $CaCO_3$ contents are lowest in this unit (Fig. 5.4). The unit does not contain any shells or shell fragments and the sediments are not bioturbated.
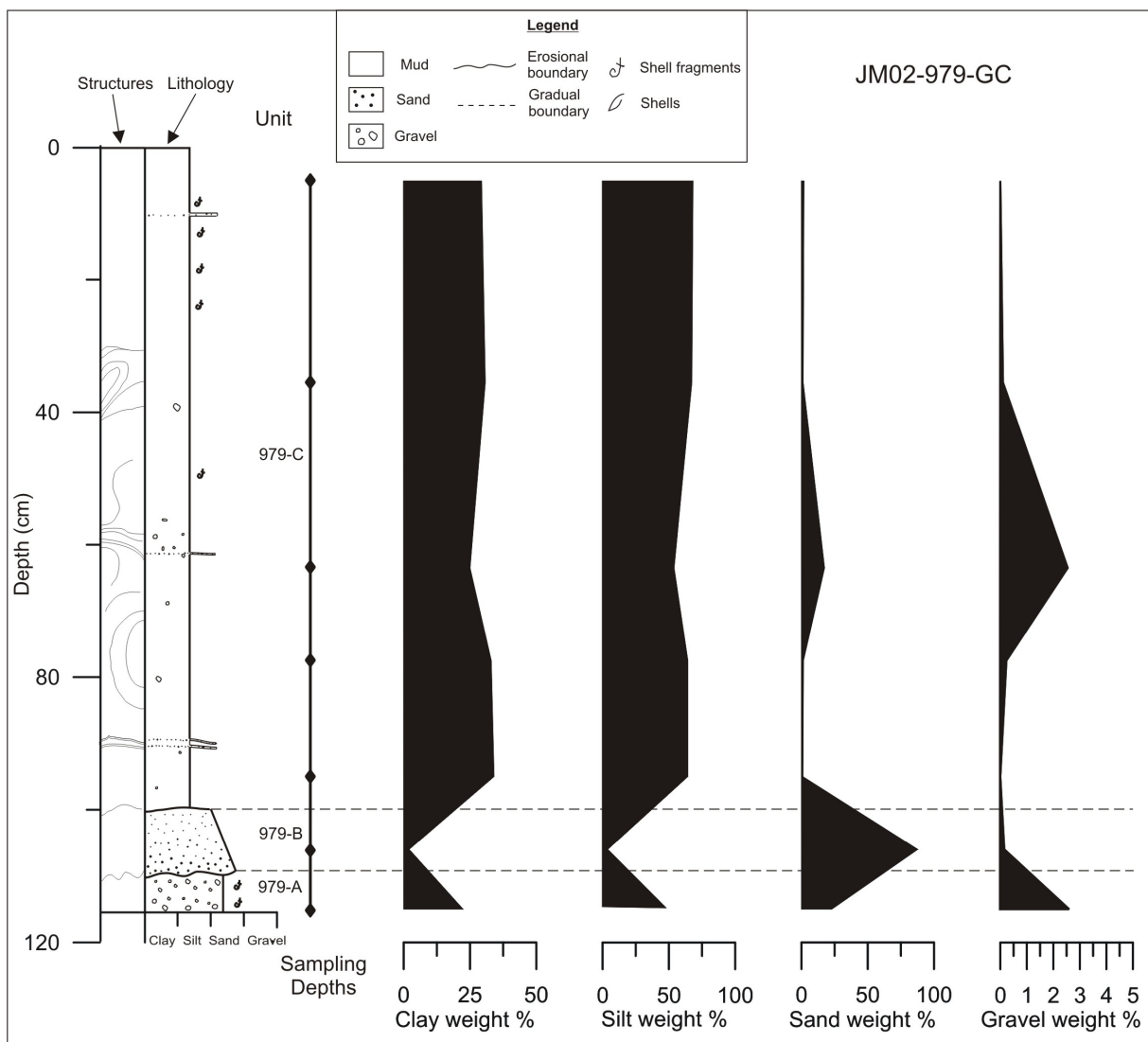
Fig. 5.1: Lithological log and the grain-size weight percentages of core JM02-979-GC
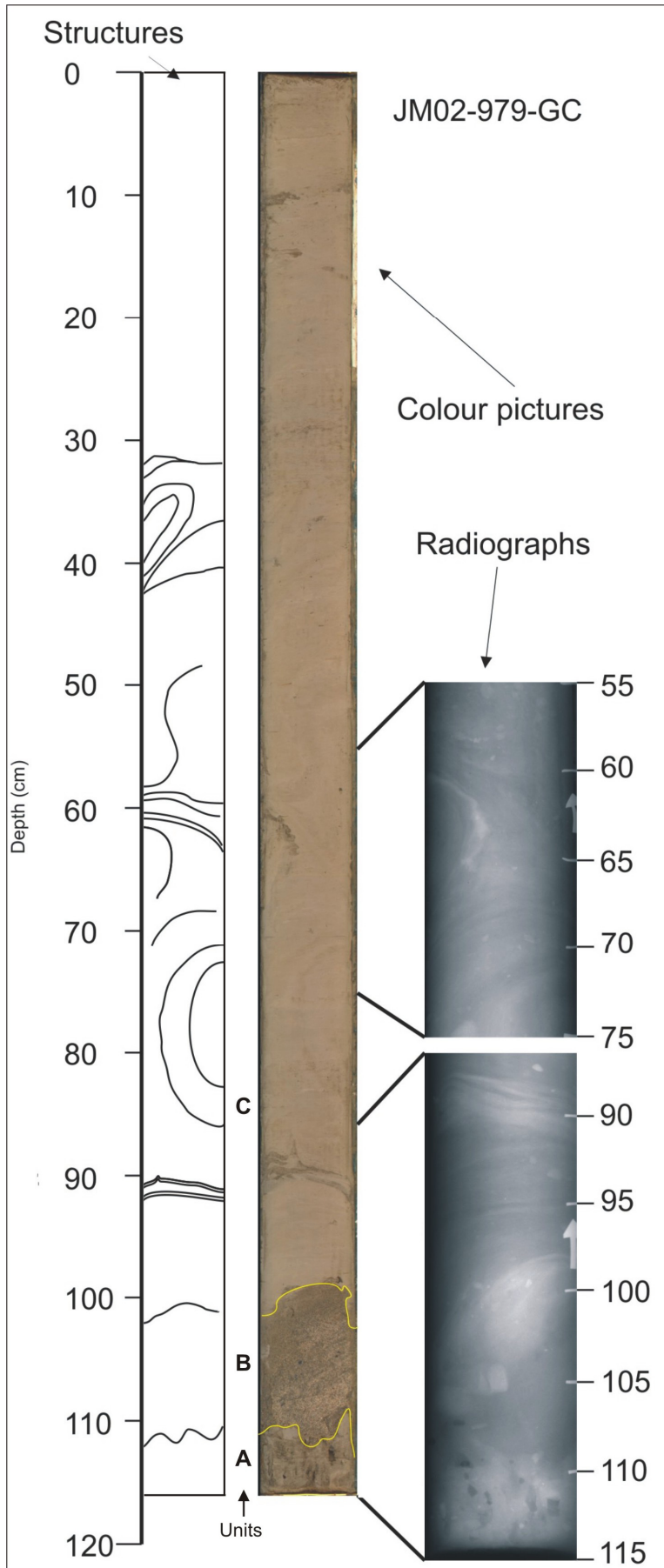
Fig. 5.2: Structures, colour picture taken with the MSCL and two radiographs of core JM02-979-GC. The yellow lines in the colour pictures indicate the unit boundaries.

5.1.3 Unit 979-C (0-100 cm)

The uppermost unit consists of mud (predominantly silt) with scattered clasts and some sandy strata (Fig. 5.1, 5.2). The colour of the sediments are greyish brown (Munsell code 10 YR 5/2). In addition to the occurrence of sandy strata, stratification can also be identified by slight colour changes. Some strata are intensely folded, as indicated on figure 5.2. Shell fragments were found between 0 and 60 cm. The physical properties (Fig. 5.3) show variation within this unit. Most variables show some change at the depth of the sandy layers. The P-wave velocity, acoustic impedance and P-wave amplitude show some spikes between 40 and 60 cm depth. The P-wave amplitude indicates if the liner is well filled with sediments. Slight changes in the TC, TOC and $CaCO_3$ contents occur; the TC is generally <2 %, TOC <0.5 % and $CaCO^3$ between 12 and 16 % (Fig. 5.4). Bioturbation occurs only in the top of the unit, where the sediments are not so strongly deformed.

5.1.3 Interpretation JM02-979-GC

979-A

The homogeneity and type of sediments found in the lowermost unit would point towards deposition in a glacimarine environment. Since this core was taken in a mass-transport deposit, the sediments were probably re-deposited.

979-B

The erosional lower boundary , the normal grading from courser to finer sand and the fact that the sediments are not bioturbated all point towards rapid deposition. The unit was interpreted as a turbidite (Middleton, 1966).

979-C

Because of the strongly deformed stratification, this unit was interpreted as a mass-transport deposit. The fact that the original stratification is deformed, but can still be detected, points towards an interpretation as a slump (Stow et al., 1996).

Fig. 5.3 Lithological log and the physical properties (MSCL) of JM02-979-GC

Fig. 5.4: Lithological log with the total carbon content (TC), total organic carbon content (TOC) and the CaCO₃ content of core JM02-979-GC.

5.2 JM97-941-GC

This core was retrieved from the basin in the inner part of the fjord (Fig. 3.1). It is 496 cm long and comprises one lithological unit.

5.2.1 Description

The colour of the sediment is light grey brownish (Munsell code between 10 YR 5/2 and 2.5 Y 5/2, Fig 5.5) almost throughout the whole core. It consists mainly of mud with sandy strata and lamina. Clasts are scattered throughout the entire core (Fig. 5.6). The sides of the core were at some places a bit oxidized and after opening the sections black mottles were visible. These black mottles disappeared after being exposed to air. The sandy strata have an erosional

lower boundary, fine upwards and are up to 4 cm thick. They occur throughout the whole core and 17 of them were counted. Thinner laminae of fine silt/sand occur very frequently. They are a few millimetres thick and do not have an erosional lower boundary (Fig. 5.5, 5.6). The granulometric composition of the beds between the sandy lamina is mainly mud. Some samples for the grain-size analyses were taken on the sandy strata and some in between the strata to give a good representation of the sediments present in the core. The physical properties of this core are very variable (Fig. 5.7). This is probably related to the stratified character of the core. The acoustic impedance and the P-wave velocity seem to follow a kind of a sea-saw pattern. The values slowly decrease towards every section top and then increase rapidly at the section boundary. All of the parameters show a considerable peak around 100 cm depth. This peak is probably caused by the fact that the core liner is less then half full around this depth, causing errors in the measurements. Due to a malfunction in the automatic settings, the magnetic susceptibility with the point sensor was measured by hand. The intervals were determined according to the stratification of the core. The TC, TOC and CaCO$_3$ contents (Fig. 5.8) fluctuate; the TC between 1 and 3, TOC < 0.4 and CaCO$_3$ between 5 and 20. All parameters increase in the uppermost 80 centimetres. The contents of all three parameters show negative excursions for the thicker sandy strata. Bioturbation only occurs in the finer sediments, not in the sandy strata.

5.2.1 Interpretation

The thicker sandy strata were interpreted as turbidites because of their erosional lower boundaries and normal grading towards finer sand in the top (Syvitski et al. 1987). They are present at irregular intervals in the core, indicating that they are most likely deposited by episodic processes (Cowan et al. 1997). The thinner sandy lamina do not have erosional lower boundaries and could have been deposited by suspension fallout of sediment laden water entering the fjord from a river entering the side of the fjord or from the glacier. Another option is that they are more distal turbidites. The variation in the magnetic susceptibility point sensor curve could point towards different sources depositing the different strata. Some of the sandy strata correlate to high magnetic susceptibility values. The clasts are most likely ice-rafted debris from icebergs or sea ice.
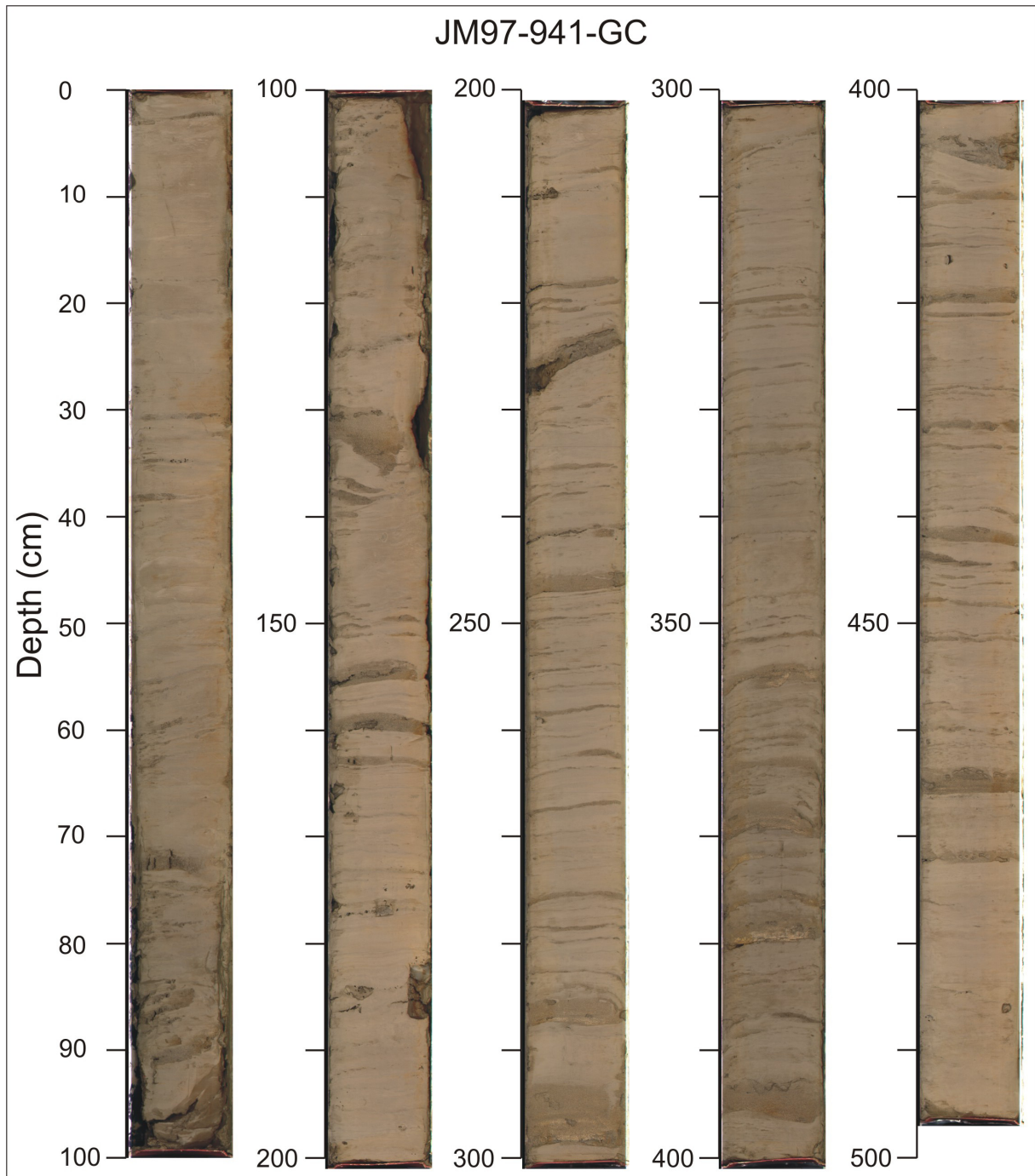
Fig. 5.5: Colour pictures of core JM97-941-GC.

Fig. 5.6: Lithological log and the grain-size weight percentages of JM97-941-GC.
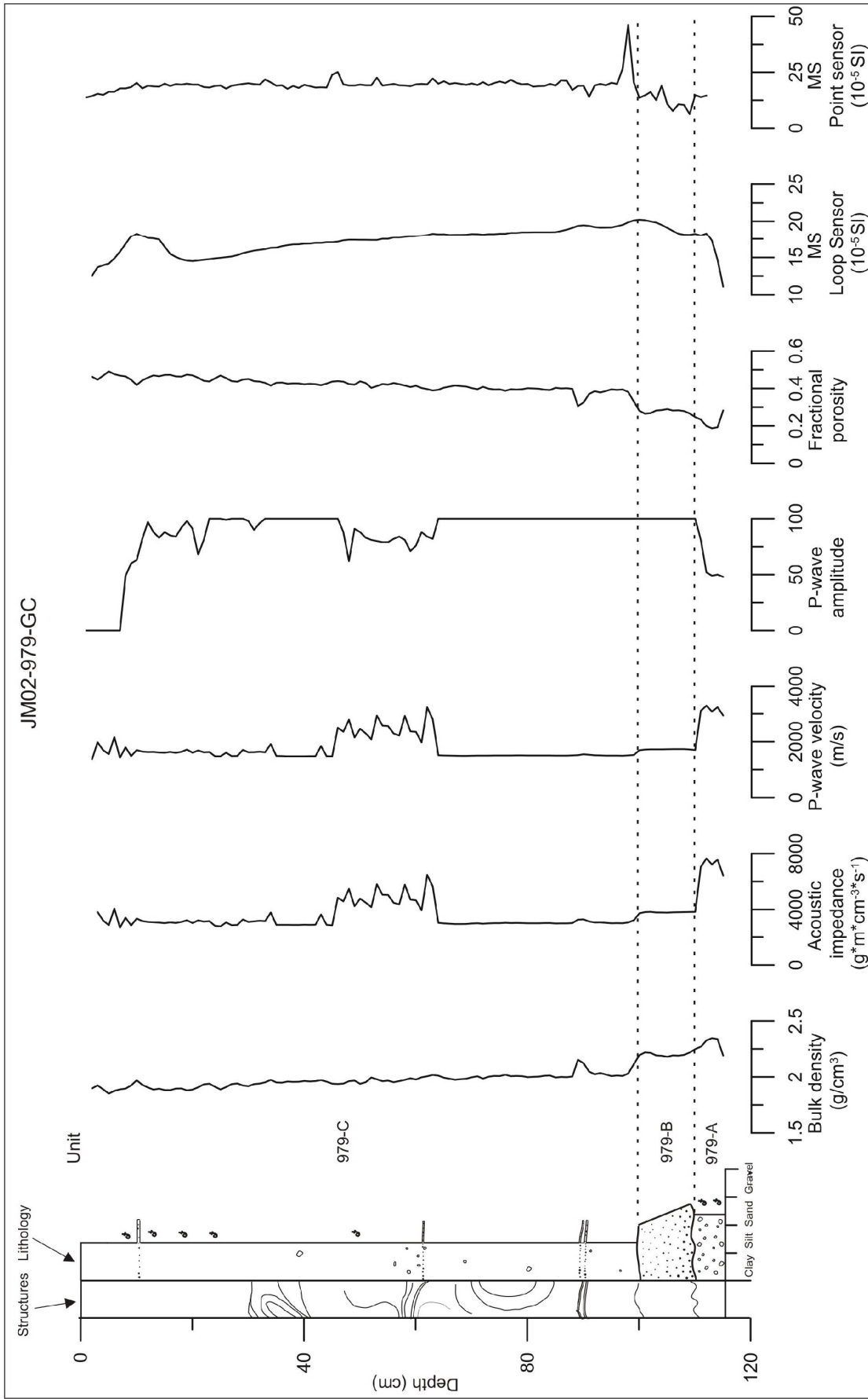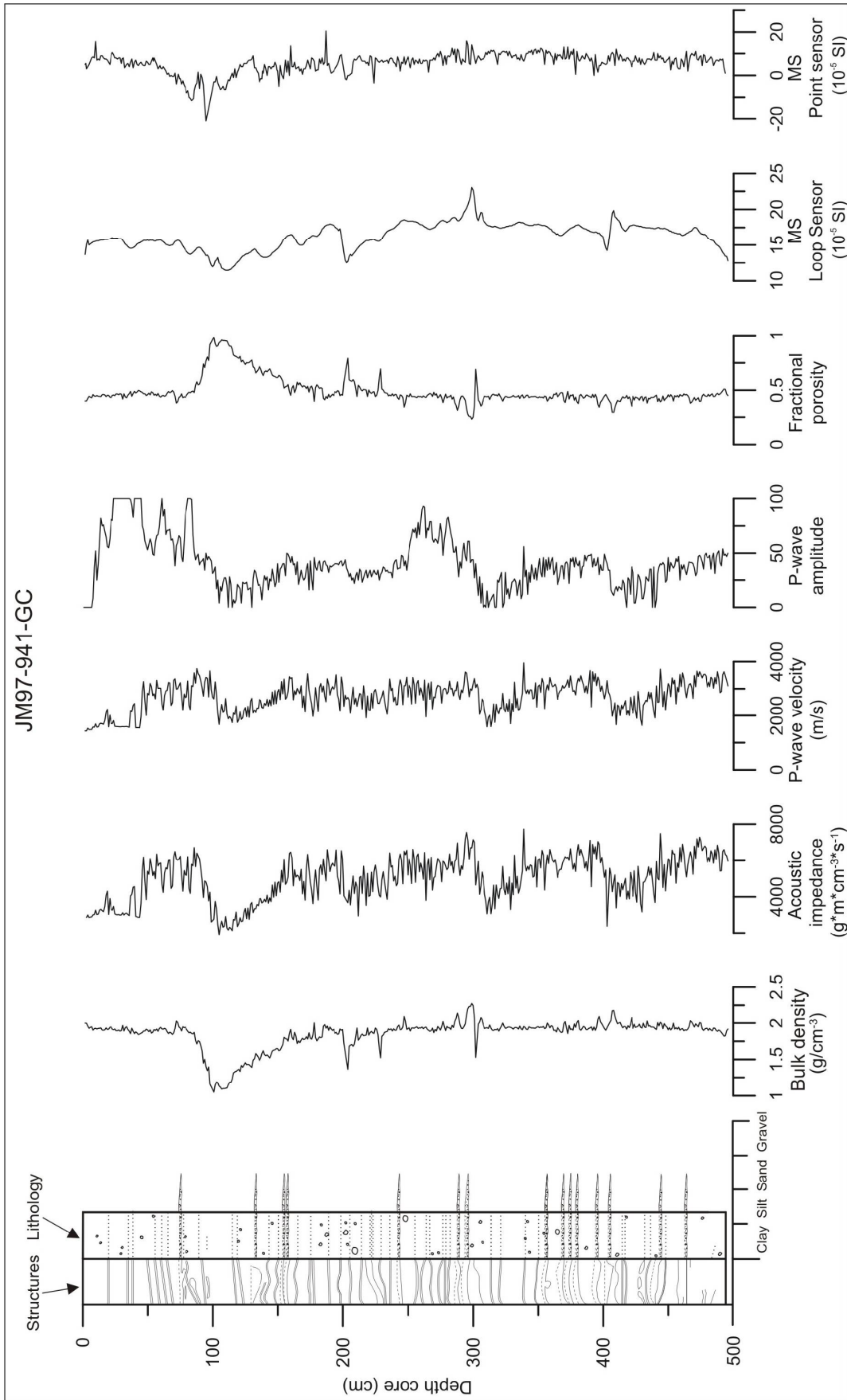
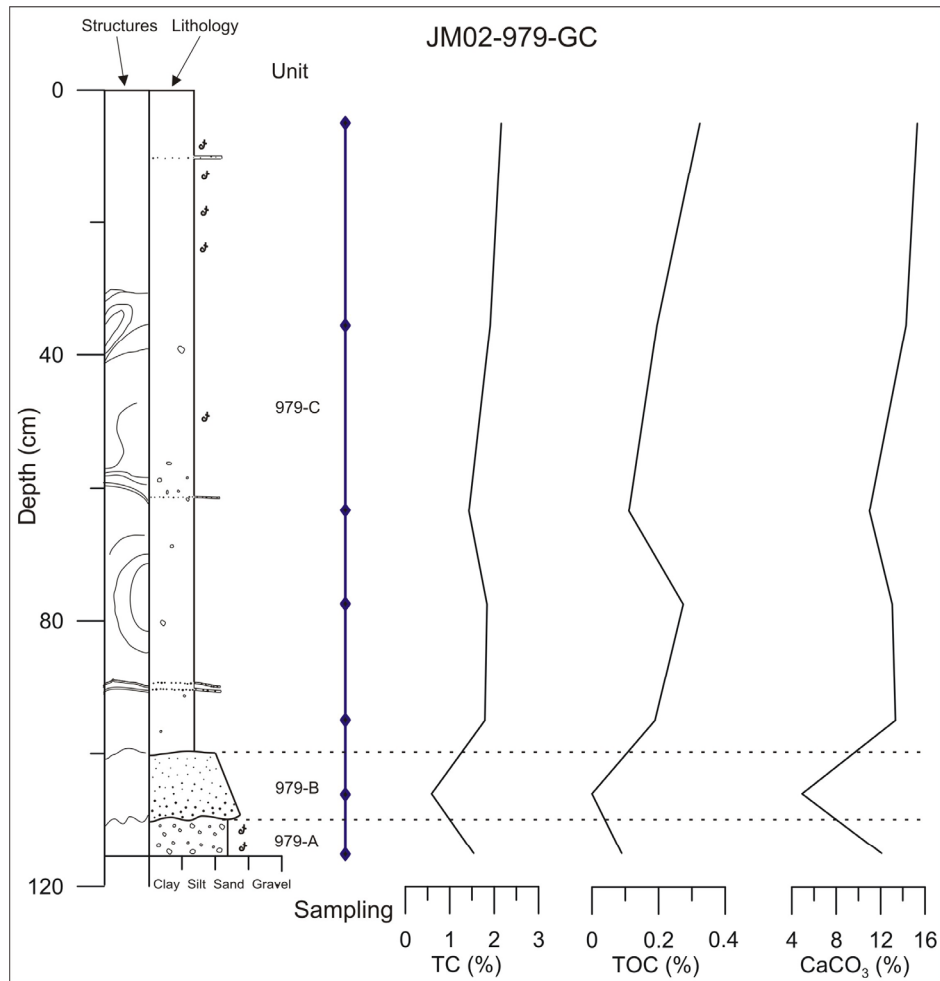**Fig. 5.7**: Lithological log and the physical properties (MSCL) of core JM97-941-GC.

48
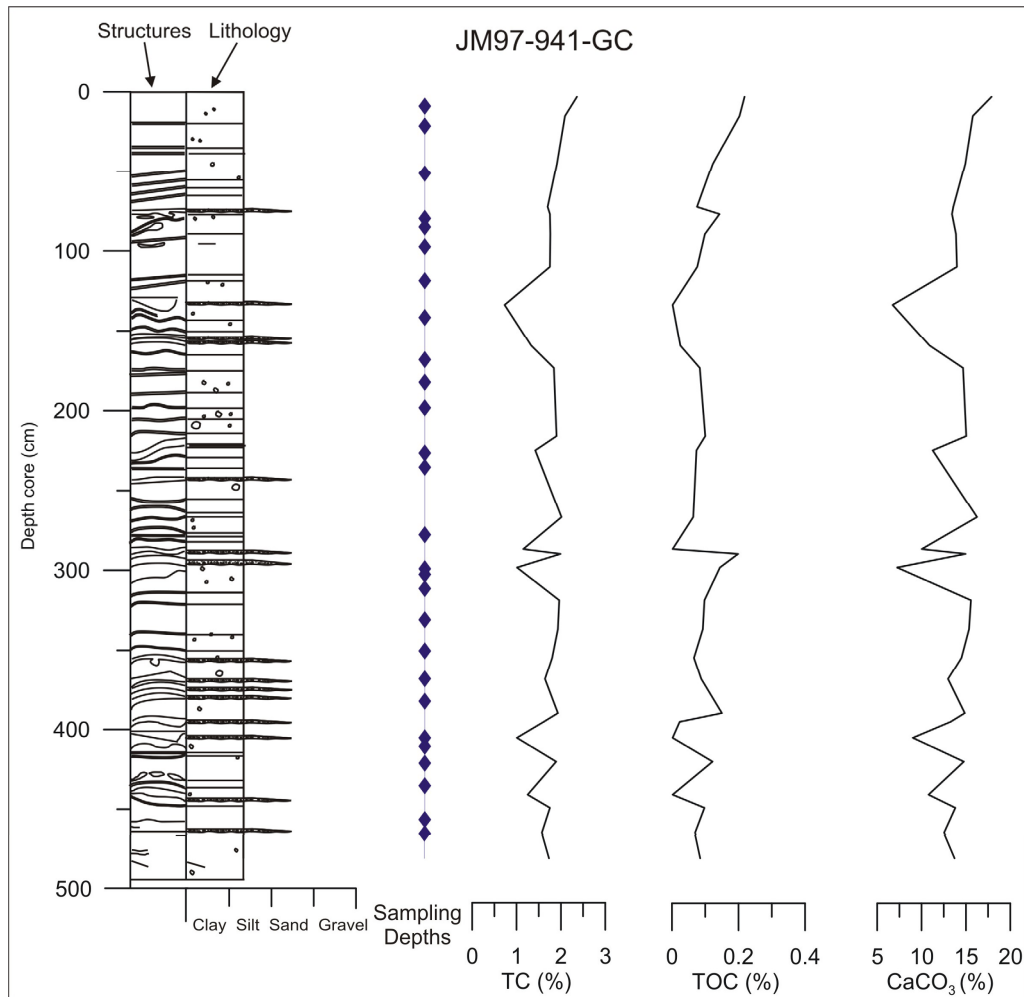
Fig. 5.8: Lithological log with the total carbon content (TC), total organic carbon content (TOC) and CaCO₃ content of the sediments in core JM97-941-GC.

5.3 JM97-943-GC

This core was taken in central parts of the fjord (Fig. 3.1). It is 460.5 cm long and comprises the units 943-A to 943-E.

5.3.1 Unit 943-A (460.5-440 cm)

Description

The lowermost unit is a massive very clast rich unit. The clasts are sub-rounded to sub-angular and the sediments have a dark greyish brown colour (Munsell code 10 YR 4/2). The upper boundary of this unit is defined by a decrease in clast content (Fig. 5.9A). The clasts vary in size and are up to 3 cm in diameter. The grain-size distribution diagram (Fig. 5.10)

shows a comparatively high percentage of sand and gravel. Probing the sediments with a needle showed that the sediments are relatively stiff compared to the other units in the core. The physical properties (Fig. 5.11) show large peaks at the depth of this unit. The magnetic susceptibility, the acoustic impedance and the bulk density are very high. They have low values below the peak, probably because there is a large hole in the sediments at that depth (Fig. 5.9A, 5.12). The fractional porosity and the P-wave amplitude are both low, and rapidly increase at the bottom of the core, where the hole occurs. The TC, TOC and $CaCO_3$ contents are low (Fig. 5.13). Possible variations are not visible since only one sample was taken in this unit. The unit does not have any internal structure or stratification (Fig. 5.9A). No shells were found in this unit and bioturbation is absent.
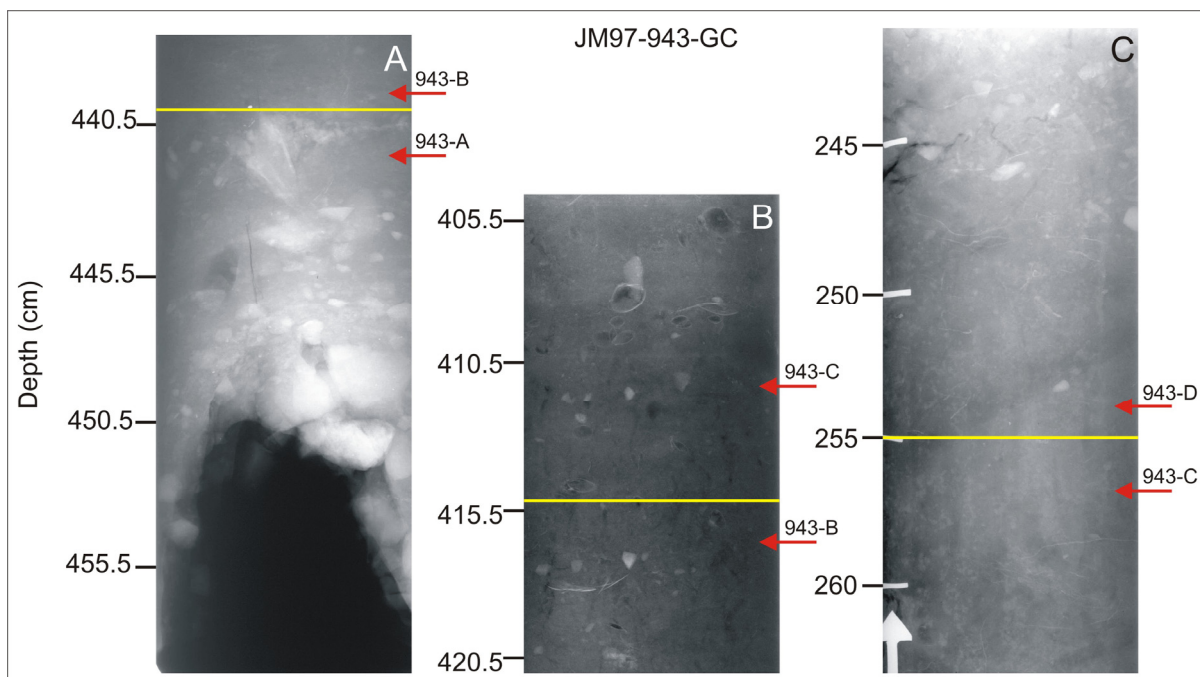
Fig. 5.9: Three radiographs from JM97-943-GC showing the boundaries between the different units. A shows the lowermost unit 943-A and the boundary to 943-B defined by a decrease in clast content. B shows the top of unit 943-B and the boundary to the overlying unit 943-C. This boundary was mainly defined by the colour of the sediment and the increase in shells. C shows unit 943-C and the boundary to overlying unit 943-D, defined by the decrease in clast content.

Interpretation

The lowermost unit in cores from the Isfjorden system and the shelf was interpreted as a till by Elverhøi et al. (1995A) & Svendsen et al. (1996). This till was described as poorly sorted, homogenous and characterized by a compact and firm consistency.

The stiffness of the sediment in unit 943-A of core JM-943-GC is suggested to be a result of compaction. The massive texture, the high amount and size of clasts, the high magnetic

susceptibility values and the absence of shells and bioturbation led to an interpretation of this unit as a basal till.
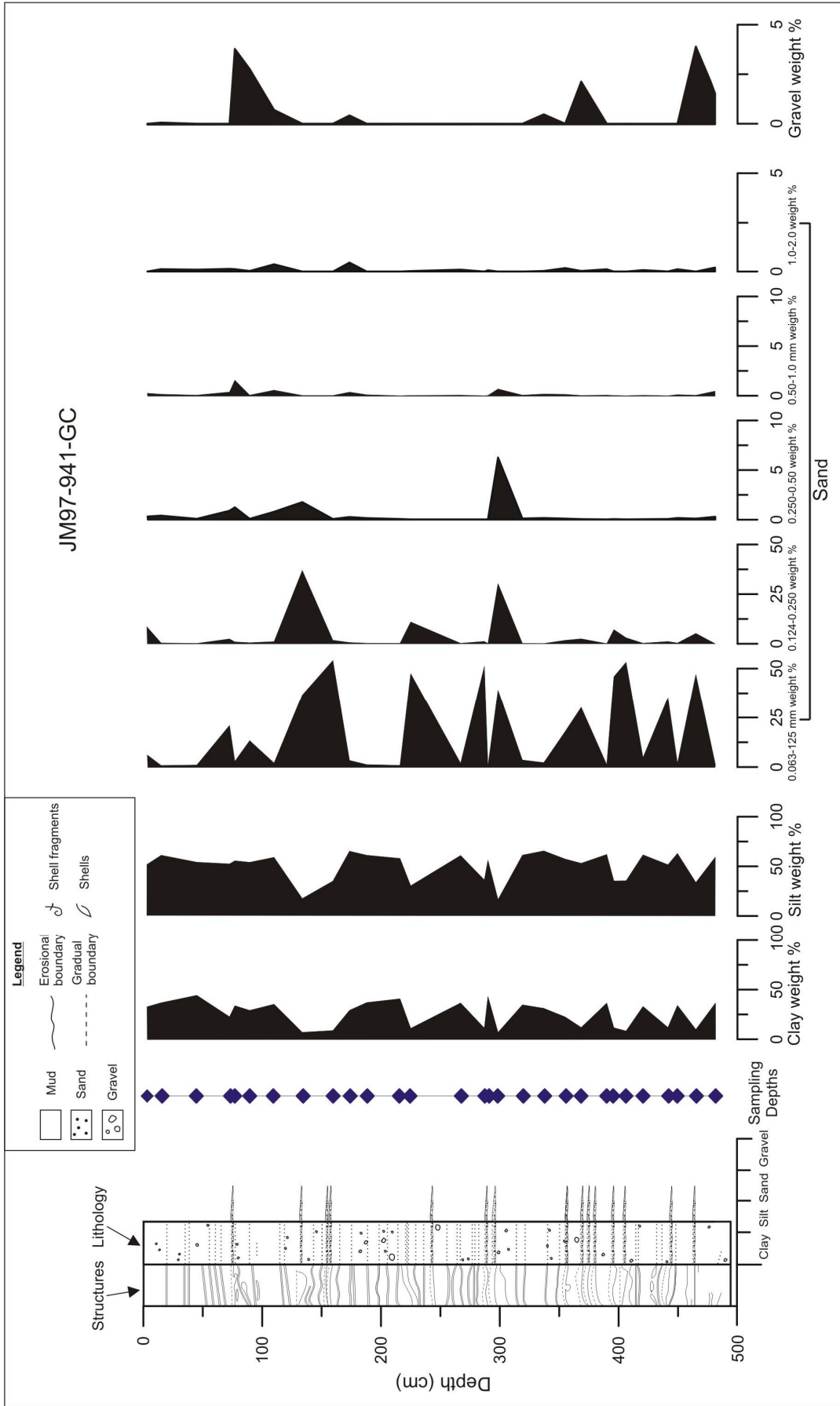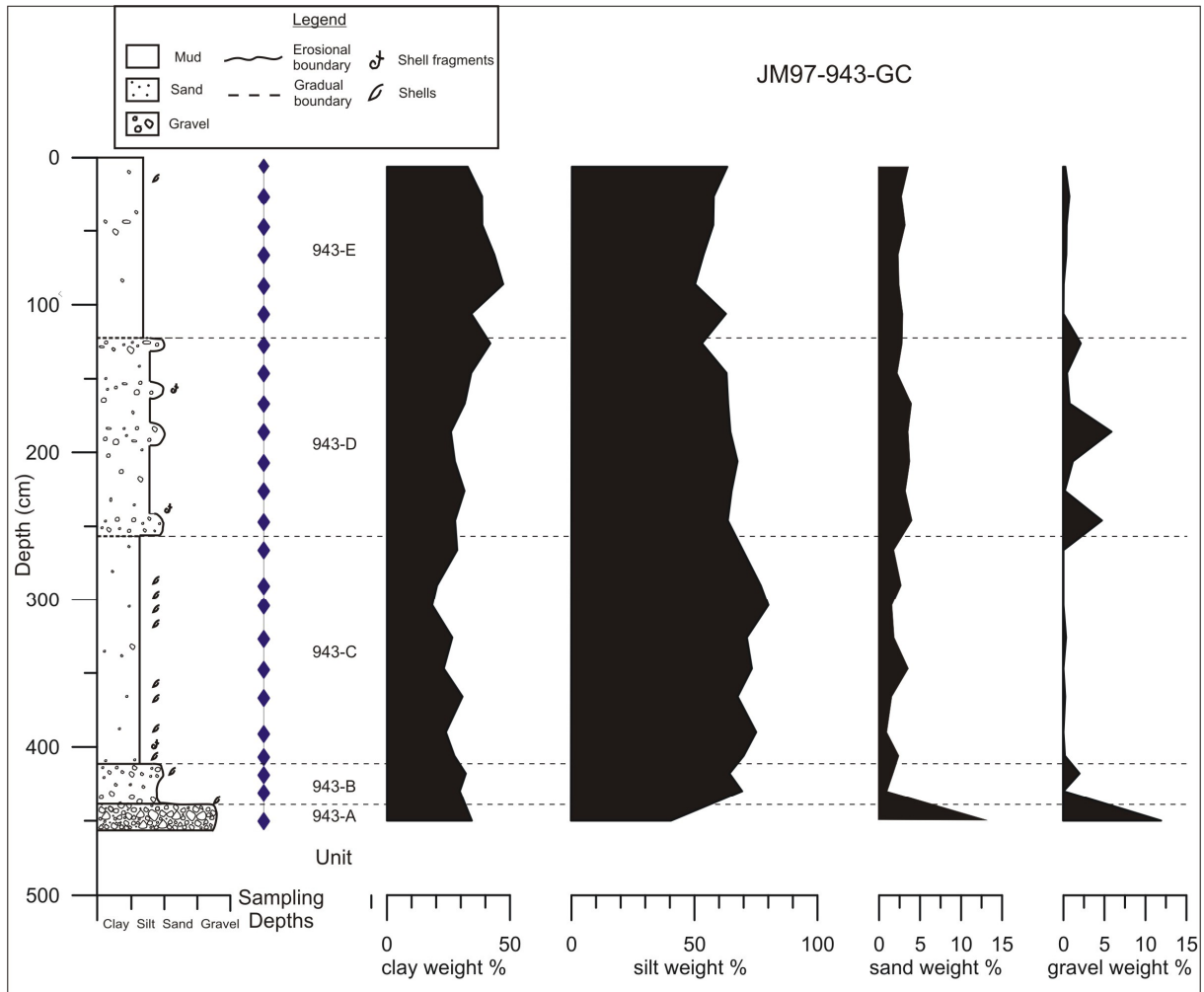

Fig. 5.10: Lithological log and the grain-size weight percentages of JM97-943-GC
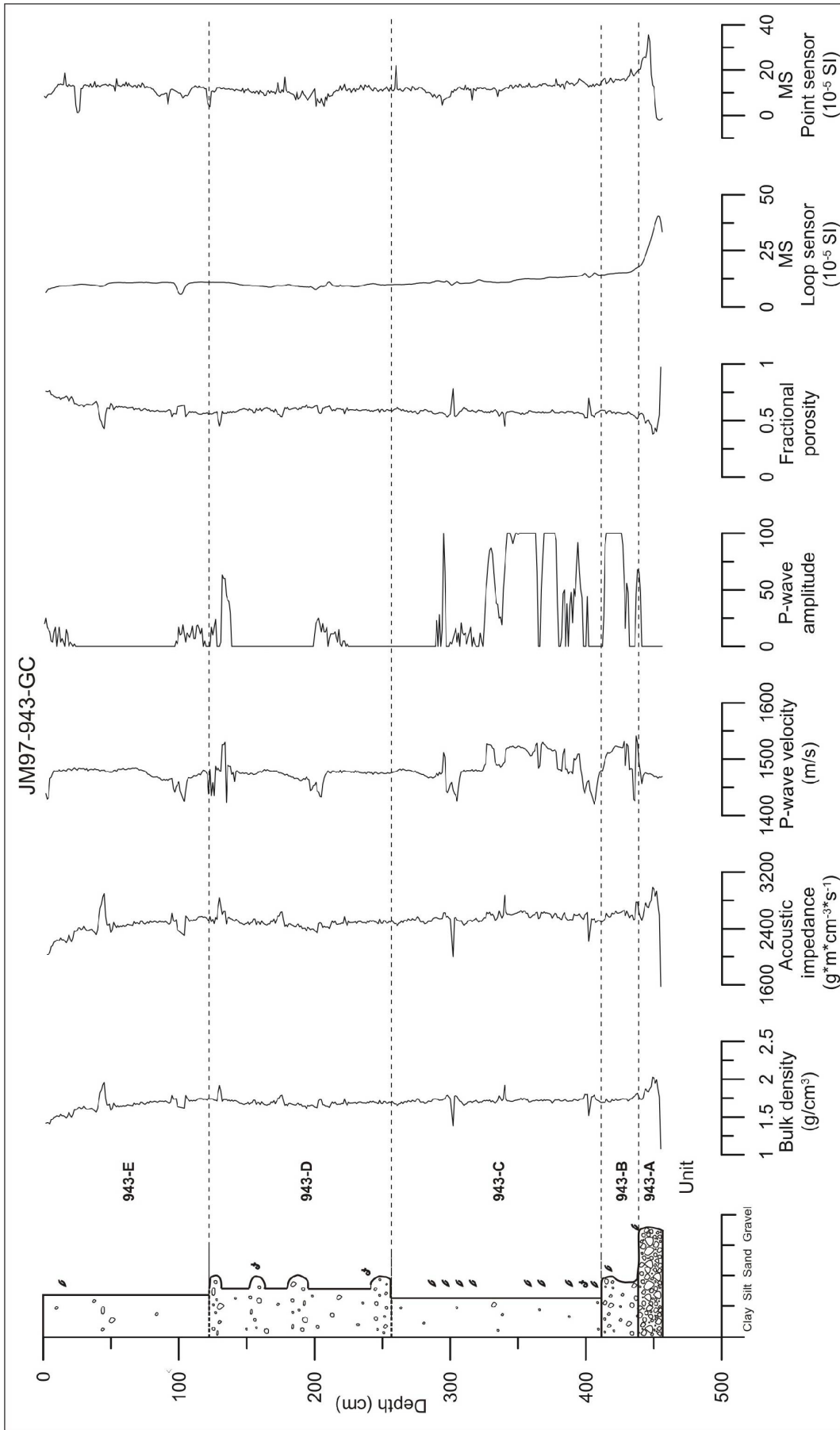
Fig. 5.11 Lithological log and the physical properties (MSCL) of core JM97-943-GC

5.3.2 Unit 943-B (440-415 cm)

Description

This unit has a dark greyish brown colour with a slight reddish glow (Munsell code 2.5 Y 4/2) and contains faintly laminated mud with a relatively high content of clasts (Fig. 5.10). The lower boundary of this unit is defined by a decrease in clast content (Fig. 5.9A). The upper boundary is defined by a colour change, as well as by an increase in shell content and a decrease in clast content (Fig. 5.9B). The magnetic susceptibility is lower than in the underlying unit, but still higher than in the overlying sediments. The bulk density and the acoustic impedance both decrease in comparison to the underlying sediments. The TC, TOC and $CaCO_3$ contents are higher in this unit then in the underlying unit, and the values increase further towards the top of the unit (Fig. 5.13). The unit contains some shells, of which most in living position and bioturbation occurs.

Interpretation

Because of the relatively high clast and low shell content compared to the overlying unit, unit 943-B was interpreted as a glacimarine diamicton. A laminated glacimarine mud was recognized from cores from Billefjorden as a less than 0.5 m thick transitional zone between the till and the Holocene mud above (Svendsen et al., 1996). Unit 943-C is 25 cm thick can be correlated to the unit described by Svendsen et al, (1996) because of its relatively high clast and low shell content compared to the overlying unit, and lower shell and clast content compared to the underlying unit.

5.3.3 Unit 943-C (415-255 cm)

Description

This unit is characterised by relatively high amounts of shells and comparatively few clasts (Fig. 5.9B; Fig. 5.10). The colour of the sediments is dark greyish brown (Munsell code 2.5 Y 4/2) and the sediments are very bioturbated. The lower boundary of this unit is defined by an abrupt decrease in the amount of clasts and increase in the amount of shells. The upper boundary is defined by an increase in the amount of clast and a decrease in the amount of shells (Fig. 5.9C). Immediately after opening the sediments in the upper part of the unit were covered with black mottles, which disappeared after being exposed to air. A large clast with a diameter of 3 cm was found at 337 cm depth (Fig. 5.12). The bulk density, acoustic impedance, fractional porosity and magnetic susceptibility remain almost constant with

generally minor fluctuations (Fig. 5.11). However, the density and the acoustic -impedance show a positive peak between 335 and 340 cm depth. The fractional porosity shows the same peak but negative. These peaks were probably caused by the large clast found at 337 cm depth (Fig. 5.12). Almost all the physical properties show an excursion around 300 and 400 cm depth (Fig. 5.11). These excursions are caused by the boundaries between the meter-long sections in which the core has been split. The p-wave velocity and the p-wave amplitude fluctuate a lot; this could indicate that the liner is not well filled with sediments. The TC, TOC and CaCO$_3$ contents are higher in this unit than in the two underlying units (Fig. 5.13). The values do not show much variation, and increase slightly towards the top of the unit. A lot of paired shells were found in situ, some to up to 4 cm in length. Between 305 and 325 a horizon is characterized by high concentration of in situ shells (Fig. 5.14A). Two shells from this unit were radiocarbon dated.

Interpretation

The high concentration of shells could indicate warmer water with more favourable living conditions for shells. Based on this and the relatively low amounts of clasts it is suggested that unit 943-C reflects deposition in a warmer climate (Hald et al., 2004; Forwick & Vorren, 2005A).
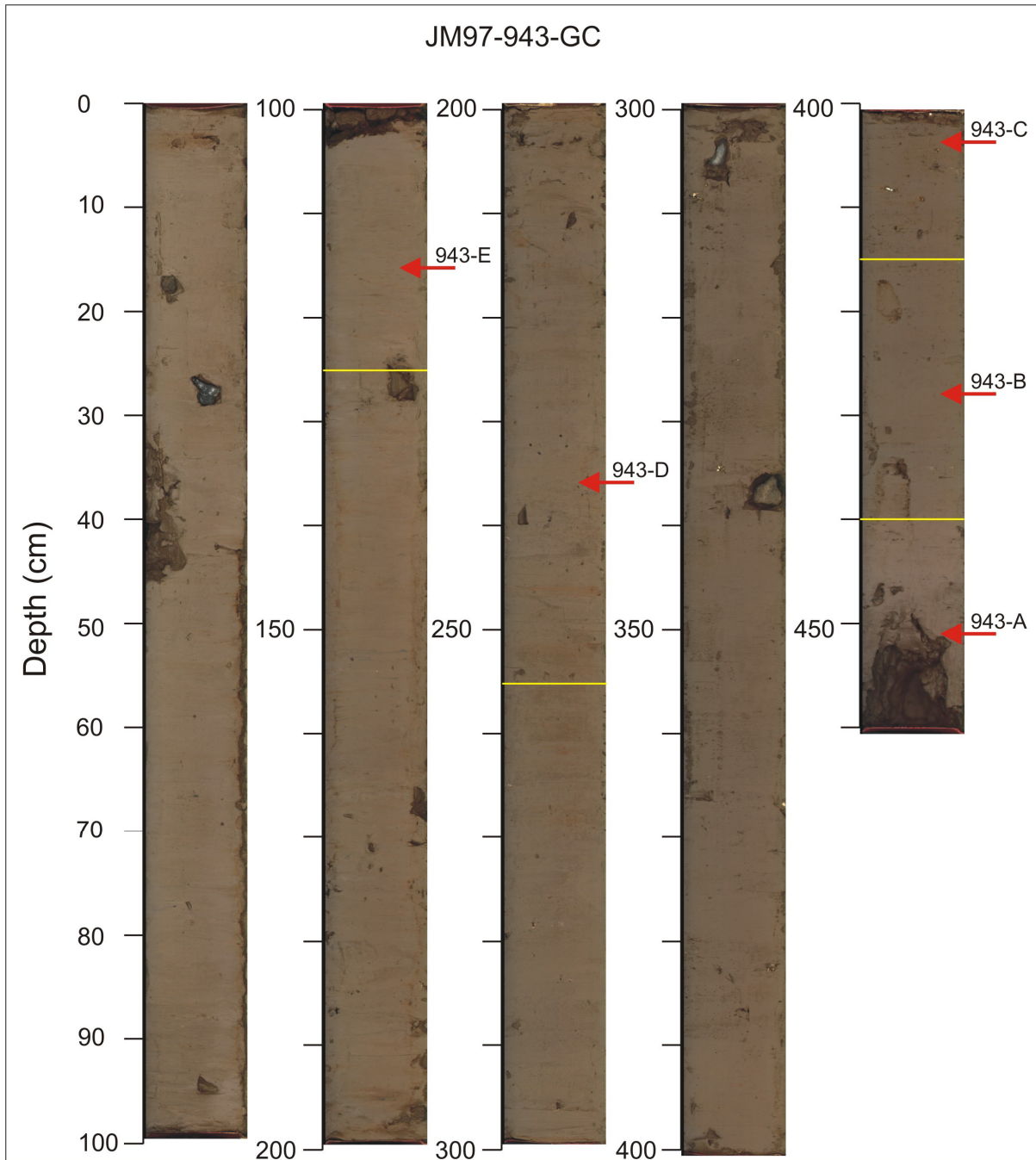
Fig. 5.12: Colour pictures of core JM97-943-GC, the section boundaries are indicated in yellow.
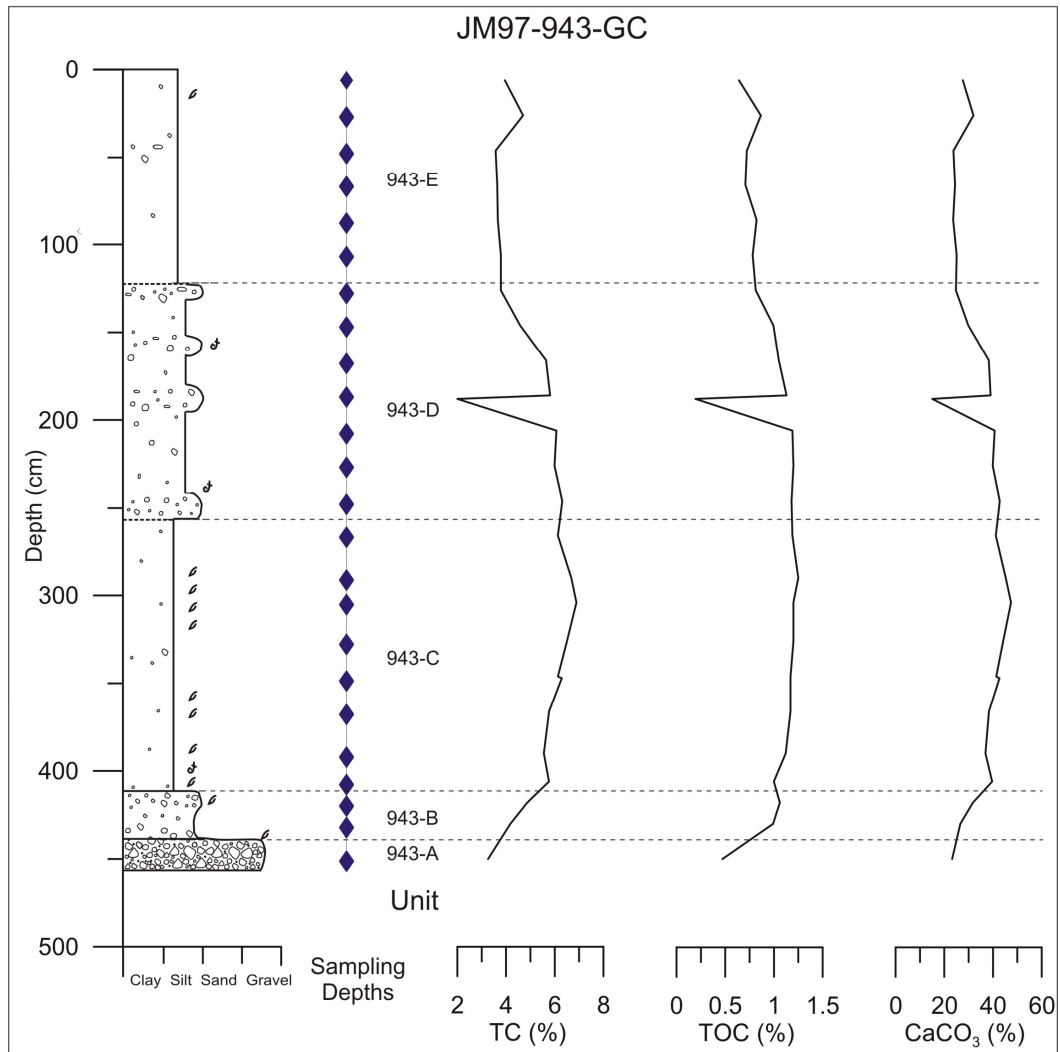
Fig. 5.13: Lithological log with the total carbon content (TC), total organic carbon content (TOC) and CaCO$_3$ content of the sediments in core JM97-943-GC.

5.3.4 Unit 943-D (255-125 cm)

Description

This unit has a higher clast and lower shell content than the underlying unit (Fig. 5.10). The lower boundary is defined by marked changes in these parameters (Fig. 5.9). The upper boundary is defined only by a decrease in clast content. Immediately after opening the sediments were covered with black mottles, which disappeared after being exposed to air. The colour of the sediments in this unit is dark greyish brown (between Munsell codes10 YR 4/2 and 2.5 Y 4/2). This unit contains four clast rich layers (Fig. 5.10, 5.14B). In between these layers, the sediments are bioturbated. The lack of high gravel contents at c. 160 depth in the grain-size distribution diagram (Fig. 5.10) is based on the fact that no sample was taken from

this clast-rich layer. The clay content increases slightly, whereas the silt content decreases upcore within the unit.
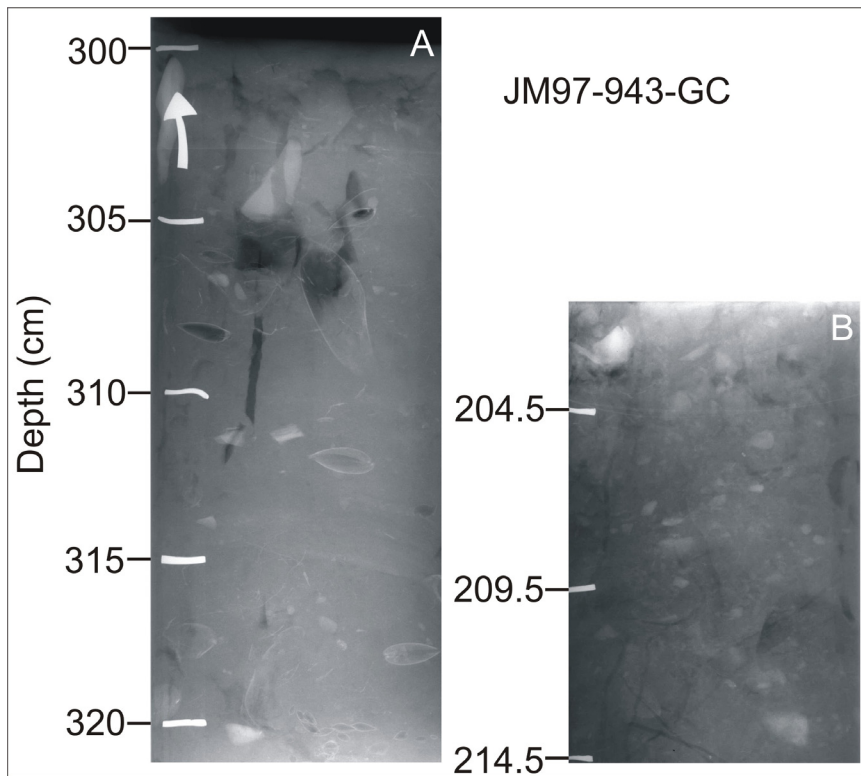
Fig. 5.14: Two radiographs from JM97-943-GC. A shows a horizon with a high concentration of (some very large) shells in unit 943-C. B shows a high concentration of small clasts in unit 943-D.

The physical properties do not show many variations in this unit (Fig. 5.11). The P-wave velocity and the P-wave amplitude show some spikes around 210 and 130 cm depth. Minor excursions at the same depths were also seen in most of the other parameters. The TC, TOC and $CaCO_3$ contents are generally lower in this unit than in the underlying unit, but higher then in the overlying unit (Fig. 5.13). The values decrease upcore within the unit, and show a marked excursion at 188 cm depth. This large excursion could be a measurement error. Only two shell fragments were found in this unit. Both have been radiocarbon dated.

Interpretation

The increase in clast content and the decrease in shell content are assumed to indicate an increase in the deposition of ice rafted debris in the central part of the fjord (compare with Hald et al., 2004; Forwick & Vorren, 2005). This increase in IRD could by caused by an increase in glacial activity in the form of glacier growth and/or the increased formation of sea ice.

5.3.5 Unit 943-E (125-0 cm)

Description

This unit contains low amounts of clasts and shells (Fig. 5.10). The colour of the sediments in the lowermost part of the unit is dark greyish brown (Munsell code 10 YR 4/2 gradually changing Munsell code 2.5 Y 4/2 at around 60 cm depth; Fig. 5.12). The surface of the sediment was covered by black mottles upon opening of the core, which disappeared after being exposed to air. The grain-size distribution diagram (Fig. 5.10) shows that this unit contains relatively little gravel and silt, but relatively much clay. The amount of sand is comparable to the amount in the underlying unit. The physical properties show an excursion in the density, acoustic impedance and the fractional porosity around 40 cm depth. This excursion could have been caused by the relatively large amount of clasts at this depth (Fig. 5.11). An excursion around 100 cm is most likely caused by the section boundary. The TC, TOC and $CaCO_3$ contents decrease slightly towards the top of the unit. They have generally low values. A small increase occurs just below the top of the core (Fig. 5.13). The unit contains one shell and some shell fragments. The sediments are intensely bioturbated. A polychaeta tube was found on the surface between 77 and 79 cm.

Interpretation

The stratigraphic position of this unit is assumed to reflect present environmental conditions. The relatively low clast content could indicate a decrease in ice rafted debris or an increase in sea-ice, blocking the way for icebergs or sea-ice transporting IRD into the fjord (Ó Cofaigh & Dowdeswell, 2001).

5.3.6 X-ray diffraction (XRD)

XRD analyses were carried out with samples from JM97-943-GC to reconstruct the influence of various sources of sediment input into the central part of Billefjorden, and to reconstruct the glacial activity in the fjord. The results are shown in figure 5.15. The plot showing the sum of clay minerals includes smectite & montmorillonite, mixed layered clays, illite & mica, kaolinite and chlorite. The highest percentage of clay minerals is from illite & mica, thus significantly influencing the shape of the plot (Fig. 5.15). The percentage of illite & mica indicates the percentage of the total sample, not only of the percentage within the clay minerals.

Description

Unit 943-A contains high percentages of clayminerals and in particular illite & mica and relatively low percentages of calcite and ankerite & dolomite (Fig. 5.15). Unit 943-B shows increasing amounts of calcite and ankerite & dolomite and decreasing amounts of clayminerals, illite & mica and quarts. The percentages of clayminerals and illite & mica decrease further in the overlying unit (943-C, Fig. 5.15). The percentage of quarts decreases first, but increases upwards from 350 cm. The percentage of ankerite & dolomite increases and also the percentage of calcite increases in the lower part of unit 943-C but starts to decrease around 340 cm depth. The percentages of clayminerals and illite & mica in unit 943-D increase from about 180-190 cm depth (Fig. 5.15). The percentages of ankerite & dolomite and calcite mirror this. The percentages of clayminerals and illite & mica decrease slightly in the uppermost unit (943-E, Fig. 5.15). The percentage of ankerite & dolomite is relatively low and remains comparatively stable with low values. The percentage of calcite increases slightly in this unit.

The percentage of quartz minerals shows high values in unit 943-A and slightly lower values in 943-B (Fig. 5.15). The values decrease in the lowermost part of unit 943-C, but slightly increase again above this unit showing some variations. The changes in the percentage of epidote behave somewhat similar to the changes of ankerite & dolomite and calcite. This means, very low values in unit 943-A with increasing values towards the top of unit 943-D. Unit 943-E contains comparatively low percentages of epidote, similar to unit 943-A.

Sediment sources

Mica occurs in almost all the metamorphic basement units described in the area underneath the glacier Nordenskiöldbreen (Dallmann et al., 2004). Quartz also occurs in one of them. High amounts of illite & mica are therefore suggested to reflect larger sediment input from Nordenskiöldbreen. Illite is a weathering product of muscovite and feldspar and occurs in sedimentary rocks as well as in metamorphic rocks. It therefore does not characterise a certain sediment source. The sides of the fjords are dominated by limestones and dolomite (Dallmann et al., 2004). Limestone is a sedimentary rock mainly composed of the mineral calcite.
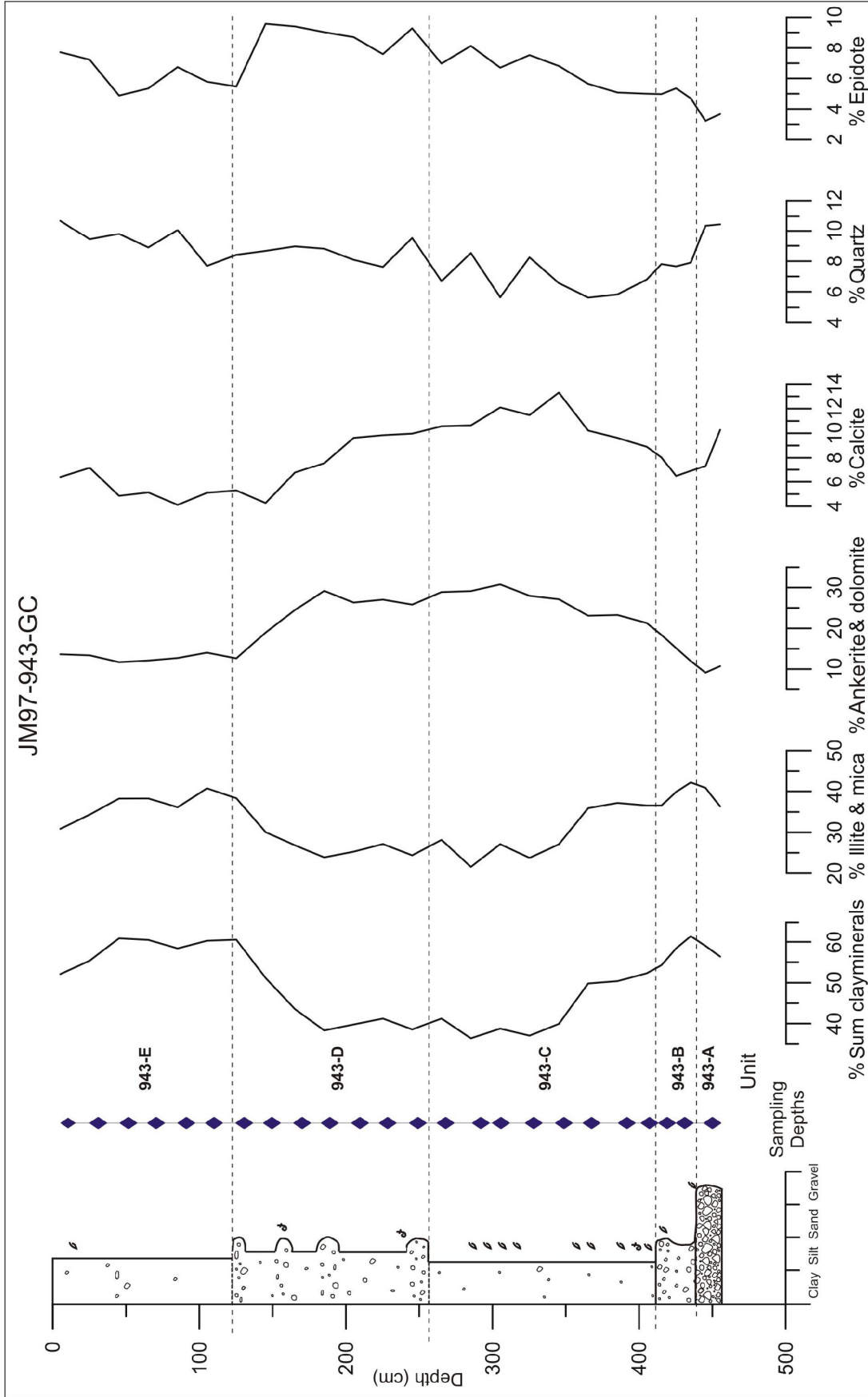
Fig. 5.15: XRD values of the different minerals from core JM97-943-GC. The % sum clayminerals consists of: smectite & montmorillonite, mixed layered clays, illite & mice, kaolinite and chlorite. The percentage of illite & mica indicates the percentage of the total sample, not only of the percentage within the clay minerals.

6. Chronology

6.1 Introduction

Sediments from Billefjorden were earlier dated by Svendsen et al. (1996) and Svendsen & Mangerud (1997). These dates were used to calculate sedimentations rates and define the timing of deglaciation of the fjord. Results from Svendsen & Mangerud (1997) showed that following deglaciation around 10 000 cal. BP, the sedimentation rate remained constant through most of the early and mid-Holocene. This was interpreted to reflect small or absent glaciers during this interval (Svendsen & Mangerud, 1997).

Seven samples from core JM97-943-GC have been radiocarbon dated (Fig. 6.1). The purpose of these dates is to:

- Establish a chronology for Billefjorden with a higher temporal resolution than done so far (Svendsen & Mangerud., 1997).
- Reconstruct the late Weichselian/ early Holocene deglaciation history in Billefjorden
- Infer the timing of Holocene glacial activity in the fjord.

6.2 Results

The radiocarbon ages and calculated calibrated calendar ages are shown in table 6.1. The radiocarbon samples will be described in more detail below.

- *439 cm, TUa-6330*

    This sample comprises a paired shell of the species *Enucula tenuis*. It was taken exactly at the base of unit 943-B and it was dated 9940 ± 50 ^{14}C yr BP, calibrated to 11230 calendar years BP (Table 6.1). This date indicates the minimum age for the deglaciation of the core site in the central part of   Billefjorden.

- *422 cm, TUa-6667*

    This sample comprises fragments of a paired shell of the species *Enucula tenuis*. It was taken just below the top of unit 943-B. It was dated to 9855 ± 50 ^{14}C yr BP, calibrated to 11190 cal. yr BP (Table 6.1). This date gives a minimum age for the

change from a glacimarine environment to a depositional environment with less glacial activity and possibly warmer water with more favourable living conditions for shells.
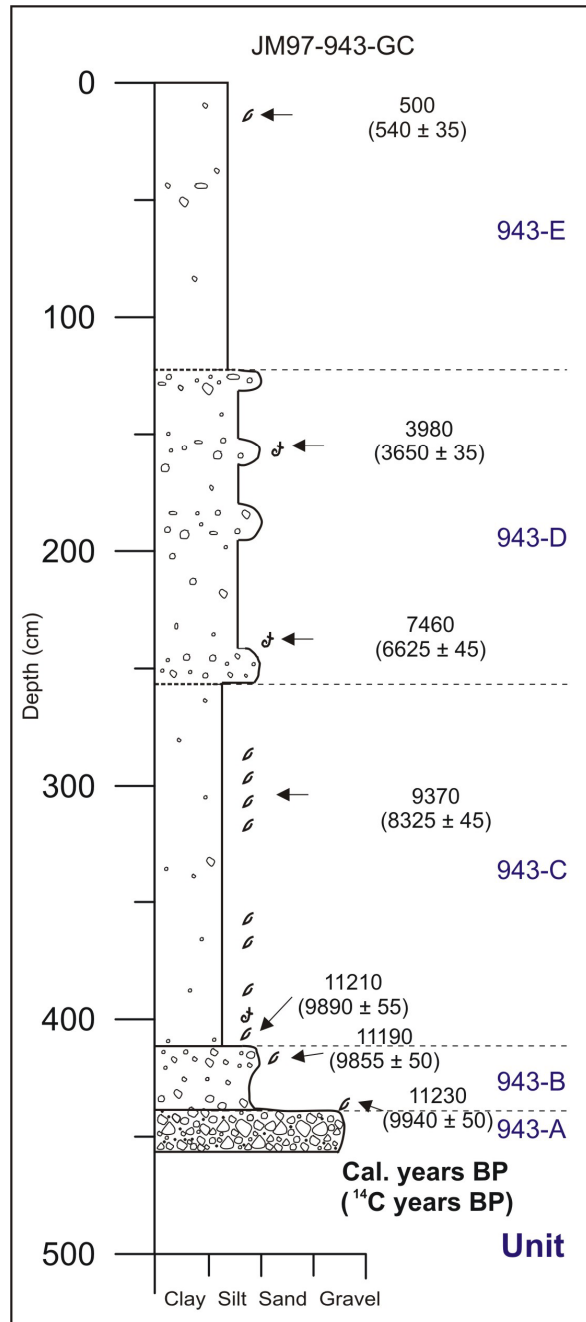
Fig. 6.1: Lithological log with the radiocarbon dates and calibrated ages of JM97-943-GC

Tab 6.1: Radiocarbon ages and calibrated ages from core JM97-943-GC. All the radiocarbon ages were corrected for a marine reservoir effect of 440 (Mangerud & Gulliksen, 1975) before calibration. For calibration the program Calib Rev. 5.0.1(Stuiver & Reimer, 1993) and the dataset *04.14C* by Hughen et al. (2004) were used.

Lab. reference	Depth (cm)	Species	^{14}C ages (^{14}C yr BP)	Calibrated ages (NTNU Lab)	Calibrated ages (BP) (Calib 5.0.1, 1σ)	Peak distr. 1σ (BP)	Calibrated ages (BP) (Calib 5.0.1, 2σ)
TUa-6330	439	*Enucula tenuis*	9940 ± 50		11191-11323	11230	11143-11423
TUa-6667	422	*Enucula tenuis*	9855 ± 50		11144-11230	11190	11096-11313
TUa-6666	408	*Enucula tenuis*	9890 ± 55		11156-11265	11210	11106-11377
TUa-6329	305-309	*Yoldia hyperborea*	8325 ± 45		9275-9419	9370	9172-9470
TUa-6665	238	*Nuculana pernula*	6625 ± 45	BC5540-5440	7416-7519	7460	7360-7575
TUa-6329	152-155	*Malcoma calcarea*	3650 ± 35	BC2130-2000	3917-4074	3980	3840-4145
TUa-6327	19	*Enucula tenuis*	540 ± 35	AD1420-1465	459-535	500	418-608

- *408 cm, TUa-6666*

    This sample comprises a paired shell of the species *Enucula tenuis*. It was taken just above the bottom of unit 943-C. It was dated to 9890 ± 55 ^{14}C yr BP, calibrated to 11210 cal. yr BP (Table 6.1). This date should give a maximum age for the same change in environments mentioned for sample TUa-6667

- *305-309 cm, TUa-6329*

    This sample comprises a paired shell of the species *Yoldia hyperborea*. It was taken in unit 943-C at the depth that contained the most and the biggest shells. It was dated to 8325 ± 45 ^{14}C yr BP, calibrated to 9370 cal. years BP (Table 6.1). This date indicates the approximate timing of favourable conditions for shells. This timing could be associated with a warm climate.

- *238 cm, TUa-6665*

  This sample comprises a shell fragment from a shell of the species *Nuculana pernula*. It was taken in unit 943-D just above the first coarser layer of sediment, in the lower part of the unit. It was dated to 6625 ± 45 ^{14}C yr BP, calibrated to 7460 cal. years BP (Table 6.1). This date gives a minimum age for the onset of an increase in ice rafted debris in the fjord.

- *152-155 cm, TUa-6328*

  This sample comprises fragments of a paired shell of the species *Malcoma calcarea*. It was taken from the second last coarser layer of sediment in unit 943-D, in the upper part of the unit. It was dated to 3650 ± 35 ^{14}C yr BP, calibrated to 3980 cal. years BP (Table 6.1). This date gives the maximum age for the change from an environment with increased amounts of ice rafted debris to conditions with less ice rafted debris.

- *19 cm, TUa-6327*

  This sample comprises a paired shell of the species *Enucula tenuis*. It was taken from unit 943-A, close to the top of the unit. It was dated to 540 ± 35 ^{14}C yr BP, calibrated to 500 cal. years BP (Table 6.1). This date gives an indication of the age of the youngest sediments in the core.

6.3 Age model

With an age model, the dates of the unit boundaries were approximated (Fig. 6.2), assuming constant accumulation rates between the radiocarbon dates. The two dates at the upper boundary of unit 943-B show an inversion of age. A possible explanation for this could be reworking of the upper date (11210 cal. years BP). However, the calendar ages presented here represent the peak distribution and the upper date could in fact be younger than the lower date because of the age range (Table 6.1). This date is therefore interpreted not to have been reworked.
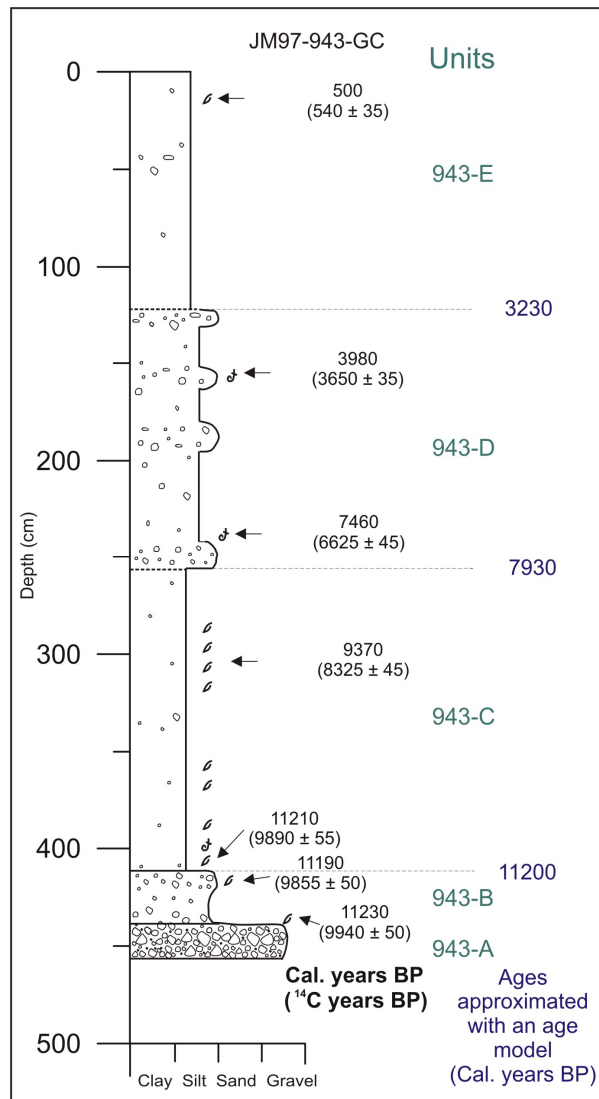
Fig. 6.2: Lithological log and the calibrated cal. years BP/ ^{14}C years BP of JM97-943-GC, with in blue the ages of the unit boundaries approximated with an age model, the ages are based on assumed constant accumulation rates between the radiocarbon dates.

6.4 Lithostratigraphy and age

6.4.1 JM02-979-GC

Core JM02-979-GC was divided into 3 units. The core penetrates the top of a sediment lobe coming down from the bedrock terrace in the inner fjord. This lobe has been deposited during the Neoglacial (Plassen et al., 2004). The sediments in core JM02-979-GC are therefore assumed to have been deposited in the late Holocene. The lowermost unit 979-A consists of redeposited glacimarine sediments. The overlying unit was interpreted as a turbidite. The

uppermost unit was interpreted as a mass-transport deposit, most likely a slump (Stow et al., 1996).

6.4.2 JM97-941-GC

This core was retrieved from the inner fjord basin; it comprises one unit and contains thicker sandy strata interpreted as turbidites. Thinner sandy/silty layers were probably deposited by meltwater or by distal turbidites. The fine sediments were probably deposited from settling of fine material. The clasts are most likely ice-rafted debris from the glacier or sea-ice. The sediments in this core penetrate the uppermost part of unit S3b (Forwick & Vorren, 2005A; see chapter 7.2.1) and are therefore assumed to have been deposited during the Late Holocene.

6.4.3 JM97-943-GC

Core JM97-943-GC was divided into 5 units. The lowermost unit 943-A comprises a stiff diamicton with a high clast content and was interpreted as a till. The unit above (943-B) contains less clasts and was interpreted to represent a glacimarine diamicton. This unit was deposited during the deglaciation of the central part of the fjord between c. 11230 and 11200 cal. yr BP. The unit above it (943-C) deposited between c. 11200 and 7930 cal. years BP has a low concentration of clasts and a high concentration of shells. This unit was interpreted to reflect a warmer climate and probably relatively little glacial activity in the fjord. The overlying unit 943-D was deposited between c. 7930 and 3230 cal. years BP and contains higher amounts of clasts and lower amounts of shells. This is suggested to indicate an increase in ice-rafted debris caused by an increase in glacial activity in the form of glacier growth and/or the increased formation of sea ice. The uppermost unit of the core is characterized by less ice rafted debris, possibly because of an increase in shorefast sea ice (Ó Cofaigh & Dowdeswell, 2001).

6.5 Accumulation rates

The accumulation rates between the radiocarbon dates of core JM97-943-GC were estimated in cm/cal. ka (centimetre per thousand calendar years) and are shown in figure 6.3. Accumulation rates of 800 cm/cal. ka during the deglaciation of the fjord decrease to 59 cm/cal. ka between c. 11200 and 9370 cal. years BP. Between c. 9370 and 7460 cal. years BP the accumulation rates decrease further to 36 cm/cal. ka and reach 24 cm/cal. ka between c.

7460 and 3980 cal. years BP. The accumulation rates increase again to 39 cm/cal. ka during the past 4000 cal. years.
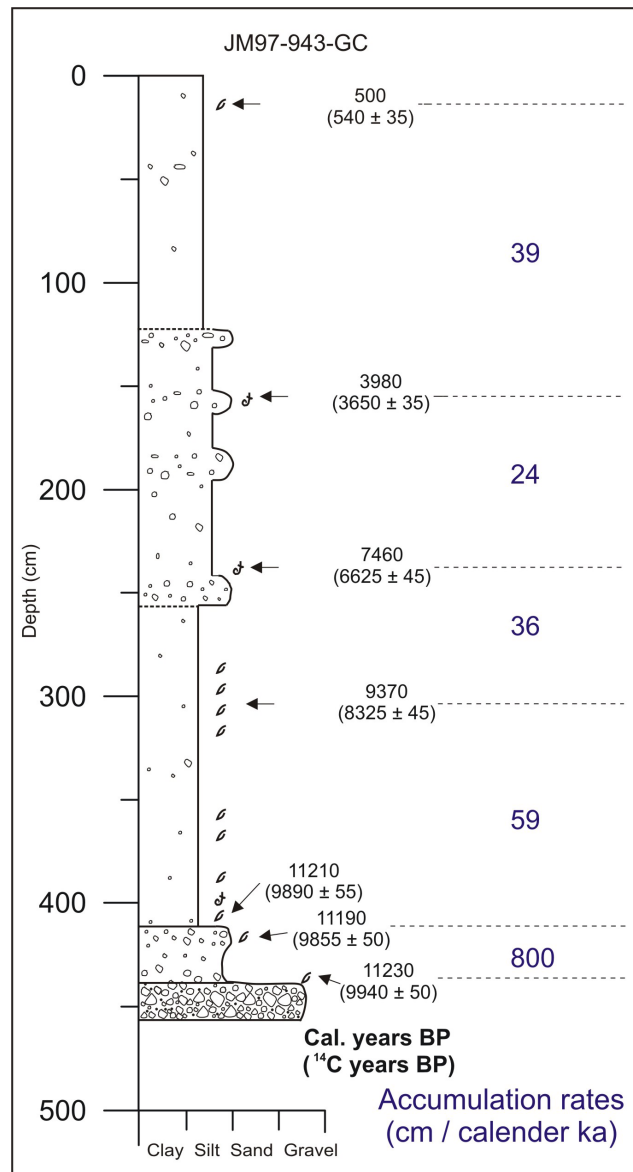
Fig. 6.3: Lithological log with the chronology of JM97-943-GC. Calculated accumulation rates in centimetre per 1000 calendar years are shown in blue.

7. Seismo-and lithostratigraphy

In the following the lateral extent of the lithological units will be discussed by correlating the lithostratigraphy with high-resolution seismic data from Billefjorden.

7.1 Seismostratigraphy in Billefjorden

High resolution seismic data (Sparker, Boomer, 3,5 kHz penetration echosounder) from Billefjorden has been interpreted by Boulton (1979), Svendsen et al. (1996), Plassen et al. (2004) and Forwick & Vorren (2005A).

Boulton (1979) distinguished till and Holocene muds on a sparker traverse at the mouth of the fjord. Results from the Isfjorden system, including Billefjorden, by Svendsen et al. (1996) describe a till, overlain by a laminated glaciomarine mud and Holocene mud on top. Plassen et al. (2004) mapped glacigenic and mass-transport deposits off Nordenskiöldbreen. Forwick & Vorren (2005A) interpreted seismic data from the entire Isfjorden area and distinguished 3 different units:

- S1, glacial sediments and landforms (including moraines and glacial lineations) deposited prior to 11300 cal BP.
- S2, glacimarine sediments deposited between 14100 and 11300 cal. BP
- S3, marine sediments deposited during the last 11300 years. These sediments were divided into two subunits:
    o S3a, lower marine sediments with a more transparent seismic signature. These were deposited between 11300 and 8800 cal. years BP.
    o S3b, upper marine sediments with a less transparent seismic signature and more distinct and continuous acoustic stratifications. These were deposited after 8800 cal. years BP.
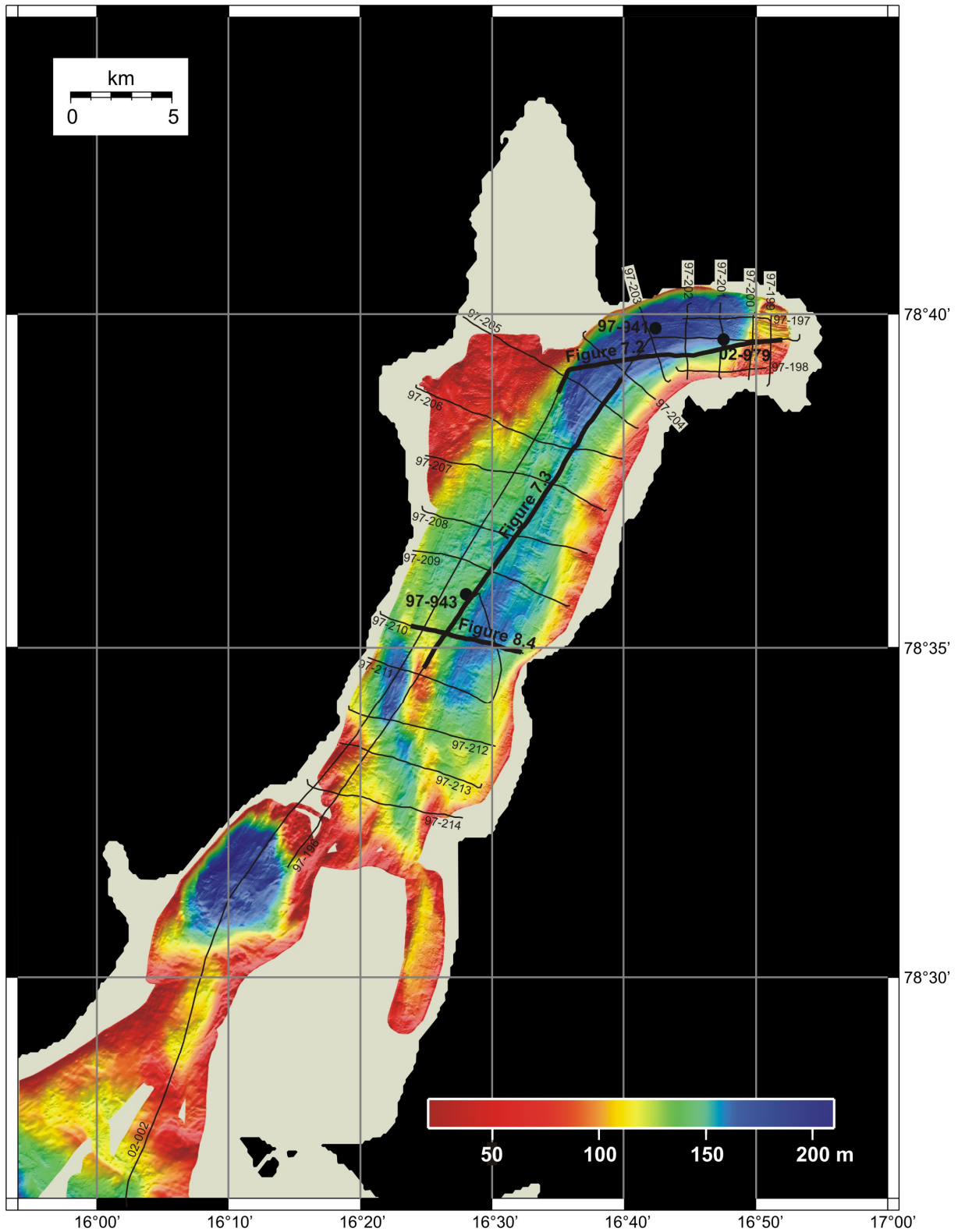
Fig. 7.1: Multibeam bathymetry dataset of Billefjorden with the core positions and seismic lines. The thicker seismic lines are displayed in the indicated figures.

7.2 Correlation sediment cores and seismostratigraphy

The sediment cores described in chapter 5 were plotted on the most recent and detailed seismic data from Billefjorden, interpreted by Forwick & Vorren (2005A). The seismic profiles used are indicated in figure 7.1.

JM97-941-GC is not located on the selected seismic lines; its position is therefore approximated in figure 7.2. JM02-979-GC is located on seismic line 02-002 (Fig. 7.2). JM97-943-GC is located on seismic line 97-196 shown in figure 7.3.

7.2.1 JM02-979-GC & JM97-941-GC

Seismic line 02-002 is located parallel to the fjord axis from the fjord mouth to the fjord head. Figure 7.2 shows the part of line 02-002 in the innermost part of the fjord (Fig. 7.1).

Core JM97-941-GC was retrieved at some distance to the north of profile 02-002 (Fig. 7.1). The approximate core location is indicated on figure 7.2. It penetrates only the upper parts of seismic unit S3b. This unit was described by Forwick & Vorren (2005; chapter 7.1). The sediments in core JM97-941-GC correlate well to those findings. This core contains 17 sandy strata interpreted as turbidites, interpreted to have been deposited during the Late Holocene.

The position of JM02-979-GC is shown on figure 7.2. It penetrates the top of the mass-transport deposit on the seismic profile. The mass-transport deposit originating from the bedrock terrace was interpreted as a debris flow related to the readvance of Nordenskiöldbreen during the Neoglacial (Plassen et al., 2004). The sediments in core JM02-979-GC consist of 3 different mass-transport deposits, the lowermost unit comprises redeposited glacimarine sediment, overlain by a turbidite and on top deformed mud interpreted as a slump. This confirms the suggestion by Plassen et al. (2004) that the proximal part of the debris lobe comprises a recent slide, and might be still active. Only the distal part of the debris lobe is covered by acoustically stratified glacimarine sediments (Plassen et al., 2004).

Blow-up 1 in figure 7.2 shows iceberg ploughmarks in the shallow areas discussed in chapter 4.5 and shown in figure 4.8. In the deepest part of the seismic line (Fig. 7.2) the sediment package is 50 ms two-way travel time; about 40 m thick.
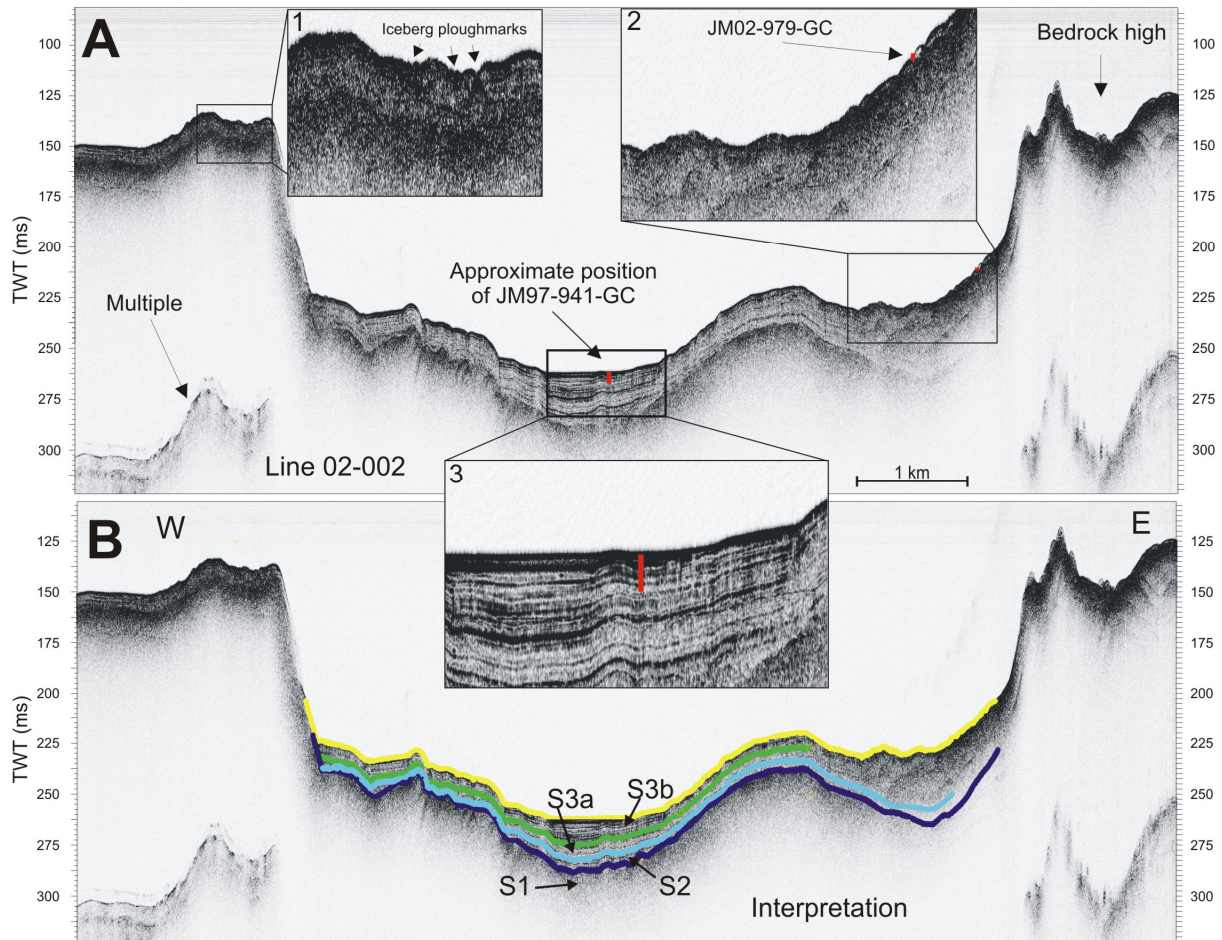
Fig. 7.2: Section of 3.5 kHz penetration echo sounder profile 02-002 in the inner part of the fjord (Fig. 3.2). Profile A shows the position of JM02-979-GC (in blow-up 2) and the position of JM97-941-GC in blow-up 3. Blow-up 1 shows the iceberg plough marks mentioned in Chapter 4.5 and figure 4.8. Profile B shows the interpretation by Forwick & Vorren (2005A). The different units are indicated.

7.2.2 JM97-943-GC

Figure 7.3 shows a part of seismic profile 97-196, located parallel to the fjord axis (for location see Fig. 7.1). A ghost reflection makes it difficult to see the acoustic signature of the units. Profile B shows the position of core JM97-943-GC. JM97-943-GC penetrates units S3, S2 and S1.

The lowermost unit (943-A) of JM97-943-GC, interpreted as a till, is correlated to the uppermost part of unit S1, containing glacial sediments and landforms deposited prior to 11300 cal. years BP (Forwick & Vorren, 2005). A shell dated just above this unit to 11,230 cal. years BP in core JM97-943-GC supports the timing of deposition of the sediments before 11300 cal. years BP.

The overlying unit (943-B) in JM97-943-GC, interpreted as a glacimarine diamicton, was correlated to seismic unit S2 interpreted as glacimarine sediments by Forwick & Vorren (2005). Unit 943-B was dated to have been deposited between approximately 11230 and 11200 cal. BP. This result is similar to the suggestion of Forwick & Vorren (2005) for the age of unit S2.

Unit 943-C, with scattered clasts is correlated to sub-unit S2a with a lower acoustic transparency than the underlying unit but a higher acouctic transparency than the overlying unit (Fig. 7.2 & 7.3). The strong reflection defining the lower boundary (Fig 7.2), and at some places also the upper boundary of unit S3a is caused by a high contrast in acoustic impedance. The lack of internal reflections and transparency compared to the overlying unit of unit S3a in figure 7.3 indicates that significant lithological changes within the unit are absent. Unit 943-C contains very little clasts in contrast to the overlying and underlying units. This is possibly the reason for the high contrast in acoustic impedance between unit S3a and the overlying and underlying seismic units. Unit 943-C was deposited between c. 11200 and 7930 cal. years BP. This fits well into the interval between 11300 and 8800 cal. years BP, in which the sediments were interpreted to have been deposited (Forwick & Vorren 2005).

The uppermost two units in core JM97-943-GC consist of mud with increasing amounts of clasts (943-D) and mud with some scattered clasts (943-E). These two units were correlated to sub-unit S3b (Forwick & Vorren, 2005). This unit is characterised by a lower acoustic transparency. The distinct internal acoustic stratification may have been caused by a few intervals with increased amounts of clasts in unit 943-D (Fig. 5.10). Both units were deposited after approximately 7930 cal. years BP. This correlates well to the interpretation by Forwick & Vorren (2005) that the deposition of this uppermost seismic unit after 8800 cal. years BP.

The location of some recessional moraines identified on the Multibeam echo sounder data (Chapter 4.2) are indicated on figure 7.3.
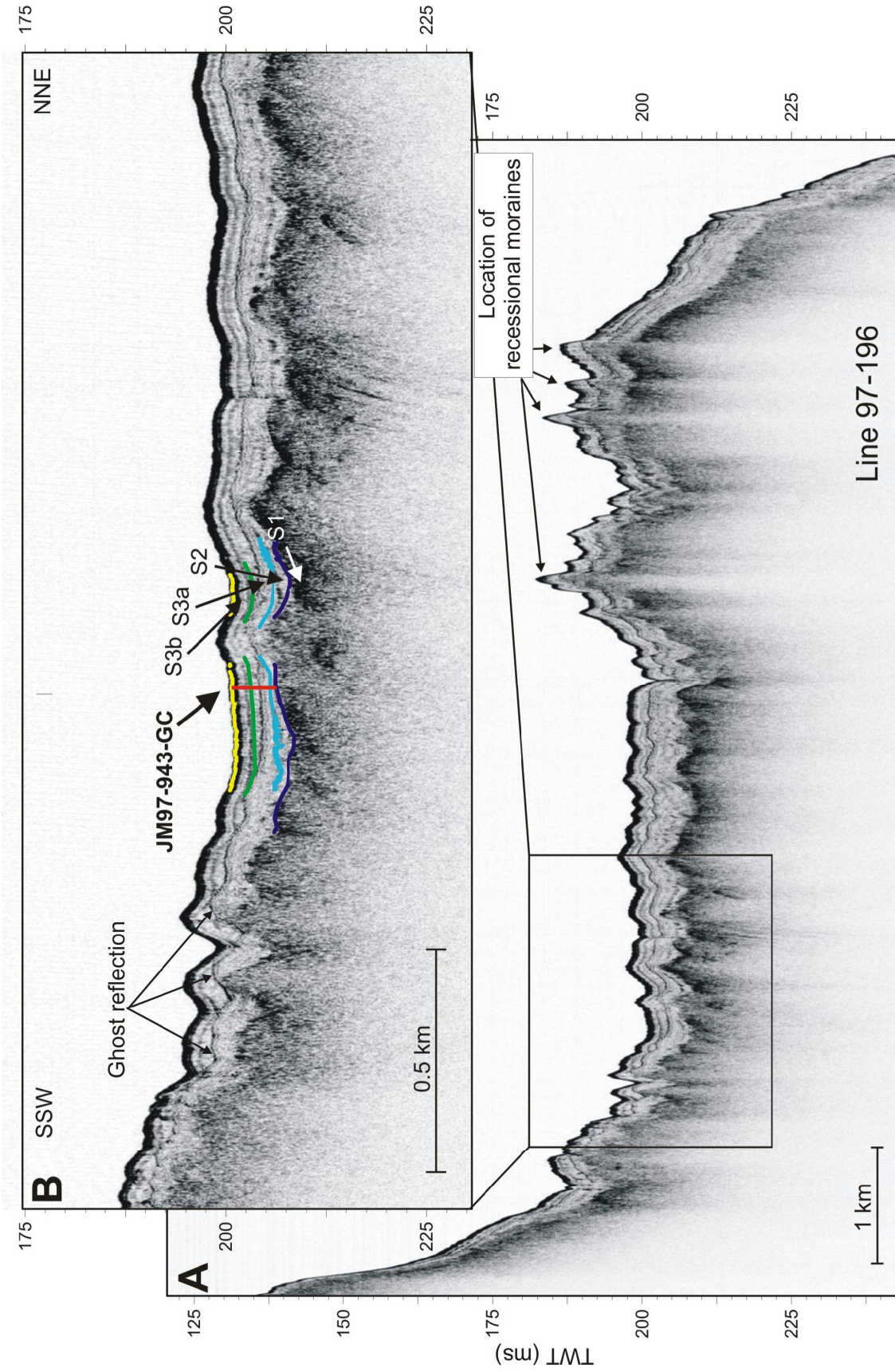
Fig. 7.3: Section of 3.5 kHz penetration echo sounder profile 97-196 in the middle of the fjord in profile A (Fig. 7.1). Profile B shows the position of JM97-943-GC and the interpretation by Forwick & Vorren (2005A). the different units are indicated. Recessional moraines are

74

8. Discussion

8.1 Fjord morphology

The fjord morphology is summarized in figure 8.1. The fact that some of the landforms are superimposed upon one another allows a reconstruction of the relative age of their deposition. The different morphological features are discussed below.

8.1.1 Glacial linear features

In the central/inner part of the fjord the linear features parallel to ice-flow show that during the time of their deposition the ice was coming from at least two different directions (Fig. 8.1B).

The majority of these features appear to have been subdued by younger sediments indicating that their formation did not occur recently. There are no indications of glacial cover in central/outer Billefjorden during the Holocene (this study). The maximum glacier extent during the Holocene was at the edge of the bedrock terrace during the Neoglacial maximum (Plassen et al., 2004). The linear features in the central part of the fjord (Fig. 8.1B) are therefore suggested to have been deposited during the Last Glacial.

The linear features in the inner part of the fjord, proximal to the glacier front (Fig. 8.1D) are assumed to have been formed during the Neoglacial advance, because they occur within the area of maximum Neoglacial ice extent.

Most of the linear features observed look like glacial lineations. Glacial lineations are elongated ridges and grooves oriented parallel to ice flow. The movement of ice over a sedimentary substrate often produces streamlined bedforms aligned parallel to the ice flow (Clark, 1994). However, a few linear features observed in the north-western part of the fjord are suggested to be crag and tail features and a few larger features with a teardrop shape are suggested to be drumlins (Fig. 8.1B; Benn & Evans 1998). Similar shaped features with corresponding sizes were found in Kongsfjorden (Howe et al., 2003). These features were suggested to have been formed during the last glacial, when the fjord was filled with ice. Mega-scale lineations were observed in several major fjords and cross-shelf troughs on the Svalbard margin (Ottesen et al., 2005, 2007), and interpreted to have been deposited from soft-sediment deformation at the base of fast-flowing ice streams (Tulaczyk et al., 2001; Dowdeswell et al., 2004B; Ó Cofaigh et al., 2005).

A

B — Glacial linear features (Last Glacial)

C — Recessional Moraines (Last Glacial)

D — Glacial linear features (Neoglacial)

E — Recessional moraines (Neoglacial)
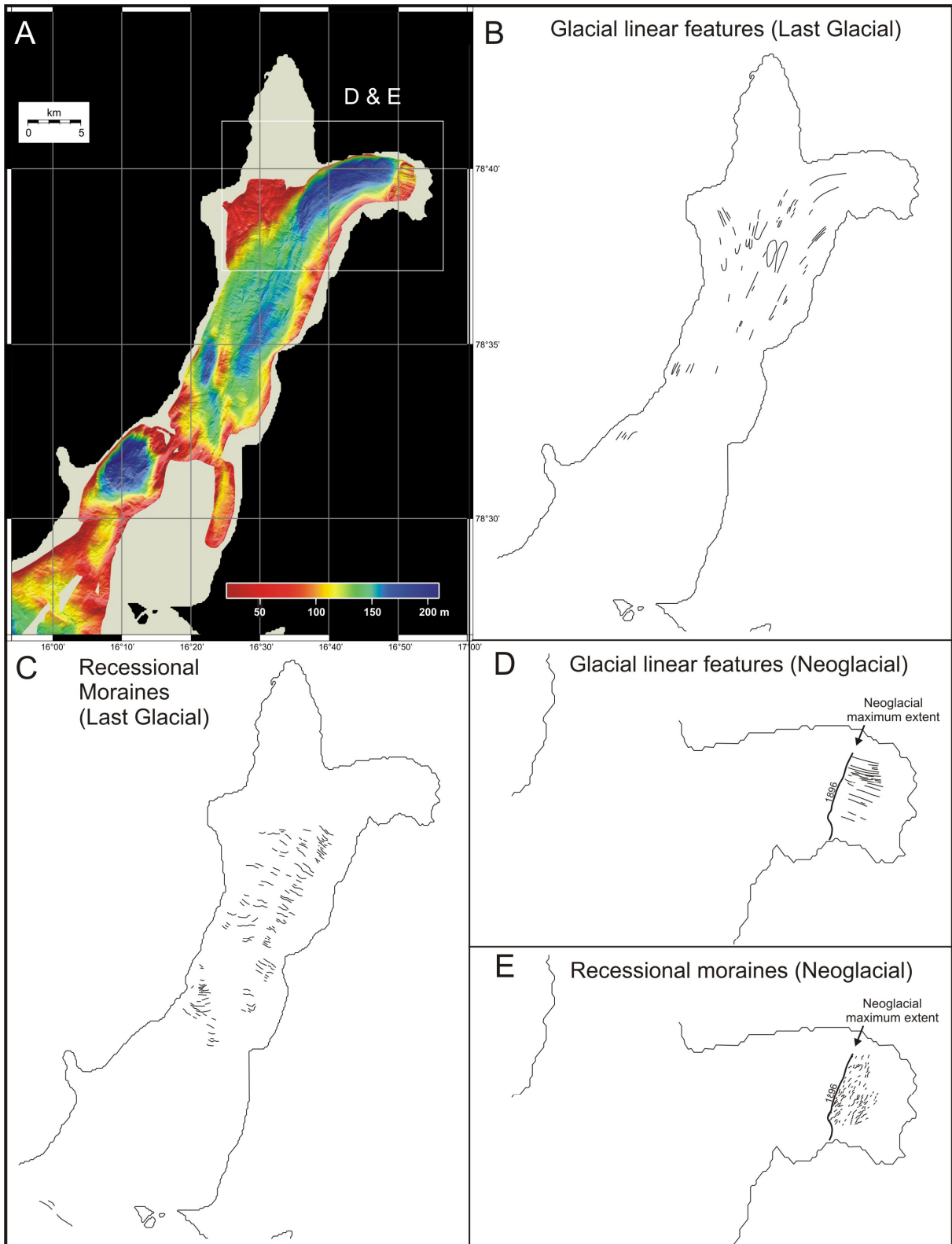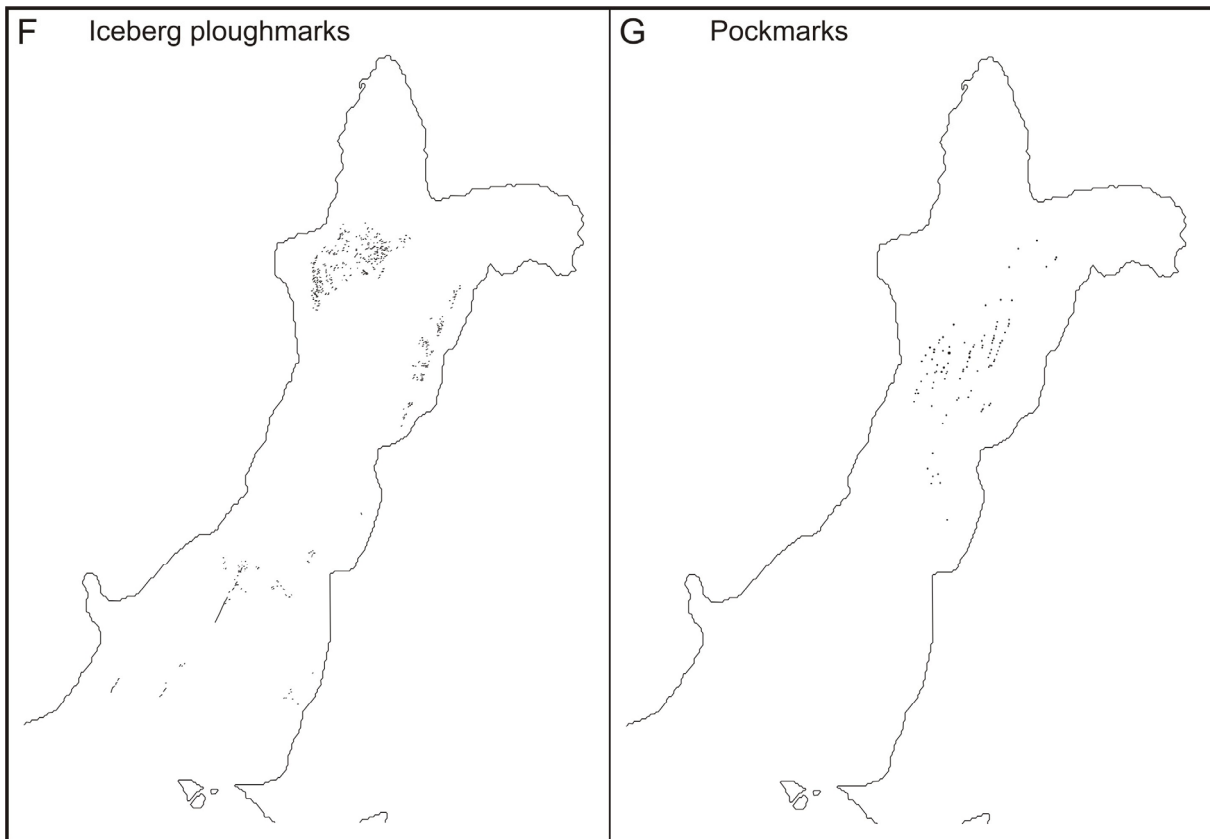
Fig. 8.1: The different morphological features and their distribution in the fjord. A: an overview map with the multibeam bathymetry of the fjord with the location of D and E; B: glacial linear features from the Last Glacial; C recessional moraines from the Last Glacial; D: Neoglacial glacial linear features; E Neoglacial recessional moraines with the maximum glacier extend documented by De Geer (1910); F: iceberg ploughmarks and G: pockmarks.

8.1.2 Moraines

The moraines in the central part of the fjord (Fig. 8.1C) superpose the linear features in figure 8.1B and are therefore assumed to be younger. They were interpreted to have been formed during the deglaciation into the fjord, during the final phase of the last glacial. In the inner part of the fjord, morainal ridges behind the Neoglacial terminal moraine at the edge of the bedrock terrace (Fig. 8.1E; Plassen et al., 2004) were most likely deposited during the retreat after the Neoglacial maximum extent of Nordenskiöldbreen before 1900 AD (Plassen et al., 2004). Both generations of moraines were interpreted as recessional moraines. The morainal ridges are however winding and discontinuous, and might thus have been deposited as crevasse squeeze ridges during possible surges of Nordenskiöldbreen.

Rhombohedral or polygonal ridge structures have been reported as landforms characteristic of surging glaciers in Svalbard (Solheim & Pfirman, 1985; Solheim, 1991; Boulton et al., 1996; Ottesen & Dowdeswell, 2006) and are suggested to be a product of soft sediment squeezing into crevasses formed at the glacier bed. No surges have been recorded for Nordenskiöldbreen

but according to a statistical analysis by Jiskoot et al. (2000) the possibility exists that it has surged. A possible reason for a lack of surge features in central/outer parts of Billefjorden is the bedrock terrace, and the steep slope to the inner fjord basin. In case the glacier would have surged at some point during the Holocene, it would most likely have developed a floating tongue, and would not have grounded beyond the break in the slope from the bedrock terrace to the basin in Adolfbukta (for location see figure 2.1; Dough Benn, pers. comm.). This suggests that the recessional moraines in the central part of the fjord are not likely to have been formed by a possible surge.

Series of small transverse ridges have been observed beyond a number of surging and non surging tidewater glaciers in Svalbard (Liestøl, 1976; Boulton, 1986; Whittington et al., 1997; Ottesen et al., 2005; Ottesen & Dowdeswell, 2006). They are not necessarily diagnostic of past surges because most of them are related to the most recent advance of Spitsbergen glaciers during the Little Ice Age and to subsequent ice retreat from about 100 yrs ago (Werner, 1993; Dowdeswell et al., 1998). Some of these sets with transverse ridges were interpreted as annual push moraines (Solheim, 1991; Whittington et al., 1997; Ottesen & Dowdeswell, 2006).

Because of the small chance that the glacier has deposited the moraines in the central part of the fjord during a post-glacial surge, and the fact that both generations of moraines (Fig. 8.1 C and E) appear to be more similar to the transverse recessional ridges than to the rhombohedral ridges described by Ottesen & Dowdeswell (2006) (Fig 8.2), it is suggested they are recessional moraines. These recessional moraines probably formed during halts or minor readvances within a period of general glacier retreat at the end of the last Glacial. Annual recessional moraines are produced during a late winter readvance, followed by a summer retreat (Boulton, 1986). A winter readvance of tidewater glaciers is a result of the suppression of iceberg calving due to the presence of winter shorefast sea ice (Ottesen & Dowdeswell, 2006). The discontinuity of the push moraines could be explained by differential movement of the glacier front and the varying amounts of material available (Solheim, 1991).

Whether the recessional moraines in the central part of the fjord are annual or not, cannot be concluded since no record of glacier frontal positions exists this far out into the fjord. However, between the position of JM97-943-GC and the basin in Adolfbukta (approximately 10 km), 28 recessional moraines were counted (Fig. 8.1C). These recessional moraines are suggested to have been deposited in the same time interval as unit 943-B (approximately 30 years), when the glaciers retreated into the fjord. A deposition within 30 years correlates very

well with the 28 recessional moraines counted in the central part of the fjord. These recessional moraines are therefore interpreted to be annual, and indicate a retreat of about 330 m/year at the end of the last Glacial. Glacial retreat velocities of probably up to several hundred meters per year during the final phase of the deglaciation have been reported for the Lyngen-Storfjord area (Corner, 1980) and of 330 m/year between the Egga-II and the Flesen events in the Andfjord-Vågsfjord area (northern Norway; Vorren & Plassen, 2002). Also in coastal areas on Svalbard it was concluded that the remaining ice-tongues in the fjord calved away quickly due to a sudden climatic warming (Lehman & Forman, 1992; Mangerud et al., 1992).
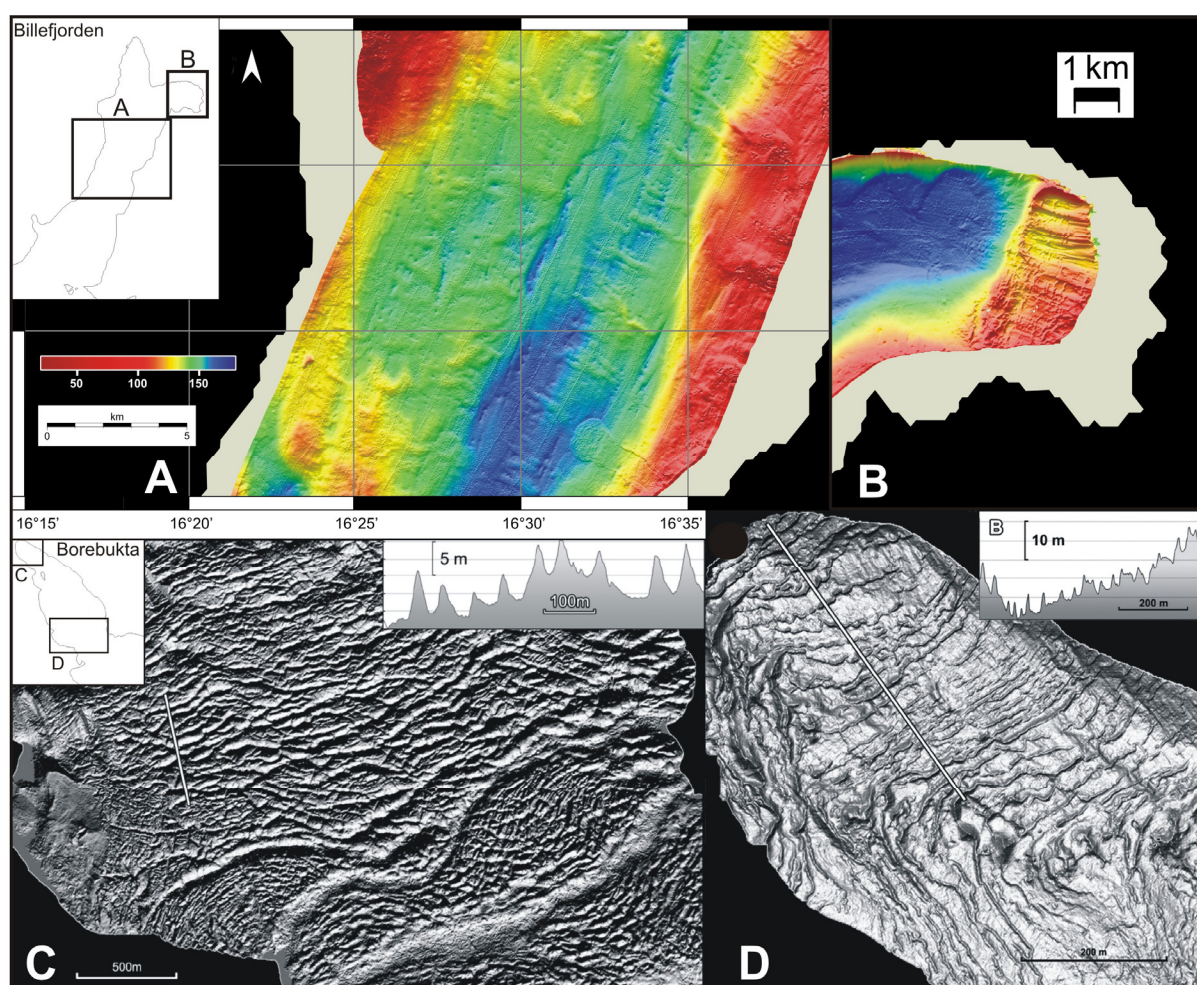

Fig. 8.2: A: Recessional moraines in the central part of Billefjorden, B: Recessional moraines in the inner part of Billefjorden (this study) C: Rhombohedral ridges in Borebukta (from Ottesen & Dowdeswell, 2006), D: Annual retreat ridges in Borebukta (from Ottesen & Dowdeswell, 2006; for location of Borebukta see figure 1.1).

The post-Neoglacial recessional moraines in the inner part of the fjord (Fig. 8.1E) cannot be counted back all the way to the present glacier front because of the limiting extent of the multibeam data. They are however assumed to be annual recessional moraines as well.

8.1.3 Iceberg ploughmarks

The 'fresh' appearance of the ploughmarks in figure 8.1F indicates that they are relatively young. The fact that they only occur in the shallow areas in the fjord indicates that they were generated by relatively small icebergs, most likely not from the last Glacial. They were therefore interpreted to have been generated at or just after the Neoglacial maximum extend of Nordenskiöldbreen around 1900 AD (Plassen et al., 2004).

Compared to iceberg ploughmarks described by King (1976), Solheim (1991), Andreassen et al. (2007), the iceberg ploughmarks in Billefjorden are relatively short. Their depths (2-5 meters) and widths (30-50 meters) are average on shelf areas (Vorren et al., 1983). The iceberg ploughmarks indicated in figure 8.1F are on average 30-80 meter long. However towards the mouth of the fjord three up to 2 km long iceberg ploughmarks were observed. In the southwestern Barents Sea, iceberg ploughmarks can be followed for up to 20 km (Andreassen et al., 2007). The magnitude of iceberg-ploughing depends on size of the iceberg, drifting velocity, bottom relief and the shear strength of the bottom sediments (Vorren et al., 1983). Wind and currents forcing on an iceberg appear to be of comparable importance on its drift (Smith & Banke, 1983). A possible explanation for the short iceberg ploughmarks might be the lack of bottom currents in Billefjorden. The longer ploughmarks towards the mouth of the fjord could be the result of an increase in windforce on the iceberg, but could probably also be related to a gradual increase in water depth in this area. A gradual increase in waterdepth towards fjord probably decreased the friction of the sediments on the icebergs, resulting in longer ploughmarks.

8.1.4 Pockmarks

The pockmarks occur only in the central part of the fjord, north-east of the Billefjorden fault zone (Fig. 8.1G). They are sharp outlined, and not smoothed by a sediment cover. Most of them are linearly aligned and occur within the linear grooves. The fact that they are so sharply outlined and the lack of infilling of the pockmarks suggests that fluid escape occurs frequently (Plassen & Vorren, 2003). Pockmarks often appear in muddy formerly glaciated areas (Kelley et al., 1994) where thick glacigenic sediments may play an important role by trapping gas that would escape more rapidly in other settings. A possibility for the generation of the pockmarks in Billefjorden might be the seepage of thermogenic gas along the Billefjorden fault zone.

Thermogenic deep earth gas from the mantle may migrate to the surface along tectonic lineaments from lower levels in the earth crusts (Söderberg & Flodén, 1991). In the northern Stockhom archipelago, Baltic Sea, thermogenic gas accumulations are found in pockmarked glacial clay along still active tectonic lineaments in the crystalline basement (Söderberg and Flodén, 1991). Passive seepage of thermogenic gas is particularly strong at major tectonic lineaments west off Spitsbergen (Knies et al., 2004). The Billefjorden fault zone is one of these tectonic lineaments. Another possibility that cannot be excluded is the presence of petroleum related gas in the sediments generating the formation of pockmarks. The rocks underneath the fjord mainly consist of the sedimentary rock in the Billefjorden trough (Chapter 2.2) and two exploration wells in the north of the fjord revealed the presence of oil (Dallmann et al., 2004).

Biogenic gas generated in the post-glacial sediments in this area is not very likely since the organic content of the sediments is very low (Fig. 5.4, 5.8, 5.13; Solheim & Elverhøi, 1985).

Since no seismic data of the pockmarks in the area was available, the source generating these pockmarks cannot be concluded. However the most likely source is the seepage of thermogenic gas. First of all because the seepage of thermogenic gas has been observed to be particularly strong at marjor tectonic lineaments west off Spitsbergen (Knies et al., 2004), and second because most of the pockmarks occur just besides the Billefjorden fault zone, around the axis of the Billefjorden through.

The reason for most of the pockmarks to occur aligned in the linear grooves is probably the presence of fine sediments in these grooves. Data from south-east of the Hopen Island in the Barents Sea (Solheim & Elverhøi, 1985) show higher concentrations of pockmarks within relict iceberg ploughmarks. These ploughmarks were formed during the Late Weichselian deglaciation period, as the ice retreated, and grounding icebergs scraping long furrows into the till underneath. The pockmarks were concluded to have been caused by the seepage of thermogenic gas and were interpreted to occur within these iceberg ploughmarks because of the occurrence of fine grained sediments (Solheim & Elverhøi, 1985). Also most and the largest pockmarks in Bellfast Bay, in the western Gulf of Maine, occur above a channel cut into glacial marine material and filled with thicker Holocene sediments (Kelley et al. 1994). Soft silty clays seem to provide the ideal sediments for pockmark formation, but examples have been reported from coarser and finer sediment types as well (Judd & Hovland, 2007).

8.2 Sedimentary environments

Because of low bottom current activity in Billefjorden, the clasts coarser than 1 mm are regarded as IRD (compare with Hald et al. 2004).

8.2.1 Accumulation rates

Elverhøi et al. (1995A) recorded a higher accumulation rate for the late Holocene in the Isfjorden area, and attributed this to the regrowth of glaciers. High accumulation rates in the early Holocene, immediately after deglaciation, lower values in the mid to late Holocene, and increasing values during the past 1,2 cal. ka BP were found in central Isfjorden (Forwick & Vorren, 2005A). The pattern of accumulation rates in van Mijenfjorden (for location see Fig. 1.1; Hald et al., 2004) shows the highest accumulation rates during the early Holocene, the lowest during the mid Holocene and increase during the late Holocene (Hald et al., 2004). A core from Billefjorden investigated by Svendsen & Mangerud (1997) showed a similar pattern (Fig. 8.3). Following deglaciation starting around 10 000 cal. BP, accumulation rates of up to 100 cm/cal. ka decreased to accumulation rates of 20 cm/cal. ka and remained constant during the early and the mid-Holocene. This low accumulation rate led to the conclusion that the glaciers were small or absent during this interval (Svendsen & Mangerud 1997). An increase in accumulation rate to about 60 cm/cal. ka at about 2800 cal. BP is attributed to glacier expansion. It was followed by a decrease in the late Holocene, and a subsequent increase during the last few hundred years correlated with the Little Ice Age expansion of Nordenskiöldbreen (Svendsen & Mangerud 1997).

Similar trends in accumulation rates were found in core JM97-943-GC (Fig. 8.3). High accumulation rates during the deglaciation (800cm/cal. ka), and a subsequent decrease in the early Holocene (to 59 cm/cal. ka) correlates well to the pattern of accumulation rates reported from Billefjorden and the Isfjorden area (Svendsen & Mangerud, 1997; Elverhøi et al., 1995A; Forwick & Vorren, 2005A). The accumulation rates in core JM97-943-GC are higher than reported by Svendsen & Mangerud (1997) because this core contains 460 cm of sediments covering the same timespan as the approximately 270 cm of sediments in the core described by Svendsen & Mangerud (1997).

A further decrease in accumulation rates to around 24 cm/cal. ka during the mid-Holocene does not correlate well with the accumulation rates reported by Svendsen & Mangerud (1997). In their core accumulation rates of 20 cm/cal. ka were already reached in early Holocene and stayed constant until about 2800 cal. BP (Fig. 8.3). This difference could be

attributed to several factors, possibly differences in dating materials used (foraminifera by Svendsen & Mangerud., 1997 and shells in this study) or because of different locations of the sediment cores. During the late Holocene, the accumulation rates in JM97-943-GC increase again to 39 cm/cal. ka. The variations in accumulation rates reported by Svendsen & Mangerud in the late Holocene are not visible in JM97-943-GC due to a lack of dates in the uppermost part of the core (Fig. 8.3).
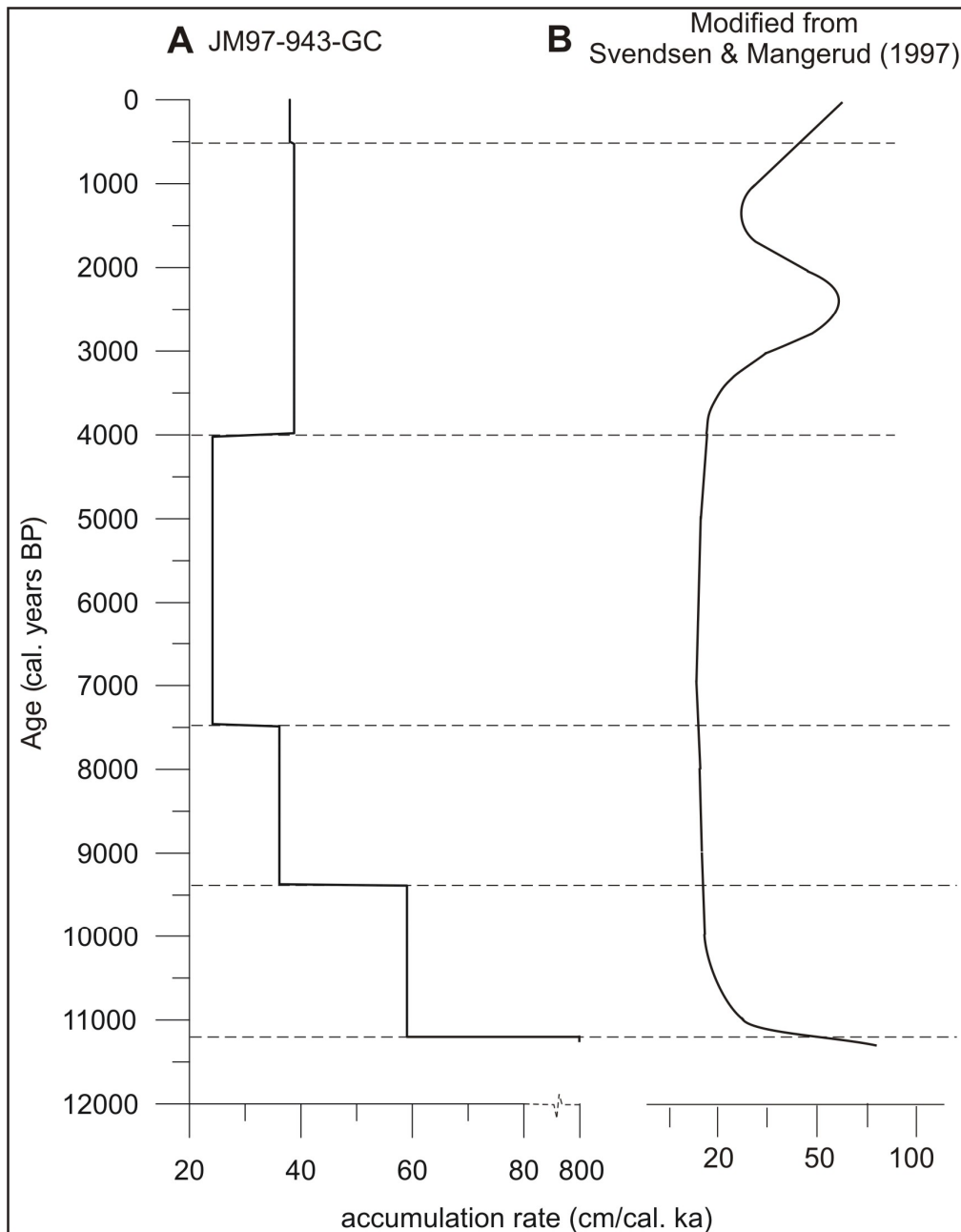

Fig. 8.3: A: accumulation rates in centimetre per 1000 calendar year of core JM97-943-GC (this study). B: accumulation rates in centimetre per 1000 calendar year of core NP-90-01 GC1, modified from Svendsen & Mangerud, (1997).

8.2.2 Sedimentary environments

Subglacial meltwater streams and calved icebergs provide the main sources of water and sediment to the Spitsbergen fjord systems (Dowdeswell, 1989). In Kongsfjorden (see for location Fig. 1.1) sedimentation is strongly influenced by the glaciers and by the seasonal generation of sea ice (Howe et al., 2003). The largest sediment input into Billefjorden occurs from Nordenskiöldbreen (Svendsen & Mangerud, 1997). Other important sediment sources into the fjord are glacier-fed river systems in Petuniabukta, Mimerbukta, Kapp Ekholm, Skansebukta and Phantomodden (for location see figure 2.1), and possibly the input of aeolian material from the valleys. Aeolian input is e.g. regarded to be significant in Adventfjorden (Christiansen & Hormes, 2005).

The distribution of sediments in the fjord is mainly controlled by the seafloor morphology and the distance to sediment sources. An important distribution mechanism of material in the fjord is rafting of material by icebergs and sea ice. Sediment dispersal patterns of icebergs and sea-ice relate mainly to water mass structure, fjord circulation including effects of Coriolis deflection, as well as wind forcing (Syvitski et al., 1987). The accumulation rates in the fjord increase in the vicinity of the different sediment sources, and are generally higher in basins than in shallow areas (Forwick & Vorren, 2005A).

Sedimentation in areas with subpolar glaciers like Spitsbergen is dominated by settling of suspended material supplied from meltwater (Elverhøi, 1984). The melt water plume has a tendency to rise to the surface of the marine water column because it is less dense than the normal-salinity sea water (Syvitski et al., 1987). Fine-grained sediments settle from these turbid surface overflows in Svalbard fjords where concentrations up to 500 mg l^{-1} have been measured (Elverhøi et al., 1980; Elverhøi et al., 1983).

The relative importance of sedimentation by iceberg rafting may increase in areas more distal to the glacier front if a significant number of icebergs is transported quickly away from the glacier front, because the sedimentation from glacier-derived meltwater decreases significantly with distance from source (Dowdeswell & Dowdeswell, 1989).

The Holocene accumulation rates in Billefjorden are continuously highest in Adolfbukta (for location see figure 2.1; Forwick & Vorren, 2005A), in front of Nordenskiöldbreen. As shown on the seismic data (Fig. 7.2 & 7.3), the sediments often drape the underlying topography. This can be related to low bottom current activity (Syvitski et al., 1987). In fjords in western Norway 90 % of the material is considered to have been deposited during the deglaciation of the late Weichselian ice sheet (Aarseth, 1997). However, in Billefjorden the majority of the sediments have been deposited during the Holocene (see e.g. Fig 7.2 & 7.3; Forwick &

Vorren 2005A). Possible explanations for this could be the rapid deglaciation in Billefjorden (see above), or differences in thickness and basal regime of the ice-sheets.

8.2.2.1 Basins

Basins in Billefjorden act as sediment traps (Forwick & Vorren, 2005A; see also Fig. 7.1). Most of the sediment input into the basin in Adolfbukta is presumably derived from Nordenskiöldbreen, but also from rivers draining into Mimerbukta and Petuniabukta (for location see Fig. 2.1). Resedimentation can occur in the deeper basins or along the fjord slopes, due to mass-transport processes like debris flows and turbidites (Howe et al., 2003). Core JM97-941-GC contains 17 turbidites.

A core from a small basin north of Ny-Ålesund (Kongsfjorden, for location see figure 1.1) comprises numerous sandy strata interpreted as turbidites (Howe et al., 2003). These strata are suggested to reflect slope instability within the fjord, possibly as a result of the high sediment supply producing oversteepened slopes in the basin and their subsequent failure. It is suggested that the turbidites in core JM97-941-GC are generated by the same process. The finer material in between the turbidites was most likely deposited from settling of material in suspension.

Another resedimentation process that can contribute to the sediment input into the basins is winnowing from the shallow areas (Vorren et al., 1984). The thick sediment package in the inner fjord basin can be explained through the fact that the basin acts as a sediment trap (Desloges et al., 2002; Plassen & Vorren, 2002), the proximity of the basin to the sediment sources mentioned and resedimentation processes.

In the distal parts of the fjord, medium high accumulation rates are explained by comparatively high sediment input from rivers (Plassen et al., 2004). In the central parts of the fjord, where JM97-943-GC was retrieved, most of the material is probably deposited by settling from suspension from river borne material. The coarser material is regarded to have been rafted from sea ice or icebergs.

8.2.2.2 Slopes

On the steeper fjord sides and the slope marking the break between the bedrock terrace in the the basin off Nordenskiöldbreen, mass-transport deposits dominate. A large debris flow on the slope between the bedrock terrace and the basin was described by Plassen et al. (2004; Chapter 4.4). The sediments in the top of this debris flow were retrieved in core JM02-979-GC, and consist of redeposited glacimarine sediments, a turbidite and highly deformed mud, most likely slump deposits.

8.2.2.3 Shallow environments

Sediment input into the shallow areas in the fjord (except from the shallow area in front of Nordenskiöldbreen) occurs mostly from rivers, but IRD input should not be excluded.

These shallow environments are influenced by icebergs and sea-ice. Iceberg ploughmarks cover most areas between 100 and 20 m water depth (Fig 8.1E). These icebergs can disturb and redeposit the sediments in these shallow areas by ploughing, but most likely also contribute sediments upon melting. The stirring action of the icebergs creates turbulence and resuspension of the sediments (Vorren et al., 1983).

Also sea-ice may cause resuspension and adfreezing of sediments at depth shallower than about 50 m (Vorren et al., 1983). Another process important in these shallow environments could probably be winnowing of the sediments, possibly by tidal currents (Syvitski, 1989).

In the shallow area in front of Nordenskiöldbreen, the glacier is regarded to be the major sediment source. Common sedimentation processes in the vicinity of a grounding-line system include (Powell & Molnia, 1989; Powell and Alley, 1997; Elverhøi et al., 1980):

- Gravity flows beyond the grounding line.

- Rapid sedimentation from a sediment plume rising up from the grounding line or from supraglacial and/or englacial riviers.

- Pushing and thrusting of glacial, fluvial and marine sediments at the grounding line.

- Iceberg rafting.

8.2.3 Mineralogy record

Changes in the mineralogical compositions of the sediments can be used as an indication of glacial activity in Billefjorden (Svendsen & Mangerud, 1997). As stated before, the occurrence of mica and quarts minerals in the sediments is regarded to indicate Nordenskiöldbreen as the provenance area. Input from the sides of the fjord mainly consists of limestones and dolomite (Dallman et al., 2004).

The till comprising unit 943-A is characterized by high percentages of illite & mica and low percentages of ankerite and dolomite (Fig. 8.4). This is suggested to indicate that Nordenskiöldbreen is the main source area. Nordenskiöldbreen is therefore regarded as the most active glacier contributing to the ice-stream draining through Billefjorden

Unit 943-B was interpreted to have been deposited in a glacio-marine environment when the glacier was retreating. After a peak of maximum input, the decreasing percentages of illite & mica indicate that the influence of Nordenskiöldbreen on the sedimentation at the core site gradually decreased, as the input of sediments from the fjord sides (calcite and ankerite &

dolomite) gradually increased. Unit 943-C was deposited in a period with little glacier activity. This is reflected by increasing percentages of ankerite & dolomite and decreasing percentages of illite & mica. These trends continue in the lower part of Unit 943-D, characterized by higher amounts of IRD. The XRD results however only show an increase in the percentage of illite and mica halfway the unit, at c. 5470 cal. years BP. This is suggested to indicate that most of the IRD in the lower part of this unit was not derived by iceberg rafting from Nordenskiöldbreen, but most likely from sea ice. In the upper part of the unit the input of material from Nordenskiöldbreen increases, indicating in increase in calving rate of the glacier. The percentage of ankerite & dolomite decreases in the upper part of the unit. This could point towards a decrease in IRD coming from the fjord sides carried by sea ice.

The percentage of illite and mica further increases in the lowermost part of unit 943-E, the lack of IRD in this unit however points towards the importance of other transport mechanisms transporting material from Nordenskiöldbreen out into the central part of the fjord. This material could have been transported in a sediment plume carrying fine material from Nordenskiöldbreen in suspension. The input of ankerite and dolomite have relatively low and stable values in unit 943-E.
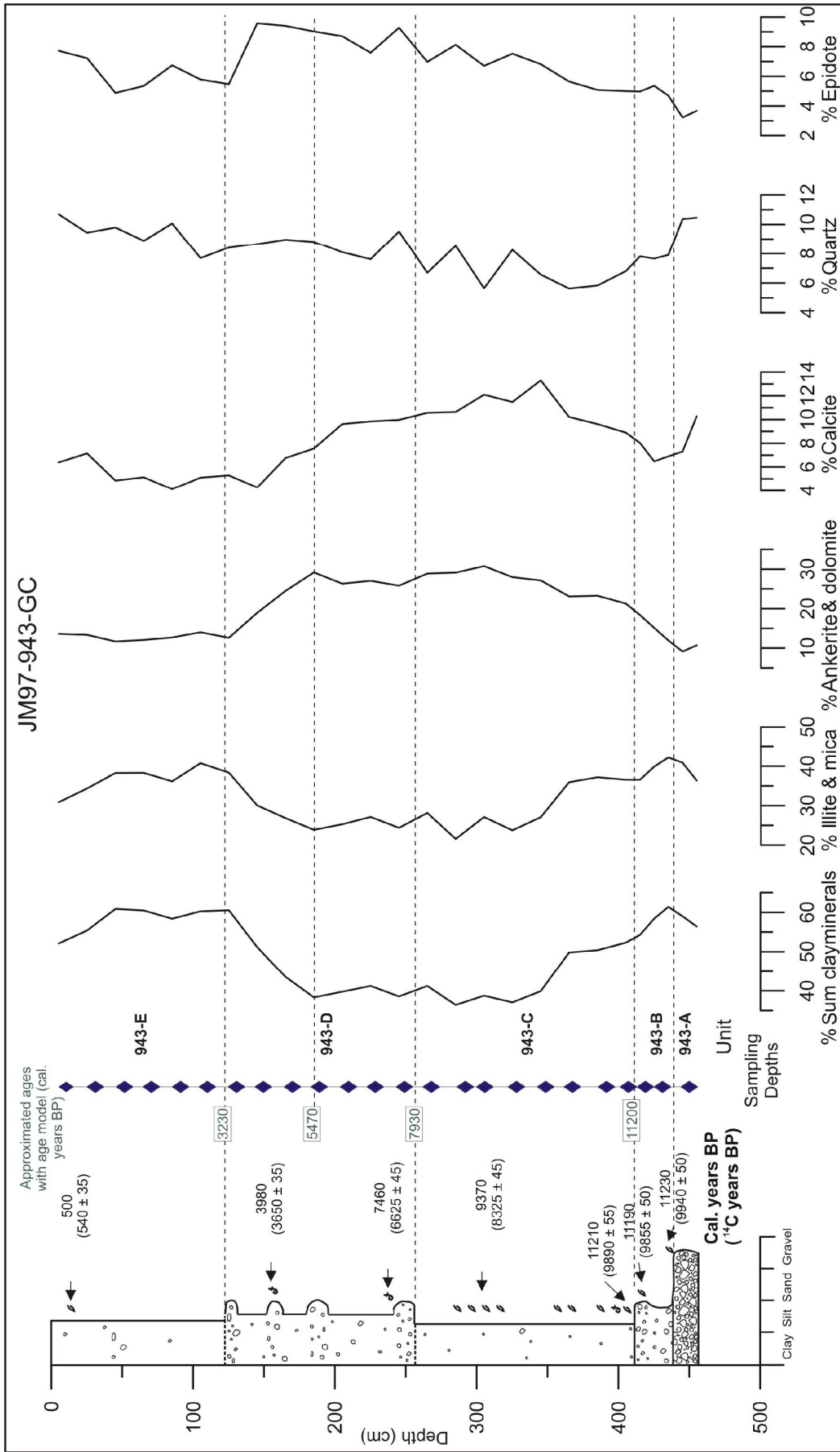
Fig. 8.4: XRD values of the selected minerals from core JM97-943-GC, with the radiocarbon dates in cal. years BP and the approximated ages of the unit boundaries and the increase in illite & mica halfway unit 943-D in cal. years BP. The ages were approximated assuming constant accumulation rates between the radiocarbon dates. The % sum clay minerals consists of: smectite & montmorillonite, mixed layered clays, illite & mice, kaolinite and chlorite. The percentage of illite & mica indicates the percentage of the total sample, not only of the percentage within the clay minerals.

8.2.4 Mass-transport deposits

8.2.4.1 Distribution and chronology

Slope failures in fjords are in general controlled by the topography, the supply of material, the physical properties of the sediments and the triggering mechanism. Triggering mechanisms include sediment loading, earthquakes, waves, sea level fluctuations, climate change and anthropogenic activity (Syvitski et al., 1987). Slope failures in Svensksunddjupet (for location see Fig. 1.1) are suggested to have been caused by earthquake activity due to rapid isostatic uplift, excess pore pressure due to relative sea-level fall, the possible presence of gas and environmental changes, respectively (Forwick & Vorren, 2007).

Mass-transport deposits (MTD's) in Billefjorden are indicated on figures 4.5 and 4.7.
Figure 8.5B shows a part of seismic profile 97-210, oriented perpendicular to the fjord axis (see for location Fig. 8.5C). The mass-transport deposit at the base of the eastern slope of the fjord is acoustically transparent and does not have any internal reflections. It is therefore interpreted to have been deposited during one single mass-transport event. The mass-transport appears to lie directly above the glacimarine sediments. This indicates that it has been deposited shortly after the deglaciation of the central parts of Billefjorden.

Mass-transport deposit B in figure 8.5C can be clearly identified on the multibeam data and is therefore interpreted to be younger than mass-transport deposit in figure 8.5B. Its 'fresh' appearance is suggested to indicate that it was deposited during the later Holocene.

Acoustic stratification in the inner basin on the seismic profile in figure 7.2 and the turbidites in core JM97-941-GC retrieved from this basin indicate mass-transport activity in this basin most likely throughout the whole Holocene.
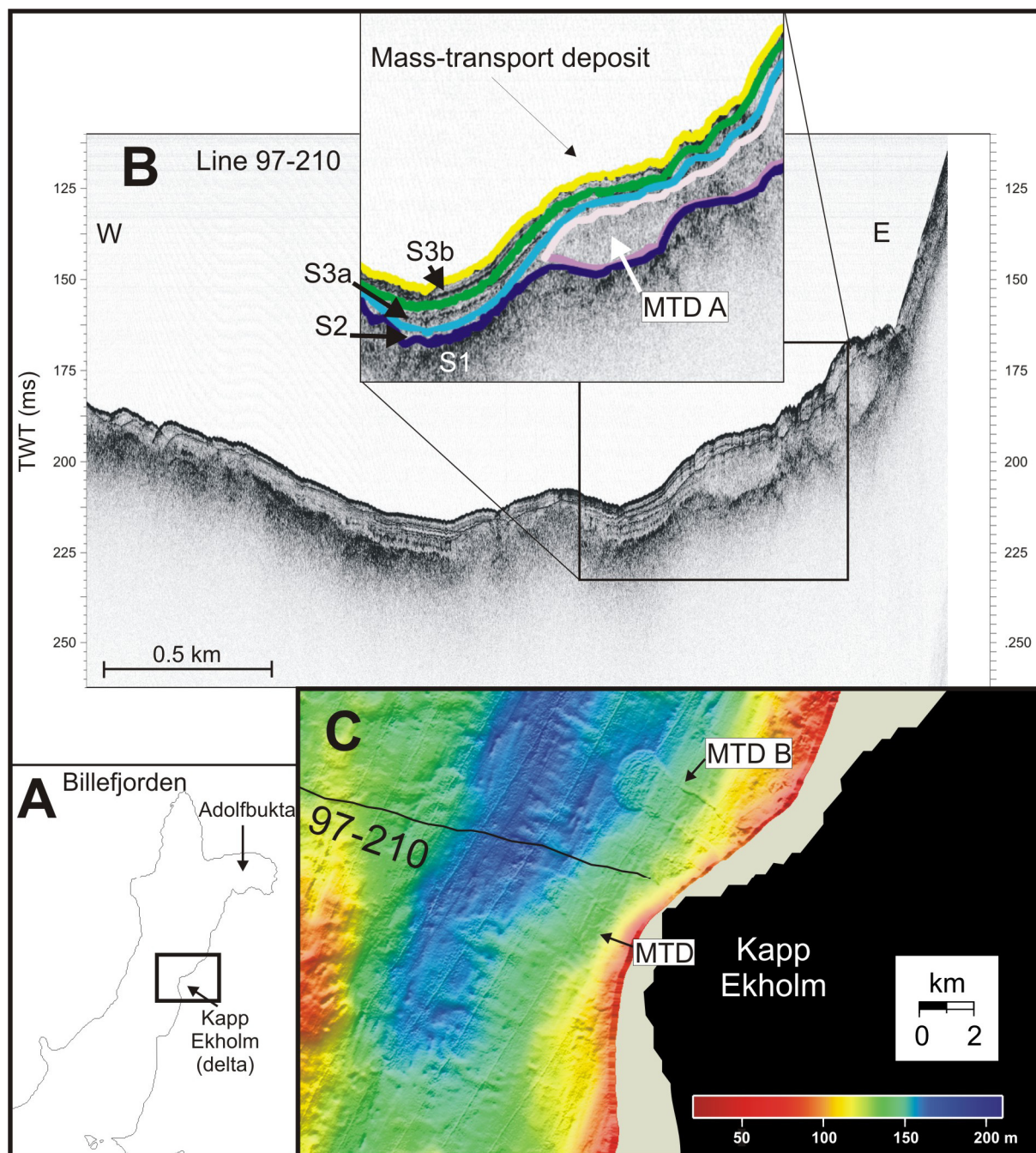
Fig. 8.5: A shows the location of the multibeam bathymetry data shown in C. B shows a part of seismic profile 97-210 in the central parts of the fjord (interpretation based on Forwick & Vorren, 2005; for location see C). In figure C two younger mass-transport deposits are indicated.

A mass-transport deposit at the base of the bedrock terrace in the inner part of the fjord was earlier described by Plassen et al. (2004) and interpreted as a debris lobe (Fig. 8.6). The debris lobe was inferred to have been deposited during the Neoglacial maximum around 1900 AD when Nordenskiöldbreen was located at the edge of the bedrock terrace (Fig 8.6).

90

An internal reflection suggests a subdivision of the debris lobe (Plassen et al., 2004). Core JM02-979-GC penetrates the top of this debris lobe. The core data indicate that more than two slope failures occurred on the slope off Nordenskiöldbreen, and that the proximal part of the debris lobe might still be active as suggested by Plassen et al. (2004). This shows that the pattern of resedimentation off glacier fronts is complex i.e. a number of different mass-transport mechanisms occur (see also Powell, 2005).
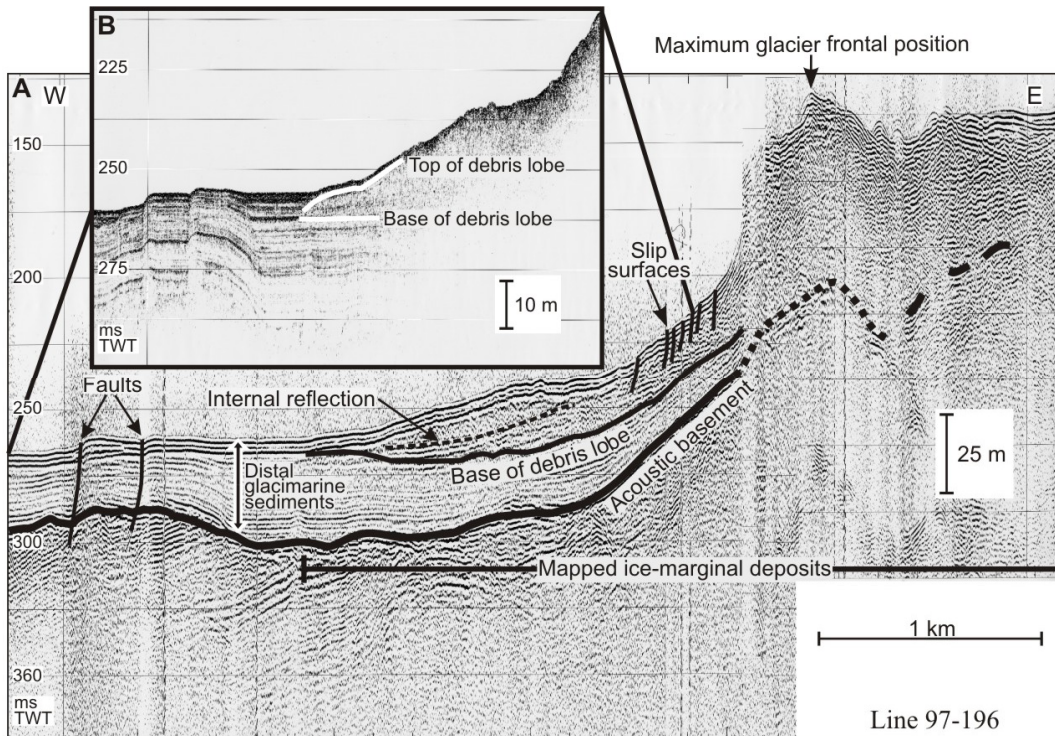
Fig. 8.6: A shows a sparker profile of the ice-marginal deposits in the inner part of the fjord. Slip surfaces and faults are indicated. B shows a 3.5 kHz profile of the debris lobe and the distal glacimarine sediments. From Plassen et al. (2004).

8.2.4.2 Triggering mechanisms

The available data suggests that mass-transport activity in Billeforden occured throughout the Holocene. There might have been an increase in mass-transport activity shortly after the deglaciation of the fjord, because high rates of isostatic uplift possibly caused seismic activity (Stewart et al., 2000; Forman et al. 2004; Forwick & Vorren, 2007). It has also been suggested that most of the mass-transport activity in fjords in western Norway took place during the deglaciation, i.e. the period of highest sediment supply, but that slope failures occurred throughout the entire Holocene (Aarseth et al., 1989; Bøe et al. 2000). This is also the case in Billefjorden. The fact that three mass-transport deposits (Fig. 8.5) are released in

91

the proximity of the Kapp Ekholm delta indicates that the supply of material is an important factor in the trigger mechanism of mass-transport deposits. Side-entry deltas are sites of intermittent slides and slumps where the frequency is related to the development of oversteepened slopes (Syvitski et al., 1987).

The debris lobe coming down from the bedrock terrace in Adolfbukta is characteristic for the areas just beyond the Neoglacial maximum extent, or maximum extents of later surges/advances of several glaciers in the Isfjorden area (Elverhøi et al., 1995B; Boulton et al., 1996; Plassen et al., 2004; Ottesen & Dowdeswell, 2006). The debris lobe sediments are inferred to be glacigenic diamicton and reworked older glacimarine deposits that were pushed and extruded from beneath the glacier at the end of a glacial advance or surge, and during stagnation (Plassen et al., 2004).

8.3 Deglaciation and Holocene history of Billefjorden

The division into 5 different sedimentary periods is based on the different units and dates of core JM97-943-GC taken in the central part of Billefjorden (Fig. 7.1). With an age model, the dates of the unit boundaries were approximated (Fig. 8.7), assuming constant accumulation rates between the radiocarbon dates.

The radiocarbon ages from other publications used in this chapter were calibrated to calendar ages for a better correlation (Table 8.1).
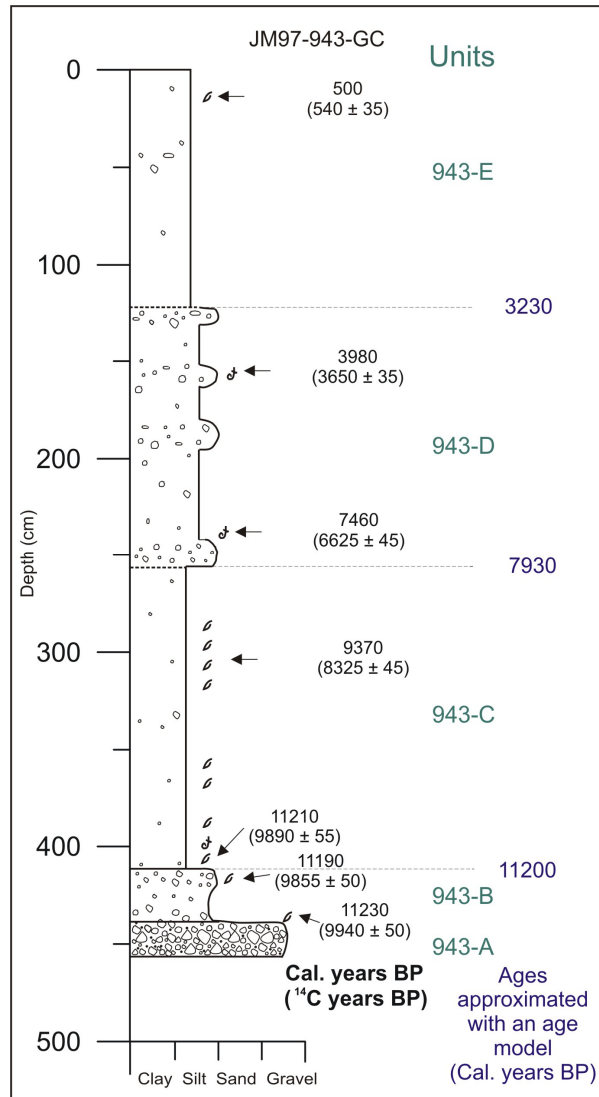
Fig. 8.7: Lithological log and the calibrated cal. years BP/ ^{14}C years BP of JM97-943-GC, with in green the units and in blue the ages of the unit boundaries approximated with an age model, the ages are based on assumed constant accumulation rates between the radiocarbon dates.

8.3.1 Deglaciation, > 11230 cal. BP, unit 943-A

Unit 943-A comprises a stiff diamicton with a high clast content, interpreted as a till. A paired shell just above this till was dated and calibrated to 11230 cal. yr BP (Table 6.1). This till is correlated to the till found by Boulton (1979) on sparker profiles in the mouth of Billefjorden. The till interpreted by Boulton (1979) has a disordered seismic texture, overlain by an up to 8 m thick surface layer displaying a parallel stratified seismic texture. Boulton (1979) correlates this till and the overlying parallel stratified sediments, which are known from cores to consist of fine-sandy and clayey silts, to the last glacial till (unit 6) and the overlying fine silty sand (unit 7) of the Kapp Ekholm sections. Only the lower part of the fjord sediments can be correlated to unit 7 of the Kapp Ekholm sequence, because the Kapp Ekholm sequence has

been uplifted above sea-level during the largest part of the Holocene (Boulton, 1979). The till described in this study (unit 943-A) can also be correlated to the Kapp Ekholm sections based on the lithology and radiocarbon dates. Dates on shells just above this last glacial till give a concluded age approximately 11290 cal. years BP (Table 8.1; Mangerud & Svendsen, 1992). Boulton (1979) interprets this till to have been deposited by a glacier readvance terminating in the mouth of the fjord, termed the Billefjorden stage. This interpretation is based on a radiocarbon date at the base of the till at Kapp Ekholm (unit 6) of approximately 12580 cal. BP (Table 8.1) and a date of approximately 11100 cal. BP (Table 8.1) above the till. In more recent investigations by Mangerud and Svendsen (1992) this date was not reproduced. Hence they question Boulton's interpretations. Forwick & Vorren (2005B) suggested that Billefjorden was covered by glacier ice during the Younger Dryas, and also in this study, no evidence for such an advance was found.

Table 8.1: Radiocarbon ages and approximated calibrated ages used in chapter 8.3. All the radiocarbon ages were corrected for a marine reservoir effect of 440 (Mangerud & Gulliksen, 1975) before calibration. For calibration the program Calib Rev. 5.0.1(Stuiver & Reimer, 1993) and the dataset *04.14C* by Hughen et al. (2004) were used.

Core/ Location	Lab. no	Depth	Material	^{14}C age (^{14}C yr BP)	Cal. age BP (2σ)	Cal. age BP (1σ)	Cal. age BP peak distr.	Reference
Kapp Ekholm			Shells	10000	11195 - 11671	11214 - 11411	11290	Mangerud & Svendsen, 1992
Kapp Ekholm			Shells	11028 ± 440	11598 - 13757	12307 - 13355	12580	Boulton, 1979
Kapp Ekholm			Shells	9709 ± 90	10702 - 11212	10896 - 11175	11100	Boulton, 1979
90-03-PC1	TUa-441	237-245	Foram (several species)	10560 ± 75	12170 - 12763	12329 - 12662	12400	Svendsen et al. 1996
90-01-PC1	TUa-187	188	Mollusc (*Lep. Coeca*)	9730 ± 110	10660 - 11256	10888 - 11200	11120	Svendsen et al. 1996
Erdmann flya	T-6535		*Modiolus*	8670 ± 90	9487 - 10039	9545 - 9839	9680	From Salvigsen et al., 1992
Dickson fjorden	T-4411		*Modiolus*	7850 ± 130	8381 - 9050	8541 - 8908	8660	Salvigsen et al., 1992
Kaffiøyra	Gd-1255		*Mytilus*	9630 ± 130	10582 - 11190	10745 - 11110	11020	From Salvigsen et al., 1992
Mytilus bekken	U 126		*Mytilus*	3810 ± 90	3948 - 4492	4089 - 4365	4220	From Salvigsen et al., 1992

Svendsen et al. (1996) also describe a till found in two cores from Billefjorden and in some cores from the shelf west of Svalbard. Like unit 943-A from core JM97-943-GC found in this study, this till is homogenous, poorly sorted and has a firm consistency (Svendsen et al. 1996). It is concluded that it all concerns the same till, interpreted to have been deposited before the ice front retreated into Billefjorden around 11290 cal. BP (Table 8.1; Mangerud et al., 1992; Svendsen et al., 1996), and 11230 cal. years BP (this study).

8.1.2 Gacimarine environment, c. 11,230 - 11,200, unit 943-B

Unit 943-B from core JM97-943-GC is similar to the laminated mud with dropstones described by Svendsen et al. (1996) and interpreted as laminated (glaciomarine) mud. They describe that the thickness of this unit decreases within the tributary fjords, and that it was found in cores from Billefjorden as a less than 0.5 m thick transitional zone between the diamicton (till) and Holocene mud. In JM97-943-GC this unit is 25 cm thick and also marks the transition between the underlying till and the overlying Holocene mud (Fig. 8.7). The dates in this unit obtained by Svendsen et al. (1996) range between 12400 and 11120 cal. BP (Table 8.1). The dates obtained from the unit in this study are 11,230 and 11,190 cal. yr BP, reflecting that it most likely concerns the same unit.

The boundary between a basal till and glaciomarine sediments above in a core from van Mijenfjorden was dated to 11,170 cal. years BP. These early deglaciation sediments are characterized by high amounts of IRD decreasing rapidly to relatively low values at 10,000 cal. years BP (Hald et al., 2004). In core JM97-943-GC relatively low values of IRD are reached at the boundary to unit 943-C dated to approximately 11,200 BP, this indicates that the glacier retreat in Billefjorden was possibly faster and terminated earlier than in Van Mijenfjorden.

According to the peak distribution of the calibrated dates (Table 6.1; Fig. 8.7), unit 943-B was deposited in approximately 30 years. As discussed before, the possibility exists that the upper date (11210 cal. years BP) was reworked. However, the suggestion that the dates are correct, and that the deglaciation of the central part of the fjord could have occurred in approximately 30 years is supported by similar retreat rates from Norway (Corner, 1980; Vorren & Plassen, 2002), and assumed rapid retreat during the deglaciation of Svalbard (Lehman & Forman, 1992; Mangerud et al., 1992).

8.3.3 Low glacial activity, c. 11200 – 7930 cal. years BP, unit 943-C

The high concentration of shells and low amounts of clasts in unit 943-C are interpreted to indicate warmer water with more favourable living conditions for shells, possibly reflecting a warmer climate (see Chapter 5.3.3). These sediments were deposited during the early Holocene when independent data give evidence of a significantly warmer climate than at present (Birks, 1991). A study on lake sediments on Bjørnøya (for location see figure 1.1) concluded that the climate optimum on that island occurred between c. 9500 and 8000 cal. BP (Wohlfarth et al., 1995), after which the temperature may have gradually declined. Dates on different mollusc species in Isfjorden and western Spitsbergen indicate optimal climate conditions around 9680 to 8660 cal. BP (Table 8.1; Salvigsen et al., 1992). This is in good agreement with the timing of the most favourable living conditions for shells around 9370 cal. BP found in unit 943-C of core JM97-943-GC. Planktic foraminifera counts from the western continental margin of the Barents Sea also show an early Holocene thermal optimum between 10700 and 7700 cal. year BP (Sarnthein et al., 2003).

A sea-surface temperature reconstruction from a core from the upper continental margin off the west of Svalbard, shows that warmer water than at present started to develop around 11,000 cal. years BP, and prevailed until 8800 cal. years BP (Hald et al., 2004). Also in a core from Van Mijenfjorden, the foraminiferal flux showed relatively high values, and the sediments contained a high abundance of bivalve shells during the early Holocene (11,000 – 7000 cal. years BP). The depletion of $\delta^{18}O$ in benthic foraminifera suggested a warming of the bottom water of the fjord. This warming in the fjord was probably caused by the influx of relatively warm oceanic water from the continental margin across the fjord sill (Hald et al., 2004).

Evidence for the absence of the glacier Linnébreen and low sedimentation rates (0.2 mm yr^{-1}) in a core from Billefjorden led to a conclusion that the glaciers were small or absent during this interval (Svendsen & Mangerud 1997). The sediments in unit 943-C, however, contain low amounts of IRD reflecting that even though Nordenskiöldbreen might have been much smaller than it is at present, it still existed. High percentages of dolomite in the XRD record (Fig. 8.4) show that the sediment supply into the fjord mainly came from the fjord sides. Low percentages of illite & mica confirm that the influence of Nordenskiöldbreen was small.

8.1.4 Increase in IRD, c. 7930 - 3230 cal. years BP, unit 943-D

This time interval is defined by the increase in IRD in unit 943-D (Fig 8.7). A similar increase in IRD starting before 7,500 cal. years BP followed by a high flux between 7,500 and 4000 cal. years BP, as well as the increase in benthic foraminiferal $\delta^{18}O$ in Van Mijenfjorden were interpreted to reflect an gradual cooling of the water in the fjord (Hald et al., 2004). The sea-surface temperature reconstruction from a core from the upper continental margin off the western Svalbard, shows a abrupt cooling of about 4 ºC around 8,800 cal. years BP (Hald et al., 2004). This apparent abruptness of the cooling might be due to the low stratigraphic resolution of the upper part of the core and probably indicates reduced influence of Atlantic Water and increased influence of Polar Water and/or runoff from land (Hald et al., 2004). The gradual cooling in Van Mijenfjorden, but possibly also in Billefjorden, may be influenced by the flux of cool water from the continental margin and due to a more restricted fjord/margin water-mass exchange across the fjord sill due to glacio-isostatic rebound (Hald et al., 2004).

A high resolution marine sea surface temperature proxy record from the Western Barents Sea at 75º N also shows an abrupt cooling at 8800 cal. years BP, after the early Holocene optimum (Sarnthein et al., 2003).

Observations contradicting the evidence of a cooling in the early Holocene have e.g. been made by Svendsen & Mangerud (1997). They suggest that the increase in sedimentation rate in a core from Billefjorden represents the formation, or reaching of the sea-shore of Nordenskiöldbreen not before 3000-4000 cal. BP, after being small or absent (Mangerud & Svendsen (1997). Also the presence of *Mytulis edulis* in Svalbard from at least 11020 to 4220 cal. BP (Table 8.1; Salvigsen et al., 1992) indicates that the water cannot have been that cold in the early Holocene.

In the study by Hald et al. (2004) it is assumed that most of the IRD reflects rafting from icebergs. The increase in IRD coincides with a gradual cooling of the water in the fjord. However, the XRD results from core JM97-943-GC point to a more complex pattern of ice rafting. The XRD results show an increase in the percentage of illite and mica in the middle of unit 943-D, not before 5470 cal. years BP (Fig. 8.4). This indicates that most of the IRD in the lower part of this unit was not transported there by iceberg rafting from Nordenskiöldbreen, but most likely from sea ice. The question remains if the IRD in unit 943-D could have been transported by sea ice and if so, why the increase of iceberg rafted debris was delayed with approximately 2500 years after the increase in sea ice rafted debris.

Sea ice

Sea ice may incorporate IRD by adfreezing in the shore zone, from rivers flowing onto the sea ice in spring (Vorren et al., 1983), or in some cases colluvial processes may contribute sediment directly to sea ice. It can locally raft sediment up to 4 m across (Gilbert, 1990), but generally sizes are less than boulder size and often smaller than that because of the lack of strength of the ice. Sea ice rafted debris cannot be carried as far as by icebergs due to the relative thinness of the ice and its speed of melting (Gilbert, 1990; Powell, 2005). The sediments may differ from iceberg rafted sediments with regard to clast roundness: most of the sea ice clasts are derived from rounded littoral gravel (Lisitzyn, 1972), but distinguishing between sea ice and iceberg rafting remains problematic (Dowdeswell et al., 1998). Conclusions about the extent of glaciation based on the interpretation of rafted sediment must be made cautiously (Gilbert, 1990). The roundness of the IRD (of grainsize > 1cm in diameter) in unit 943-D was studied on x-radiographs but no changes were observed.

A gradual cooling of the water could have increased the formation of sea ice and the transport of IRD from the fjord sides to location of core JM97-943-GC.

However, the cooling could not have been too strong, because the development of multi year shorefast sea ice, known in Greenland as sikussak (Koch, 1945), would prevent sea ice and icebergs from drifting (Ó Cofaigh & Dowdeswell, 2001), and hence from transporting material to the core site.

Calving

The input of IRD from Nordenskiöldbreen into the fjord depends on the calving rate of the glacier. Calving fluxes can change through changes in terminus position or changes in glacier velocity or both (Benn & Evans, 1998). There is a strong positive correlation between calving rates and water depth at the calving front. A possible explanation is that the glacier retreated higher up into shallower water depth during the Holocene climatic optimum, and that it took a long time for the glacier to advance in deeper waters again before it could increase its calving rate.

However, a dynamic response of glaciers and ice-caps to a change in climate takes usually up to 100 years (Hagen, 2007). Nordenskiöldbreen is an outlet glacier of the Lomonosovfonna ice-cap (for location see Fig. 1.1) and therefore would not need more than 100 years to react to a shift in climate. The at a relatively higher elevation lying Lomonosovfonna does not show a correlation to the sea ice records as the lower lying Austfonna ice-cap and may therefore be less sensitive to changes in sea ice, and primarily record free atmospheric changes instead

(Isaksson et al., 2005). The fact that Nordenskiöldbreen sits on bedrock (Dallmann et al., 2004) could slightly prolongue the dynamic response to a climate change.

And an increase in the calving flux of a glacier can be caused by both advance and retreat of the glacier. If the ELA (equilibrium line altitude) falls, as a result of a climatic shift, the glacier margin will advance to a point where the fjord widens or deepens, thus to increase the calving rate to balance the ice flux (Benn & Evans, 1998). On the other hand, many Arctic and Antarctic ice shelves have undergone accelerated calving over the past century, probably owing to climatic warming causing, first, less widespread sea-ice, and second, enhanced basal melting and surface ablation (Benn & Evans, 1998).

IRD as a single parameter does not seem to provide enough information about the behavior of the glacier and climatic conditions, but indications of a generally cooler climate and the XRD data point to a glacier growth from around 5470 cal. years BP.

Foraminifera and IRD analyses from a core in Kongsfjordrenna indicate a middle Holocene transitional period between the warmer early Holocene and colder late Holocene (Skirbekk, 2007). This period is suggested to last from c. 7200 to 4700 cal. years BP. It is characterised by low glacial influence and a gradual increase of inflow of colder Arctic water into the fjord (Skirbekk, 2007). The period between c. 7930 and 5470 cal. years BP might be regarded as a similar transitional period in Billefjorden, because of the comparatively high concentration of sea-ice rafted debris and low input of iceberg rafted debris.

Another possible explanation for the comparatively high amounts of IRD in unit 943-D is an increased input of finer sediments during the early and the late Holocene. The accumulation rate in the middle Holocene was comparatively low (Fig. 8.3). The high amount of IRD in this part of the core could therefore be a result of the very low input of fine material, rather than an increase in IRD flux Plassen et al. (2004). However, the differences in accumulation rates are not regarded to be high enough to mask similar amounts of IRD in the early and the late Holocene, if they would have been present. It is suggested that the high concentrations of IRD in the lower part of unit 943-D is related to an increase in the amount of sea ice and in the upper part of unit 943-D is related to the growth of Nordenskiöldbreen in addition to the contribution by sea ice.

8.1.5 Late Holocene glacial maximum, < c. 3230 cal. years BP, unit 943-E

The late Holocene on Svalbard was defined by a relatively cold climate, termed the Neoglacial. In many areas of Svalbard, the Neoglacial terminal deposits represent the Holocene glacial maximum. According to Svendsen & Mangerud (1997), the Neoglacial started during at about 4000 ^{14}C years BP. They claim that the regrowth of tide water glaciers in Isfjorden seems to have occurred during the late Holocene, culminating during the Little Ice Age, about 100 yr ago (Liestøl, 1976; Sexton et al., 1992). Nordenskiöldbreen had its maximum extend around 1900 AD (Plassen et al., 2004). At this time the glacier front was located at the break from the bedrock terrace to the basin in Adolfbukta and a terminal moraine as well as a debris lobe were deposited (Plassen et al., 2004).

Even though this period is assumed reflect the coldest period in the Holocene, the IRD content in unit 943-E is very low. It however increases slightly towards the top of the unit (Fig. 5.10). Furthermore, the content of material from Nordenskiöldbreen (illite & mica; Fig. 8.4) in the XRD record decreases towards the top of the unit. A possible explanation for the lack of IRD and decrease of material coming from Nordenskiöldbreen could be an increase in sea ice. With a colder climate, sea-ice could cover the fjord (almost) the year round, blocking the way for icebergs from the glaciers (Ó Cofaigh & Dowdeswell, 2001). Most icebergs were possibly held in the sea ice for several years before release, and their basal debris-rich ice largely melted off in front of the glacier during this period (Syvitski et al., 1996). Also material incorporated in the sea ice would not reach the fjord easily if the sea ice would break up seldom.

9. Summary and conclusions

Three sediment cores, swath bathymetry data and high-resolution seismic data provided the basis for investigating sedimentary processes and glacigenic deposits as well as to reconstruct the glacial activity during the Late Weichselian and Holocene in Billefjorden, Svalbard.
The following conclusions are drawn:

- Prior to c. 11230 cal. years BP, glacial linear features have been formed in the central part of Billefjorden when glaciers occupied the fjord, draining the Svalbard-Barents Sea ice sheet (Fig. 9.1-1). Unit 943-A in core JM97-943-GC from the central part of the fjord is a till inferred to have been deposited before the ice front retreated into central Billefjorden.

- The glacier retreated from the central parts of Billefjorden to the fjord head between c. 11230 and 11200 cal. years BP (Fig. 9.1-2). 28 moraines in the central part of the fjord were interpreted to be annual recessional moraines, suggesting a glacier retreat rate about 330 m/year at the end of the Last Glacial

- High concentration of shells and low amounts of IRD in unit 943-C indicate a Holocene climatic optimum with reduced glacial activity between c. 11200 – 7930 cal. years BP (Fig. 9.1-3). Low amounts of IRD in addition to low percentages of illite & mica (regarded to indicate Nordenskiöldbreen as the provenance area) reflect that Nordenskiöldbreen existed during the Holocene climatic optimum. However, its size might have been much smaller than it is today.

- Unit 943-D reflects a period with increased ice rafting between 7930 and 3230 cal. years BP (Fig. 9.1-4 & 9.1-5). XRD results point to a complex pattern of ice rafting. An increase in the percentage of illite and mica indicates that most of the IRD between 7930 and 5470 cal. years BP was not transported there by iceberg rafting from Nordenskiöldbreen, but most likely from sea ice (Fig. 9.1-4). The XRD data point to a glacier growth from around 5470 cal. years BP (Fig. 9.1-5). Why the increase of iceberg rafted debris was delayed with approximately 2500 years after the increase in sea ice rafted debris remains to be understood. IRD as a single parameter does not seem to provide enough information about the behavior of the glacier and the climatic conditions.

- The late Holocene on Svalbard was defined by a relatively cold climate. A lack of IRD and a decrease in the material coming from Nordenskiöldbreen are explained by suppressed sea-ice and iceberg rafting because of the possible presence of multi-year shorefast sea ice during the Neoglacial maximum (Fig. 9.1-6). Glacial lineations on a bedrock terrace in the inner part of the fjord have presumably been formed during the Neoglacial readvance of Nordenskiöldbreen. At its maximum Neoglacial extent, the glacier front was located at the edge of the bedrock terrace in the inner part of the fjord, and a terminal moraine as well as a debris lobe was deposited (Plassen et al., 2004). Recessional moraines on the bedrock terrace in the inner part of the fjord were deposited during the subsequent retreat. Iceberg ploughmarks in the shallow areas were most likely generated by icebergs calving from Nordenskiöldbreen during the retreat (Fig. 9.1-7).

- Mass-transport activity in Billefjorden probably occurred throughout the entire Holocene. There might haven been an increase in mass-transport activity shortly after the deglaciation of the fjord, due to seismic activity related to high rates of isostatic uplift (Fig. 9.1-2 to 9.1-7). Other triggering mechanisms include the development of oversteepened slopes by high sediment supply and pushing of sediments at the grounding line of the glacier. Types of mass-transport deposits present in Billefjorden are include turbidites, slumps and debris flows (Plassen et al., 2004).
- Pockmarks in the central part of the fjord were most likely generated by the seepage of thermogenic gas along the Billefjorden fault zone (Fig. 9.1-3 to 9.1-7).
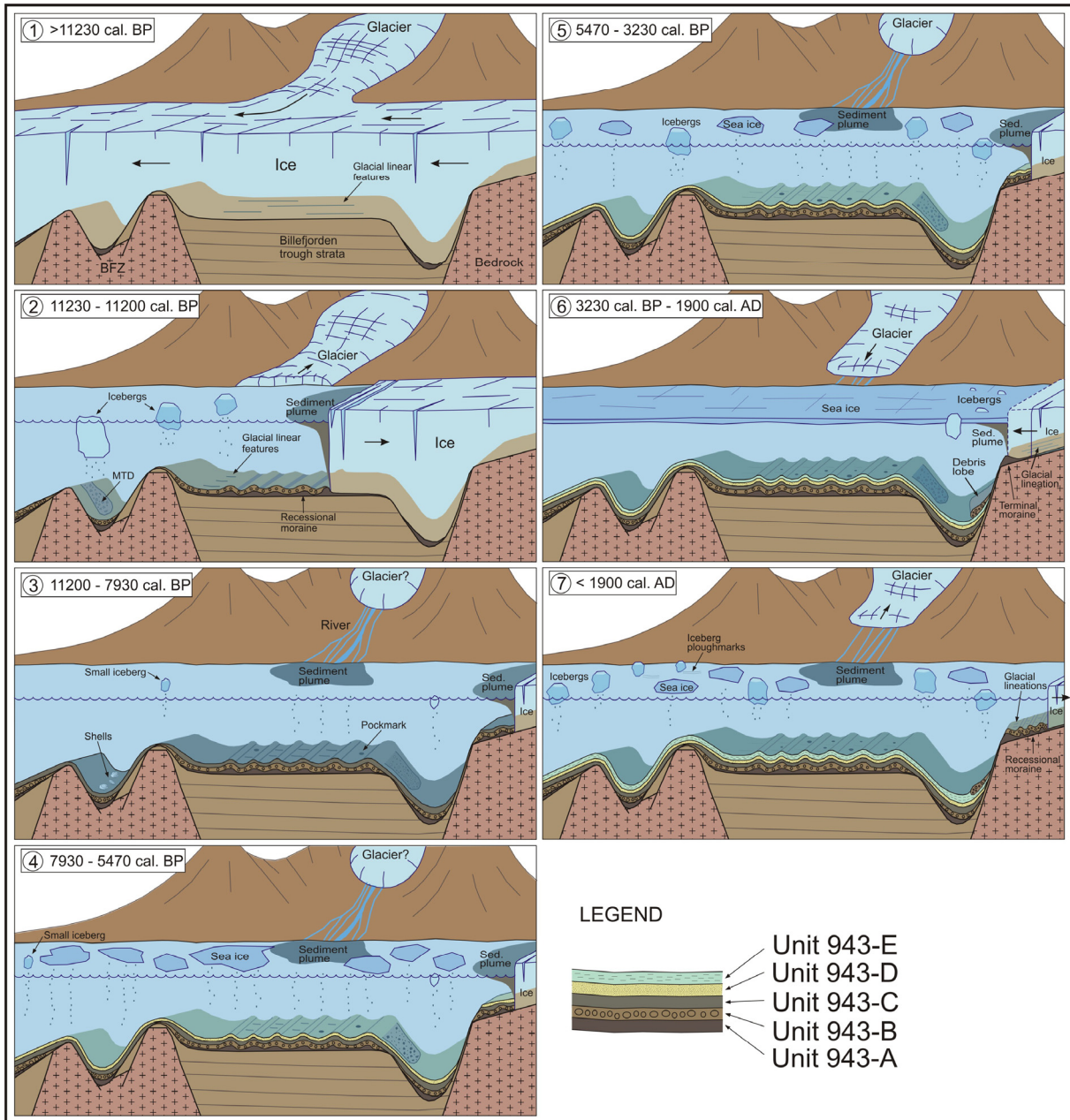
Fig. 9.1 Schematic overview of the glacial and sedimentological processes in Billefjorden during the Late Weichselian and Holocene. The units are from core JM97-943-GC from the central part of the fjord.

References

Aagaard, K., Foldvik, K., Hillman, S.R., 1987. The west Spitsbergen current: Disposition and water mass transformation. Journal of Geophysical Reasearch 92, 6729-6740.

Aarseth, I., Lønne, Ø., Giskeødegaard, O., 1989. Submarine slides in glaciomarine sediments from some western Norwegian fjords. Marine Geology 88, 1-21.

Aarseth, I., 1997. Western Norwegian Fjord sediments: age, volume, stratigraphy, and role as temporary depository during glacial cycles. Marine Geology 143, 39-53.

Andreassen, K., Nilssen, E.G., Odegaard, C.M., 2007. Analysis of shallow gas and fluid migration within the Plio-Pleistocene sedimentary succession of the SW Barents Sea continental margin using 3D seismic data. Geo-Marine Letters 27, 155-171.

Barnes, P.W., Lien, R., 1988. Icebergs rework shelf sediments to 500 m off Antarctica. Geology 16, 1130–1133.

Benn, I. D., Evans, D.J.A., 1998. Glaciers & Glaciation. Arnold, London.

Birks, H., 1991. Holocene vegetation history and climatic change in west Spitsbergen—plant macrofossils from Skardtjørna, an Arctic lake. The Holocene 1, 209–218.

Boulton, G.S., 1979. Glacial history of the Spitsbergen archipelago and the problem of the Barents Shelf ice sheet. Boreas 8, 31-57.

Boulton, G.S., 1986. Push-moraines and glacier-contact fans in marine and terrestrial environments. Sedimentology 33, 677-698.

Boulton, G.S., Van der Meer, J.J.M., Hart, J., Beets, D., Ruegg, G.H.J., Van der Wateren, F.M., Jarvis, J., 1996. Till and moraine emplacement in a deforming bed surge – an example from a marine environment. Quaternary Science Reviews 15, 961-987.

Bøe, R., Hovland, M., Instanes, A., Rise, L., Vasshus, S., 2000. Submarine slide scars and mass movements in Karmsundet and Skudenesfjorden, southwestern Norway: morphology and evolution. Marine Geology 167 (1-2), 147-165.

Christiansen, H.H., Hormes, A., 2005. Holocene periglacial landscape development in Adventdalen, Svalbard – modern activity and palaeoenvironmental reconstruction. Abstracts and Proceedings of the Geological Society of Norway 1, 21-22.

Clark, C.D., 1994. Large-scale ice-moulding: A discussion of genesis and glaciological significance. Sedimentary Geology 91, 253-268.

Corner, G.D., 1980. Preboreal deglaciation chronology and marine limits of the Lyngen-Storfjord area, Troms, North Norway. Boreas 9, 239-249.

Cowan, E.A., Cai, J., Powell, R.D., Clark, J.D., Pitcher, J.N., 1997. Temperate glacimarine varves: An example from Disenchantment Bay, Southern Alaska. Journal of Sedimentary Research 67, 536-549.

Dallmann, W.K., Piepjohn, K., Blomeier, D., 2004. Geological map of Billefjorden, Central Spitsbergen, Svalbard, with geological excursion guide. Norsk Polarinstitutt Temakart Nr. 36.

De Geer, G., 1910. Guide de l'excursion au Spitsberg. Excursion Al. (Guide to excursions on Spitsbergen Al.) Stockholm: XI International Geological Congress.

Desloges, J.R., Gilbert, R., Nielsen, N., Christiansen, C., Rasch, M., Øhlenschläger, R., 2002. Holocene glacimarine sedimentary environments in fjords of Disko Bugt, West Greenland. Quaternary Science Reviews 21, 947-963.

Dowdeswell, J.A., 1989. On the nature of Svalbard icebergs. Journal of Glaciology 35, 224-234.

Dowdeswell, J.A. & Dowdeswell, E.K., 1989. Debris in icebergs and rates of glaci-marine sedimentation: observations from Spitsbergen and a simple model. Journal of Geology 97, 221-231.

Dowdeswell, J.A., Elverhøi, E., Spielhagen, R., 1998. Glacimarine sedimentary processes and facies on the Polar North Atlantic margins. Quaternary Science Revieuws 17, 243-272.

Dowdeswell, J.A., Uenzelmann-Neben, G., Whittington, R.J., Marienfeld, P., 2004B. The Late Quaternary sedimentary record in Scoresby Sund, East Greenland. Boreas 23, 294-311.

References

Elverhøi, A., 1984. Glacigenic and associated marine sediments in the Weddel Sea, fjords of Spitsbergen and the Barents Sea: a revieuw. Marine Geology 57, 53-88.

Elverhøi, A., Andersen, E.S., Dokken, T., Hebbeln, D., Spielhagen, R., Svendsen, J.I., Sørflaten, M., Rørnes, S., Hald, M., Forsberg., C.F., 1995A. The Growth and Decay of the Late Weichselian Ice Sheet in Western Svalbard and Adjacent Areas Based on Provenance Studies of Marine Sediments. Quaternary Research, 44: 303-316.

Elverhøi, A., Liestøl, O., Nagy, J., 1980. Glacial erosion, sedimentation and microfauna in the inner part of Kongsfjorden, Spitsbergen. Norsk Polarinstitutt Skrifter 172, 33-58.

Elverhøi, A., Lønne, Ø, Seland, R., 1983. Glaciomarine sedimentation in a modern fjord environment, Spitsbergen. Polar Research 1, 127-149.

Elverhøi, A., Svendsen, J.I., Solheim, A., Andersen, E.S., Milliman, J., Mangerud, J., leB. Hooke, R., 1995B. Late Quaternary Sediment Yield from the High Arctic Svalbard Area. Journal of Geology 103, 1-17.

Forman, S.L., Lubinski, D.J., Ingólfsson, Ó., Zeeberg, J.J., Snyder, J.A., Siegert, M.J., Matishov, G.G., 2004. A review of postglacial emergence on Svalbard, Franz Josef Land and Novaya Zemlya, northern Eurasia. Quaternary Science Reviews 23, 1391-1434.

Forman, S.L., Mann, D., Miller, G.H., 1987. Late Weichselian and Holocene relative sea-level history of Brøggerhalvøya, Spitsbergen, Svalbard Archipelago. Quaternary Research 27, 41-50.

Forwick, M. & Vorren, T.O., 2005A. Late Weichselian and Holocene sedimentation and environments in the Isfjorden area, Svalbard. In Forwick, M. (ed.): Sedimentary processes and palaeoenvironments in Spitsbergen fjords. Dr.Scient. Thesis, University of Tromsø, 34 p.

Forwick, M. & Vorren, T.O., 2005B. Late Weichselian deglaciation history of the Isfjorden area, Spitsbergen. In Forwick, M. (ed.): Sedimentary processes and palaeoenvironments in Spitsbergen fjords. Dr.Scient. Thesis, University of Tromsø, 10 p.

Forwick, M., Vorren, T.O., 2007. Holocene mass-transport activity and climate in outer Isfjorden, Spitsbergen: marine and subsurface evidence. The Holocene 17 (6), 707-716.

Førland E.J., Hanssen-Bauer, I., Nordli, P.Ø., 1997. Climate statistics & longterm series of temperature and precipitation at Svalbard and Jan Mayen. DNMI-KLIMA Report, 21-97.

Gascard, J.C., Richez, C., Rouault, C., 1995. New insights from large-scale oceanography in Fram Strait: The West Spitsbergen Current. In Smith, W. and Grebmeier, J. (eds.). Oceanography of the Artic: Marginal ice zones and continental shelves. Coastal and estuarine studies series, American Geophysical Union, Whashington DC, 131-182.

Gilbert, R., 1990. Rafting in glacimarine environments. Glacimarine environments: processes and sediments. J.A. Dowdeswell and J.D. Scourse (eds.), Geological Society Londen, Special Publications 53, 105-120.

Grove, J.M., 1988. The little Ice Age. Methuen, Londen.

Hagen, J.O., 2007. Lecture notes for AG-325 Glaciology at UNIS, March 2007.

Hagen, J.O., Liestøl, O., Roland, E. Jørgensen, T., 1993. Glacier atlas of Svalbard and Jan Mayen, Medd. Norsk Polarinstitutt 129, 5-41.

Hald, M., Ebbesen, H., Forwick, M., Godtliebsen, F., Khomenko, L., Korsun, S., Ringstad Olsen, L. & Vorren, T.O., 2004. Holocene paleoceanography and glacial history of the West Spitsbergen area, Euro-Arctic margin. Quaternary Science Reviews 23, 2075-2088.

Hjelle, A., 1993. Geology of Svalbard, Norsk Polarinstitutt, Oslo, 162 p.

Hovland, M., Judd, A.G., 1988. Seabed pockmarks and seepages. Graham and Trotman, 239 p.

Howe, J.A., Moreton, S.G., Morri, C., Morris, P., 2003. Multibeam bathymetry and the depostitional environment of Kongsfjorden and Krossfjorden, western Spitsbergen, Svalbard. Polar Research, 22(2), 301-316.

Hughen, K.A., Baillie, M.G.L., Bard, E., Bayliss, A., Beck, J.W., Bertrand, C., Blackwell, P.G., Buck, C.E., Burr, G., Cutler, K.B., Damon, P.E., Edwards, R.L., Fairbanks, R.G., Friedrich, M., Guilderson, T.P., Kromer, B., McCormac, F.G., Manning, S., Bronk Ramsey, C., Reimer, P.J.,

Memmele, S., Southon, J.R., Stuiver, M., Talamo, S., Taylor, F.W., van der Plicht, J., Weyhenmeyer, C.E., 2004. Marine04, Marine radiocarbon age calibration, 26-0 ka BP. Radiocarbon 46, 1059-1086.

Isaksson, E., Hermanson, M., Hicks, S., Igarashi, M., Kamiyama, K., Moore, J., Motoyama, H., Muir, D., Pohjola, V., Vaikmäe, R., van de Wal, R., Watanebe, O., 2003. Ice cores form Svalbard – useful archives of past climate and pollution history. Physics and Chemistry of the Earth 28, 1217-1228.

Isaksson, E., Kohler, J., Pohjola, V., Moore, J., Igarashi, M., Karlöf, L., Martma, T., Meijer, H., Motoyama, H., Vaikmäe, R., van de Wal, R.S.W., 2005. Two ice-cored delta^{18}O records from Svalbard illustrating climate and sea-ice variability over the last 400 years. The Holocene 15(4), 501-509.

Jiskoot, H, Murray, T., Boyle, P., 2000. Controls on the distribution of surge-type glaciers in Svalbard. Journal of Glaciology 46, 412–422.

Judd, A.G., Hovland, M., 1992. The evidence of shallow gas in marine sediments. Continental Shelf Research 12 (10), 1081-1096.

Judd, A.G., Hovland, M., 2007. Seabed fluid flow, the impact on geology, biology and the marine environment. Cambridge University Press, Cambridge.

Kelley, J.T., Dickson, S.M., Belknap, D.F., Barnhardt, W.A., Henderson, M., 1994. Giant sea-bed pockmarks: Evidence for gas escape from Belfast Bay, Maine. Geology 22, 59-62.

King, L.H., 1976. Use of a conventional echo-sounder and textural analyses in delineating sedimentary facies: Scotion shelf. Canadian Journal of Earth Science 13, 1082-1092.

Knies, J., Damm, E., Gutt, J., Mann, U., Pinturier, L., 2004. Geochemistry Geophysics Geosystems 5, number 6.

Koch, L., 1945. The East Greenland ice. Meddelelser om Grønland, 130, 1-373.

Kongsberg, 2003. EM300 Multibeam echosounder, Operator manual.

Kromer, B., Spurk, M., 1998. Revision and tentative extension of the tree-ring based 14C calibration, 9200 to 11855 cal BP. Radiocarbon 40(3), 1117-1125.

Lehman, S.J., Forman, S.L., 1992. Late Weichselian Glacier Retreat in Kongsfjorden, West Spitsbergen, Svalbard. Quaternary Research 37, 139-154.

Liestøl, O., 1976. Årsmorener foran Nathorstbreen? Norsk Polarinstitutt Årbok, 1976, 361-363.

Lisitzyn, A.P., 1972. Sedimentation in the world's ocean. Society of Economic Paleontologists and Mineralogists Special Publication No. 17, 218 p.

Mangerud, J., Bolstad, M., Elgersma, A., Helliksen, D., Landvik, J.Y., Lønne, I., Lycke, A.K., Salvigsen, O., Sandahl, T. & Svendsen, J.I., 1992. The Last Glacial Maximum on Spitsbergen. Quaternary Research 38, 1-31.

Mangerud, J., Dokken, T., Hebbeln, D., Heggen, B., Ingólfsson, Ó., Landvik, J.Y., Mejdahl, V., Svendsen, J., Vorren, T.O., 1998. Fluctuations of the Svalbard-Barents Sea ice sheet during the last 150 000 years. Quarternary Science Reviews 17, 11-42.

Mangerud, J., Gulliksen, S., 1975. Apparent radiocarbon ages of recent marine shells from Norway, Spitsbergen, and Arctic Canada. Quaternary Research 5, 73-263.

Mangerud, J., Svendsen, J.I., 1990. Deglaciation chronology inferred from marine sediments in a proglacial lake basin, western Spitsbergen, Svalbard. Boreas 19, 249-272.

Mangerud, J., Svendsen, J.I., 1992. The last interglacial-glacial period on Spitsbergen, Svalbard. Quaternary Science Reviews 11, 633-664.

Middleton, G.V., 1966. Experiments on density and turbidity currents: II. Uniform flow of density currents. Canadian Journal of Earth Sciences 3, 627–637.

Nordli, P.Ø., Hanssen-Bauer, I., Førland, E.J., 1996. Homogeneity analyses of temperature and precipitation series from Svalbard and Jan Mayen. Det Norske Meteorologiske Institutt (DNMI) – Klima. Report No. 16/96, 41 p.

Ó Cofaigh, C., Dowdeswell J.A., 2001. Laminated sediments in glacimarine environments: diagnostic criteria for their interpretation. Quaternary Science Reviews 20, 1411-1436.

Ó Cofaigh, C., Dowdeswell, J.A., Allen, C.S., Hiemstra, J.F., Pudsey, C.J., Evans, J., Evans, D.J.A., 2005. Flow dynamics and till genesis associated with a marine-based Antarctic palaeo-ice stream, Quaternary Science Reviews, 709–740.

Ottesen, D., Dowdeswell, J.A., 2006. Assemblages of submarine landforms produced by tidewater glaciers in Svalbard. Journal of Geophysical Research 111, 1-16.

Ottesen, D., Dowdeswell, J.A., Rise, L., 2005. Submarine landforms and the reconstruction of fast-flowing ice streams within a large Quaternary ice sheet: The 2500-km-long Norwegian Svalbard margin (57°–80°N). Geological Society of America Bulletin 117(7/8), 1033-1050.

Plassen, L., Vorren, T.O., 2002. Late Weichselian and Holocene sediment flux and sedimentation rates in Andfjord and Vågsfjord, North Norway. Journal of Quaternary Science 17 (2), 161-180.

Plassen, L., Vorren, T.O., 2003. Fluid flow features in fjord-fill deposits, Ullsfjorden, North Norway. Norwegian Journal of Geology 83, 37-42.

Plassen, L., Vorren, T.O., Forwick, M., 2004. Integrated acoustic and coring investigation of glacigenic deposits in Spitsbergen fjords. Polar Research, 23(1), 89-110.

Powell, 2005. Subaquatic landsystems: Fjords, in Glacial Landsystems, edited by D.J.A. Evans. Edward Arnold, London 532, 313-347.

Powell, R.D., Alley, R.B., 1997. Grounding-line systems: processes, glaciological inferences and the stratigraphic record. In P.F. Barker and A.C. Cooper (eds), Geology and seismic stratigraphy of the Antarctic Margin, 2. Antarctic Research Series, 71. AGU, Washington, DC, 169-187.

Powell, R.D., Molnia, B.F., 1989. Glacimarine sedimentary processes, facies and morphology of the south-south-east Alaska Shelf and fjords. Marine Geology 85, 359-390.

Salvigsen, O., 1979. The last deglaciation of Svalbard. Boreas 8(2), 229-231

Salvigsen, O., Forman, S.L., Miller, G.H., 1992. Thermophilous molluscs on Svalbard during the Holocene and their paleoclimatic implications. Polar Research 11 (1), 1-10.

Sarnthein, M., Van Kreveld, S., Erlenkeuser, H., Grootes, P.M., Kucera, M., Pflaumann, U., Schulz, M., 2003. Centennial-to-millennial-scale periodicities of Holocene climate and sediment injections off the western Barents shelf, 75ºN. Boreas 32, 447-461.

Sexton, D.J., Dowdeswell, J.A., Solheim, A., Elverhøi, A., 1992. Seismic architecture and sedimentation in northwest Spitsbergen fjords. Marine Geology 103, 53-68.

Skirbekk, K., 2007. Rekonstruksjon av paleomiljø i Kongsfjordrenna, vest for Svalbard, de siste ~ 11 800 år, basert på bentiske foraminiferer of sedimentologiske undersøkelser. Mastergradsoppgave i Geology, Universitetet i Tromsø.

Smith, S.D., Banke, E.G., 1983. The influence of winds, currents and towing forces on the drift of icebergs. Cold Regions Science and Technology 6, 241-255.

Solheim, A., 1991. The depositional environment of surging sub-polar tidewater glaciers: a case study of the morphology, sedimentation and sediment properties in a surge affected marine basin outside Nordaustlandet, the Northern Barents Sea. Norsk Polarinstitutt Skrifter 194, 1-97.

Solheim, A., Elverhøi, A., 1985. A pockmark field in the central Barents Sea: gas from a petrogenic source? Polar Research 3, 11-19.

Solheim, A., Pfirman, S.L., 1985. Sea-floor morphology outside a grounded, surging glacier; Bråsvellbreen, Svalbard. Marine Geology 65, 127-143.

Stewart, I.S., Sauber, J., Rose, J., 2000. Glacio-seismotectonics: ice sheets, crustal deformation and seismicity. Quaternary Science Revieuws 19, 1367-1389.

Stow, D.A.V., Reading, H.G., Collinson, J.D., 1996. Deap Seas. In H.G. Reading (Editor), Sedimentary Environments – Processes, Facies and Stratigraphy. Blackwell Science, 395-453.

Stuiver, M., Reimer, P.J., 1993. Extended 14C database and revised CALIB radiocarbon calibration program. Radiocarbon 35, 215-230.

Stuiver, M., Reimer, P.J., Bard, E., Beck, J.W., Burr, G.S., Haugen, K.A., Kromer, K.A., McCormac, F.G., Van der Plicht, J., Spurk, M., 1998. INTCAL98 Radiocarbon age calibration 24,000–0 cal BP. Radiocarbon 40, 1041-1083.

Stuiver, M., Polach, H.M., 1977. Discussion: Reporting of 14C Data. Radiocarbon 19 (3), 355-363.

Svendsen, H., Beszczynska-Møller, A., Hagen, J.O., Lefauconnier, B., Tverberg, V.,
Gerland, S., Ørbæk, J.B., Bischof, K., Papucci, C., Zajaczkowski, M., Azzolini, R., Bruland, O., Wiencke, C., Winther, J., Dallman, W., 2002. The physical environment of Kongsfjorden-Krossfjorden, an Artic fjord system in Svalbard. Polar Research 21 (1), 133-166.

Svendsen, J.I., Elverhøi, E., Mangerud, J., 1996. The retreat of the Barents Sea Ice Sheet on the western Svalbard margin. Boreas 25, 244-256.

Svendsen, J.I. & Mangerud, J., 1997. Holocene glacial and climatic variations on Spitsbergen, Svalbard. The Holocene 7 (1), 45-57.

Syvitski, J.P.M., 1989. On the deposition of sediment within glacier-influenced fjords: oceanographic controls. Marine Geology, 85, 301-329.

Syvitski, J.P.M., Andrews, J.T., Dowdeswell, J.A., 1996. Sediment deposition in an iceberg-dominated glacimarine environment, East Greenland: basin fill implications. Global and Planetary Change 12, 251-270.

Syvitski, J.P.M., Burrel, D.C., Skei, J.M., 1987. Fjords: processes and products. Springer-Verlag.

Söderberg, P., Flodén, T., 1991. Pockmark developments along a deep crustal structure in the northern Stockholm Archipelago, Baltic Sea. Beiträge zur Meereskunde 62, 79-102.

Tulaczyk, S.M., Scherer, R., Clark, C.D., 2001. A ploughing model for the origin of weak tills beneath ice streams: a qualitative treatment. Quaternary International 86, 59-70.

Vogt, C., Lauterjung, J. and Fischer, R.X., 2002. Investigation of the clay fraction (<2 μm) of the clay mineral society reference clays. Clays and Clay Minerals, 50(3), 388-400.

Vorren, T.O., Hald, M., Edvardsen, M., Lind-Hansen, O., 1983. Glacigenic sediments and sedimentary environments on continental shelves: General principles with a case study from the Norwegian shelf. In J. Ehlers (ed.), Glacial deposits in north-west Europe. Balkema, Rotterdam, 61-73.

Vorren, T.O., Hald, M., Thomsen, E., 1984. Quaternary sediments and environments on the continental shelf off northern Norway. Marine Geology 57, 229-257.

Vorren, T., Plassen, L., 2002. Deglaciation and palaeoclimate of the Andfjord-Vågsfjord area, North Norway. Boreas 31, 97-125.

Weber, M.E., Niessen, F., Kuhn, G., Wiedicke, M., 1997. Calibration and application of marine sedimentary physical properties using a multi-sensor core logger. Marine Geology 136, 151-172.

Werner, A., 1993. Holocene moraine chronology, Spitsbergen, Svalbard: lichenometric evidence for multiple Neoglacial advances in the Arctic. The Holocene 3, 12-137.

Whittington, R.J., Forsberg, C.F., Dowdeswell, J.A., 1997. Seismic and side-scan sonar investigations of recent sedimentation in an ice-proximal glacimarine setting, Kongsfjorden, north-west Spitsbergen. In Glaciated Continental Margins: an Atlas of Acoustic Images, CRC Press, Boca Raton, Fla, 175-178.

Wohlfarth, B., Lemdahl, G., Olssen, S., Persson, T., Snowball, I., Ising, J., Jones, V., 1995. Early Holocene environment on Bjørnøya (Svalbard) inferred from multidisciplinary lake sediment studies. Polar Research 14 (2), 253-275.